Master's thesis

NTNU
Norwegian University of Science and Technology
Faculty of Engineering
Department of Marine Technology

Bjørn Theodor Torp Brørby

Wave load compensation in DP control systems

Master's thesis in Marine Technology
Supervisor: Roger Skjetne
Co-supervisor: Mathias Marley
June 2022

NTNU
Norwegian University of
Science and Technology

Bjørn Theodor Torp Brørby

Wave load compensation in DP control systems

Master's thesis in Marine Technology
Supervisor: Roger Skjetne
Co-supervisor: Mathias Marley
June 2022

Norwegian University of Science and Technology
Faculty of Engineering
Department of Marine Technology

NTNU
Norwegian University of
Science and Technology

NTNU Trondheim
Norwegian University of Science and Technology
Department of Marine Technology

MASTER OF TECHNOLOGY THESIS DEFINITION (30 SP)

Name of the candidate:	Brørby, Bjørn Theodor Torp
Field of study:	Marine cybernetics
Thesis title (Norwegian):	Kompensasjon av bølgelaster i kontrollsystemer for DP.
Thesis title (English):	Wave load compensation in DP control systems.

Background

For dynamic positioning (DP) operations in ocean waves, the DP control system must compensate the hydrodynamic wave-drift loads. This is done by feedback control, where slowly-varying 2nd order wave loads are compensated through the integral action of the DP feedback control law. Typically, these feedback mechanisms are subject to changes caused by low-frequency (and possibly mid-frequency) contributions, which are forcing an offset in DP stationkeeping accuracy. The research question in this master thesis is if a feedforward mechanism can be designed to eliminate such offsets, and how effective will such strategies be compared to the conventional DP feedback control?

In this project, the goal is to develop and compare different strategies for wave load compensation, by utilizing acceleration measurements as well as estimation of wave load parameters. The strategies shall be compared as fairly as possible in both a simulation model and possibly in a physical test setup using the C/S Arctic Drillship (CSAD) in MC-lab.

Scope of Work

1. Perform a background and literature review to provide information and relevant references on:
    - Hydrodynamic wave models and loads on ships and ocean structures.
    - Sea state and wave spectrum estimation, in particular online methods.
    - Relevant instruments for wave load estimation and prediction.
    - DP control system: Objective, typical topology, and methods for DP feedback and feedforward control, including use of acceleration feedforward disturbance rejection.
    - MC-Lab and CSAD model.

    Write a list with abbreviations and definitions of terms and symbols, relevant to the literature study and project report.
2. Develop and discuss several strategies for wave-drift load compensation, considering:
    - DP-observer bias estimate and feedforward compensation.
    - Direct integral action in DP PID control law.
    - Acceleration feedforward compensation of residual disturbance loads.
    - Estimation of harmonic “residual loads” given by the internal model principle using e.g. a Fourier series.
    - Spectrum-based method, if applicable.
3. Decide on some promising methods for wave load compensation, and implement and test these strategies on a (high-fidelity) simulation model, and possibly conduct lab experiments with CSAD in MC-Lab, if applicable. Analyze and discuss, with good critical evaluation, the results.

Specifications

Every weekend throughout the project period, the candidate shall send a status email to the supervisor and co-advisors, providing two brief bulleted lists: 1) work done recent week, and 2) work planned to be done next week.

The scope of work may prove to be larger than initially anticipated. By the approval from the supervisor, described topics may be deleted or reduced in extent without consequences with regard to grading.

The candidate shall present personal contribution to the resolution of problems within the scope of work. Theories and conclusions should be based on mathematical derivations and logic reasoning identifying the steps in the deduction.

The report shall be organized in a logical structure to give a clear exposition of background, problem/research statement, design/method, analysis, and results. The text should be brief and to the point, with a clear language. Rigorous mathematical deductions and illustrating figures are preferred over lengthy textual descriptions. The report shall have font size 11 pts., and it is not expected to be longer than 70 A4-pages, 100 B5-pages, from introduction to conclusion, unless otherwise agreed. It shall be written in English (preferably US) and contain the elements: Title page, project definition, preface (incl. description of help, resources, and internal and external factors that have affected the project process), acknowledgement, abstract, list of symbols and acronyms, table of contents, introduction (project background/motivation, objectives, scope and delimitations, and contributions), technical background and literature review, problem formulation or research question(s), method/design/development, results and analysis, conclusions with recommendations for further work, references, and optional appendices. Figures, tables, and equations shall be numerated. The contribution of the candidate shall be clearly and explicitly described, and material taken from other sources shall be clearly identified. Work from other sources shall be properly acknowledged using quotations and a Harvard citation style (e.g. natbib Latex package). The work is expected to be conducted in an honest and ethical manner, without any sort of plagiarism and misconduct, which is taken very seriously by the university and will result in consequences. NTNU can use the results freely in research and teaching by proper referencing, unless otherwise agreed.

The thesis shall be submitted with an electronic copy to the main supervisor and department according to NTNU administrative procedures. The final revised version of this thesis definition shall be included after the title page. Computer code, pictures, videos, data, etc., shall be included electronically with the report.

Start date: 15 January, 2022 **Due date:** As specified by the administration.

Supervisor: Roger Skjetne
Co-advisor(s): Mathias Marley (NTNU AMOS)

Signatures:

Roger Skjetne

Digitally signed by rskjetne
Date: 2022.05.27 14:35:50
+02'00'

Abstract

This master thesis presents alternative methods for wave load compensation in dynamic positioning (DP) operations, where stable and robust conventional feedback DP controllers typically are used. Such DP feedback control laws, compensates slowly-varying second order wave loads through the integral action. The problem is that these mechanisms are subject to changes caused by low-frequency (and possible mid-frequency) contributions, which are forcing an offset in DP stationkeeping accuracy. In addition, feedback mechanisms requires such offsets to be induced before the control law can mobilize any counteractions, making the control system less reactive to disturbances. Therefore, this thesis aims to find better strategies for eliminating offsets due to slowly varying second order wave loads.

A background study and literature review have been performed, in order to gain fundamental knowledge on relevant topics; that is, hydrodynamical theory in terms of wave models and loads, sea state estimation, relevant instruments for wave load estimation, DP control systems in general, and information on C/S Arctic Drillship in the Marine Cybernetics Laboratory.

In order to test different control strategies, a high-fidelity simulator in six degrees of freedom have been developed and implemented, such that relevant sensor measurements and wave loads are provided. The simulator is based on parameters from the physical model vessel C/S Arctic Drillship, such that the implemented control systems can be tested directly on the physical model vessel in MC-Lab. However, the latter have not been performed due to external factors.

Five control strategies have been presented, including a DP-observer estimate as feedforward compensation, direct integral action in DP PID-control, acceleration feedforward compensation, adaptive control using the internal model principle, and a spectrum-based method. The two first were considered as conventional DP feedback controllers, and were used as baseline to compare the effectiveness against the other developed methods.

A performance analysis was submitted, based on results from the control systems applied to the high-fidelity simulator. In order to compare the results as fairly as possible, much time was put into tuning the control laws. Consequently, only surge direction was tuned properly enough to be part of the analysis. The performance was evaluated and compared based on key performance indicators, in terms of positioning performance and thrust effort.

Results showed that the adaptive control method, using the internal model principle, was able to counteract the second order wave loads well in a long term perspective, while on a short term, the adaption was unable to match the conventional controllers, and the overall thrust effort was significantly higher than the conventional feedback controllers. The acceleration feedforward held, in general, the best performance in both a long term and short term period, by providing an aggressive response to all accelerations. However, mean-drift loads were not successfully compensated, since these lead to zero acceleration. Moreover, the latter method showed tendencies to be sensitive towards uncertain measurements. Finally, a spectrum based method, utilizing a wave spectrum estimate to compensate mean-drift loads, was implemented. However, the algorithm was too time-consuming for the control system, but alternatives to overcome the issue were discussed.

Taken into consideration that only surge direction was analyzed, there are reasons to believe that there exists better strategies for wave load compensation, than the conventional feedback mechanisms.

Sammendrag

Denne masteroppgaven presenterer alternative metoder for bølgelastkompensasjon i dynamiske posisjonering (DP) av marine fartøy, der stabile og robuste konvensjonelle kontrollere med tilbakekopling vanligvis brukes. Slike tilbakekoplinger kompenserer saktevarierende andreordens bølgebelaster gjennom integralvirkning. Problemet er at disse mekanismene er gjenstand for endringer, forårsaket av lavfrekvente (og muligigens mellom-frekvente) bidrag, som tvinger fram et posisjonsavvik. I tillegg krever mekanismer med slik tilbakekopling at slike avvik induseres før kontrollsystemet kan mobilisere motkrefter. Dette gjør kontrollsystemet mindre reaktivt overfor forstyrrelser. Derfor har denne oppgaven som mål å finne bedre strategier for å eliminere forskyvninger på grunn av sakte varierende andreordens bølgelaster.

Det er utført en bakgrunnsstudie og litteratur-gjennomgang, for å få grunnleggende kunnskap om relevante tema; det vil si hydrodynamisk teori som angår bølgemodeller og laster, sjøtilstandsestimering, relevante instrumenter for sjøtilstandsestimering, kontrollsystemer for DP generelt, og informasjon om C/S Arctic Drillship i MC-Lab.

For å teste ulike kontrollstrategier er det utviklet og implementert en naturtro simulator i seks frihetsgrader, som også gir realistiske sensormålinger og bølgelaster. Simulatoren er basert på parametere fra det fysiske modellfartøyet C/S Arctic Drillship, slik at de implementerte kontrollsystemene kan testes direkte på det fysiske modellfartøyet i MC-Lab. Sistnevnte har imidlertid ikke blitt utført på grunn av ytre faktorer.

Fem kontrollstrategier er presentert, deriblandt et DP-observer estimat som feedforward kompensasjon, direkte integral virkning i en PID kontroller, akselerasjons-feedforward kompensasjon, adaptiv kontroll ved bruk av et intern modell prinsipp, samt en spektrum-basert metode. De to første ble betraktet som konvensjonelle kontrollere med tilbakkompling, og ble brukt til å sammenligne ytelsen mot de andre utviklede metodene.

Det ble gjort en analyse av metodene, basert på resultater simulatoren. For å sammenligne resultatene så rettferdig som mulig, ble det brukt mye tid på å tune kontrollerne. Følgelig ble bare jag-retningen godt nok justert til å være en del av analysen. Ytelsen ble evaluert og sammenlignet basert på to indikatorer; hvor god posisjoneringen var og hvor mye arbeidskraft som kreves.

Resultatene viste at den adaptive metoden, ved bruk av den interne modellen, var i stand til å motvirke andre ordens bølgelaster i et langsiktig perspektiv, mens tilpasningen på kort sikt ikke var i stand til å matche de konvensjonelle kontrollerene. Den totale arbeidsytelsen var betydelig høyere enn de konvensjonelle kontrollerne på både lang og kort sikt. Akselerasjon-tilbakekoplingen viste seg å være den generelt beste både på lang og kort sikt, ved å gi en aggressiv respons på alle akselerasjoner. Imidlertid egnet metoden seg dårlig til å motvirke gjennomsnittlige bølgedriftlaster, da disse ikke induserer akselerasjoner. I tillegg viste sistnevnte metode tendenser til å være sensitiv mot usikkerhet i målinger. Til slutt ble den spektrum-baserte metoden implementert. Den benyttet et bølgespektrum-estimat for å kompensere gjennomsnittlige bølgedriftlaster. Algoritmen var imidlertid for tidkrevende for kontrollsystemet, men alternativer for å løse problemet ble diskutert.

Tatt i betraktning at kun jag-retning ble analysert, er det grunn til å tro at det finnes bedre strategier for kompensasjon av bølgelaster, enn de konvensjonelle tilbakekoblings-mekanismene.

Preface

This master thesis is the final part of my master's degree in Marine Cybernetics at the Department of Marine Technology, and was written in the spring of 2022. This is a continuation of my preproject, delivered in December 2021, which also focused on wave load compensation.

My supervisor, Professor Roger Skjetne, has helped enlighten me on possible strategies and suggested ideas for wave load compensation, through discussions and follow-up, in a control theoretical perspective. The knowledge I have gained about hydrodynamical aspects of this thesis has been well-supported by my co-advisor, PhD Candidate Mathias Marley, and has been crucial in both my approach to the problem, and in designing the simulator.

The developed control designs were supposed to be tested in the Marine Cybernetics Laboratory, in order to study a physical test case on the C/S Arctic Drillship. Due to issues, possibly related to a hardware problem, I did not manage to connect to the vessel's actuators. Therefore, only simulations made the basis for testing and performance analysis.

Through the period of working with this master thesis, I have enriched my knowledge and experience in designing, programming, and testing control systems. In addition, my passion for applying control theory on relevant problems has developed even further.

Acknowledgement

First of all I would like to thank my supervisor, Professor Roger Skjetne, for showing genuine interest in my work in this master thesis, giving the impression of that someone other than me cares about the outcome of my work. This has helped me to keep up my motivation during this period. I am also grateful for the help I have received to overcome the different problems that I have run into, when designing the control systems presented in this thesis.

I am also grateful for all the follow-up I have got from my co-advisor, PhD Candidate Mathias Marley, in order to understand and gain knowledge of the hydrodynamical theory which has been definitive for understanding and approaching the problem in question.

I would also like to direct a huge thanks to my fellow students for five great years. A special thanks to my fellow students sharing office with me, for making the final year fun, and for going through a period of hard work together.

Finally, I thank my family for their love, and for always being supportive in my choices, especially during challenging periods through my education.

Table of Contents

List of Tables

List of Figures

Abbreviations

Acronyms

ARS	Attitude rate sensor
CDM	Control design model
CLF	Control Lyapunov function
CO	Center of origin
CSAD	C/S Arctic Drillship
DNV	Det Norske Veritas
DOF	Degree of freedom
DP	Dynamic positioning
FFT	Fast Fourier transform
FOV	Field of view
GNSS	Global navigation satellite system
GPS	Global positioning system
IMU	Inertial measurement unit
INS	Inertial navigation system
JONSWAP	Joint North Sea Wave Project
KM	Kongsberg Maritime
KPIs	Key performance indicators
LF	Low frequency
MC-Lab	Marine cybernetics teaching laboratory
MIMO	Multi-input-multi-output
MRU	Motion reference unit
NED	North-east-down reference frame
NLO	Nonlinear observer
NTNU	Norwegian University of Science and Technology
PMS	Power management system
QTF	Quadratic transfer function
QTM	Qualisys track manager system
RAO	Response amplitude operator
ROS	Robot Operating System
SSH	Secure shell
WF	Wave-frequency

Definitions

η	NED frame position
ν	Velocity vector in body-fixed reference frame
ψ	Heading angle of vessel's x-axis relative to North
τ	Forces and moments in body reference frame
b	Bias due to unmodelled dynamics and slowly varying loads
R	Rotation matrix for Euler angle transformation
H_s	Significant wave height
T_p	Peak wave period
ω_p	Peak wave frequency
β	Wave propagation direction in body-frame
ζ	Wave elevation
g	Gravitational acceleration

Chapter 1

Introduction

1.1 Motivation

For dynamic positioning (DP) operations in ocean waves, the DP control system must compensate the hydrodynamic wave-drift loads. This is conventionally done by feedback control, where slowly-varying second order wave loads are compensated through the integral action of the DP feedback control law. Typically, these feedback mechanisms are subject to changes caused by low-frequency (and possibly mid-frequency) contributions, which are forcing an offset in DP stationkeeping accuracy. In addition, feedback mechanisms requires such offsets to be induced before counteractions can be carried out. This delay the process of counteractions, and decreases the system's capability of stationkeeping accuracy, making it less effective against slowly-varying loads.

Conventional feedback control methods have been proved to be stable and robust in a large range of sea states, and is therefore the state-of-the-art method for wave load compensation. However, there exists methods more effective compensation in other applications; for instance, feedforward mechanisms for wind load compensation. Other strategies may include mathematical models describing the oncoming disturbance, using this in either adaptive control or feedforward mechanisms.

If better strategies for compensating second order wave loads more efficiently can be achieved, it could lead to larger weather windows in DP operations; and consequently, savings in terms of costs and emissions would be significant.

1.2 Objectives

This master thesis includes several objectives, where the first is to gain relevant knowledge and background theory within the fields of hydrodynamic wave theory, methods for estimation of sea state parameters, instruments needed for sea state estimation, and DP control systems in general. Gaining relevant information about the C/S Arctic Drillship (CSAD) and the Marine Cybernetics Laboratory (MC-Lab) was also part of the background study. This is presented in Chapter 2, where some parts were done in the preproject study by the author in Brørby (2021).

The second objective is to develop and implement a high-fidelity simulator in six degrees of freedom, providing relevant sensor measurements, and realistic wave loads for a DP control system to compensate for. The simulator is based on the CSAD model and implemented with its parameters prepared by Bjørnø (2016).

The third objective is to develop and possibly implement different strategies for wave load compensation; in particular, second order wave loads. This includes a DP-observer estimate as feedforward compensation, direct integral action in DP PID control, acceleration feedforward compensation, adaptive control using the internal model principle, and a spectrum-based method. Both the second and third objective are presented in Chapter 4.

A fourth objective is to carry out a performance analysis of the designed control strategies from the previous objective. The analysis is based on simulations done with the high-fidelity simulator. Comparisons and discussions are made in order to investigate whether the proposed strategies can challenge state-of-the-art DP control systems. This is presented in Chapter 5.

1.3 Scope and Delimitations

The design presented in this thesis is based on a case study on CSAD, which is the largest model in the MC-Lab fleet at the moment. It is in a relatively good condition, and is well suited for dynamic positioning.

Based on simulations, the most promising strategies were supposed to be tested in a physical case study on CSAD in MC-Lab. Due to problems connecting to the vessel's actuators, this was impracticable. Hence, the thesis is discussing and concluding based on results from simulations only.

Due to time-consuming work, the implemented DP controllers are only properly tuned in surge direction, hence results and analysis presented in this master thesis is only considering one direction. Consequently, waves propagating along the vessel's surge axis is the only wave-direction that is considered.

The scope of the thesis is about compensating wave loads; therefore, disturbances due to wind and current is not considered.

1.4 Contributions

The contributions of this master thesis are focused on methods for wave load compensation in DP control systems. Extensive work have been done, and we summarize:

- A high-fidelity simulator in six degrees of freedom is implemented, including modules for sensor measurements and wave loads. All implementations are done by the author, while parameters and data used in the implementations are inherited from earlier work in Bjørnø (2016). Frameworks like the Robot Operating System, numpy, etc. are assumed to be fundamental for the implementations, and the author is of course not taking credits for these.
- Five control methods are implemented, including two self designed methods; that is, an adaptive control law, and a wave spectrum-based method. The latter was first proposed by the author in the project thesis (Brørby, 2021), and is improved here. A third method including acceleration feedforward is earlier presented by Kjerstad and Skjetne (2016), but whether the method has been applied for suppressing slowly-varying loads in earlier work, is unknown to the author.
- Experimental verification, performance analysis and comparisons of the control methods are done, based on simulations from the high-fidelity simulator.

Chapter 2

Background and Literature Review

This chapter presents relevant and necessary background theory, to make a foundation for understanding the work presented in the following chapters. A literature review on relevant studies and work is also presented. Parts of this chapter were done in the preproject in Brørby (2021), and are here reproduced and extended for this master thesis.

2.1 Wave Models and Loads

A surface vessel operating at sea will encounter different sea states that will induce wave loads, affecting the vessel's motions. This section encompasses how waves can be modelled, and how a surface vessel is affected by the wave induced loads. The theory in this section is mainly taken from Faltinsen (1999) and OrcaFlex (2021), with support from some other references.

2.1.1 Wave Models

Sea states are often divided into two categories: short crested and long-crested waves. long-crested waves are defined as waves that propagates from one direction, while short crested waves are a sum of long-crested wave components that propagates from multiple directions. long-crested sea states can either be regular or irregular. The natural sea state in oceans is irregular, but it will often be convenient to apply regular wave theory before examining irregular sea states. Irregular waves are more complicated in many ways, and the hydrodynamic effects that follows are less explored and difficult to describe with mathematical models.

Equation (2.1a) shows how irregular long-crested waves can be modelled as a sum of N different regular waves, in the time domain. ζ_{aj} is the wave amplitude, ω_j is the wave frequency, k_j is the wave number defined by $\omega_j^2 = gk_j$, according to the dispersion relation, and ε is the phase angle between 0 and 2π. The same sea state can also be modelled based on a wave spectrum. Given the energy of a wave component in (2.2), we can rewrite the model as in (2.1b). Here, $S(\omega_j)$ is the wave spectrum as a function of frequency, and $\Delta\omega$ is the constant difference between successive frequencies.

$$\zeta(x,t) = \sum_{j=1}^{N} \zeta_{aj} sin(\omega_j t - k_j x + \varepsilon_j) \tag{2.1a}$$

$$= \sum_{j=1}^{N} \sqrt{2S(\omega_j)\Delta\omega} sin(\omega_j t - k_j x + \varepsilon_j) \tag{2.1b}$$

$$\frac{1}{2}\zeta_{aj}^2 = S(\omega_j)\Delta\omega \tag{2.2}$$

Figure 2.1 illustrates the connection between the time domain and the frequency domain. It shows how different frequencies represented by a spectrum adds up, giving a wave elevation in the time domain. The area under the graph of $S(\omega)$ for a given frequency interval, express the total energy for the corresponding wave component.

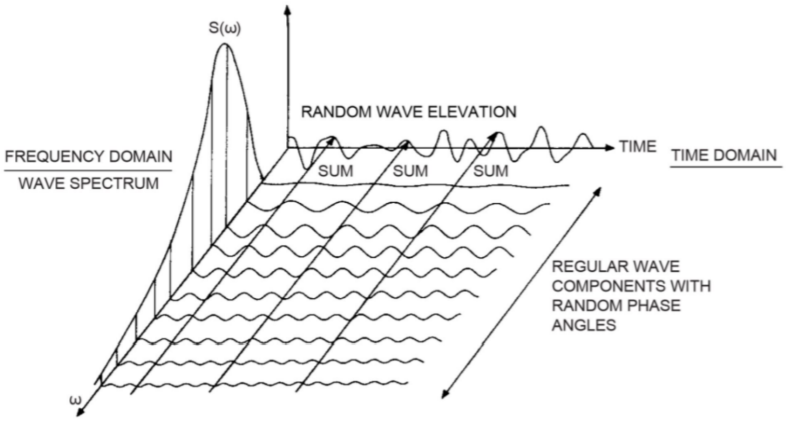

Figure 2.1: Connection between representation of time domain and frequency domain of long-crested waves. Courtesy of (Faltinsen, 1999, chap. 2).

Significant wave height H_s and peak frequency ω_p can be provided by a spectrum, like the standardized Joint North Sea Wave Project (JONSWAP) spectrum Figure 2.2. That is obtained from a Rayleigh distribution of wave components (Faltinsen, 1999, chap. 2). The γ parameter determines how sharp the peak shape is. A value of $\gamma = 3.3$ was determined by Hasselmann et al. (1973) from data collected in the North Sea, and therefore often used when modelling sea states. This parameter is also what makes the JONSWAP spectrum different from the Pierson-Moskowitz spectrum. (2.3) describes the JONSWAP spectrum, where α defines the spectrum shape in the high frequency range, and the variance is defined by (2.4).

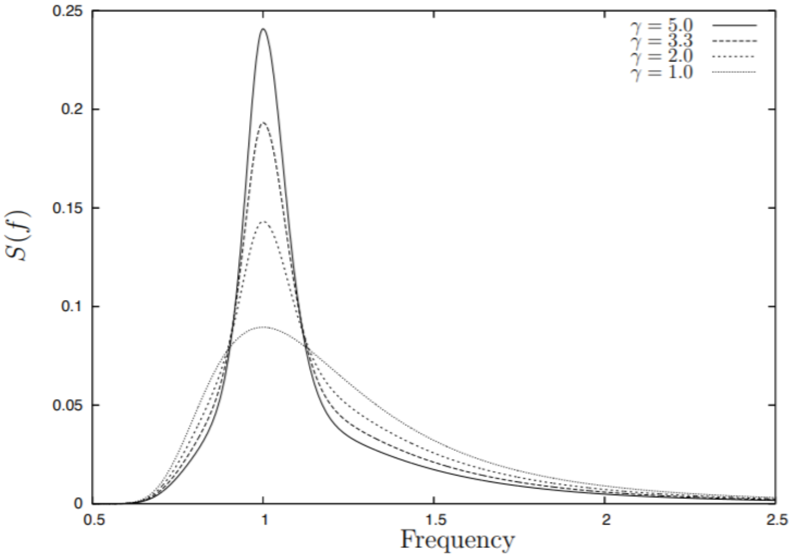

Figure 2.2: JONSWAP spectrum with different values for γ. Courtesy of Shiach (2008).

$$S(\omega) = \alpha \frac{g^2}{\omega^5} \exp\left[-\frac{5}{4}\left(\frac{\omega_p}{\omega}\right)^4\right] \gamma^{\exp\left[-\frac{1}{2}\left(\frac{\omega-\omega_p}{\sigma\omega_p}\right)^2\right]} \tag{2.3}$$

$$\sigma = \begin{cases} \sigma_a & \text{for } \omega \leq \omega_p \\ \sigma_b & \text{for } \omega > \omega_p \end{cases} \tag{2.4}$$

2.1.2 Wave Loads

Second order wave loads are smaller than first order wave loads, but second order loads are proportional to the square of the wave amplitude. This implies that second order wave loads are very important for large sea states (Sørensen, 2011).

Wave loads acting on a vessel can be expressed as a sum of first order, second order and higher order terms. The first order terms are often called wave-frequency (WF) loads. The induced motion from WF loads are observed as an oscillatory motion with a zero mean. These are motions that are typically filtered in a dynamic positioning system. Therefore, first order terms are not considered in detail in this thesis. The second-order terms are called wave-drift forces, and are observed as slowly-varying components that have a non-zero mean (Fossen, 2021, chap. 10). An illustration of this is presented in Figure 2.3. Higher order effects are outside the scope for this thesis and will not be further discussed.

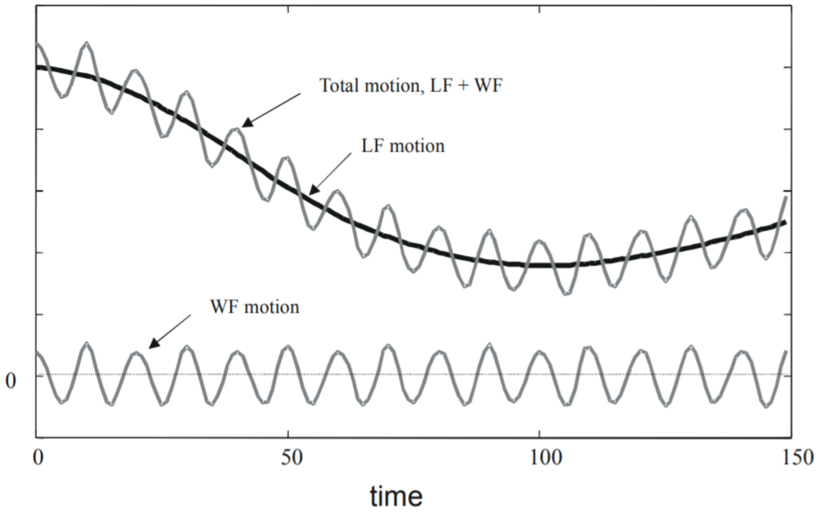

Figure 2.3: Superposition of wave frequency and wave-drift. Courtesy of Torsetnes et al. (2005).

Consider first a surface vessel in a regular sea state. Even though regular waves form a sinusoidal propagation, it is not only oscillatory WF motions which are observed as vessel motions. Wave-drift motions are present as well. A surface vessel in regular waves will experience vertical body motions. If there exists relative vertical motions between the wave surface and the vessel, this will lead to some of the body being part-time out of water and part-time in water. This causes a non-zero pressure that will induce a non-zero mean load (Faltinsen, 1999, chap. 5). Therefore, a non-zero mean load is present whenever the wet surface is varying along the vessel's hull; hence, both roll, pitch, and heave motions will induce such loads.

Now consider a regular sea state where the incoming wave's length is much longer than the characteristic length of the vessel. Assume that the relative vertical motion is zero and the wet surface can be considered constant. Then the vertical motion can no longer contribute to wave-drift motions, but still wave-drift motions are observed. Long waves tend to have higher amplitude than shorter waves. Since second order effects are proportional to the square of wave amplitude (Faltinsen, 1999, chap. 5), there will be a significant contribution to wave-drift loads in long waves. In addition, viscous effects may dominate for long waves since particle velocity for long waves are large compared to particle acceleration. That is, viscous terms are proportional to the square of particle velocity (Faltinsen, 1999, chap. 5).

With that being said, linear wave theory applies only to small waves, since kinematics above the mean surface level is not encountered for. Therefore, linear theory will not be able to estimate the velocity potential above mean water level. Linear wave theory implies equal absolute value of velocity at wave crests and trough (with opposite directions), but in reality the crest velocity is higher. In addition, larger waves will in reality not have a sinusoidal form, but a more narrow form at the wave crest. Therefore, the theory needs to be stretched to cover these velocities. There are several approaches that either will overestimate or underestimate the actual velocity potential (OrcaFlex). DNV have published a standard DNVGL-RP-E306 where a recommended practice for these estimates are stated (DNV, 2010).

Now consider an irregular sea state. In second order wave loads, there are pairs of wave elements that contribute. Let the wave element pair have frequencies ω_1 and ω_2. The contribution of these pairs are divided in two types: sum-frequency loads and difference-frequency loads. The sum-frequency loads have a frequency equal to the sum of the wave component's frequencies ($\omega_1 + \omega_2$). Therefore, the sum-frequency can be significantly high, and potentially much higher than the wave frequency itself (OrcaFlex, 2021). This is an important contribution for systems that has high natural frequency properties, such as tension-leg platforms, due to high stiffness in the tension-legs (Xie et al., 2020). This is not relevant for the natural frequencies in surge, sway, and yaw in a DP system; thus, the sum frequencies have no physical meaning for this purpose.

Difference-frequency loads have frequency equal to the difference of the wave component's frequency ($\omega_1 - \omega_2$). If $\omega_1 = \omega_2$ the difference frequency becomes zero, which gives a constant contribution. Adding up all the constant contributions, constitute the mean-drift load. The mean-drift load induces a constant offset of a DP vessel. If the pair frequencies are almost equal, a low frequency load is exited, which is observed as a slowly-varying wave-drift load. Finally, $\omega_1 \ll \omega_2$ represents a high frequency contribution, but these are in general negligible (OrcaFlex, 2021). Consequently, the second order wave loads are only considered as a sum of a mean wave-drift component and a slowly-varying component for the rest of the thesis.

Second order wave loads can be expressed by second order transfer functions, which can be considered as matrices dependent of wave frequencies and independent of wave amplitudes. These functions are also known as quadratic transfer functions (QTF). Off-diagonal terms in the QTF represent the difference-frequencies $\omega_1 - \omega_2$ and $\omega_2 - \omega_1$. The diagonal elements represent the frequency pairs, where $\omega_1 = \omega_2$ i.e., the constant contributions to second order loads. This is why the mean wave-drift load in direction i can be expressed by (2.5), where T is the diagonal of the QTF, and A_j is the amplitude of the j-th wave element (Faltinsen, 1999, chap. 5).

$$\bar{F_i} = \sum_{j=1}^{N} A_j^2 T(\omega_j) \quad ; \quad i = \{1, ..., 6\} \tag{2.5}$$

Slow-drift excitation loads can be written as a large double sum which is computational tiring (Faltinsen, 1999, chap. 5), but an approximation of the QTF constitute (2.6), which is known as the Newman approximation.

$$F_i^{SV} = 2\left(\sum_{j=1}^{N} A_j T^{\frac{1}{2}}(\omega_j) cos(\omega_j t + \varepsilon_j) \right)^2 \tag{2.6}$$

If (2.6) was written out, one could see that the load from each wave component in (2.6) will vary over time with $cos(\omega_j t + \varepsilon)^2$. This can be rewritten as $\frac{1}{2}(cos(2\omega_j t + 2\varepsilon) + 1)$. The constant term represents the mean-drift, and the cosine term represent the non-physical sum-frequencies. This means that the Newman approximation includes effects that have nothing to do with slowly-varying loads (Faltinsen, 1999, chap. 5).

Mean-drift load is a constant force contribution in higher order loads when the vessel has obtained a stationary response in a stationary sea state with infinite duration. What does this mean? In a regular sea state, it is intuitive to understand that a sea state is stationary when sinusoidal motions are obtained. An irregular sea state is stationary when collected data are sufficient to describe the sea state. By experience, it has been seen that 20 minutes is typically long enough to express the statistical properties of a sea state, and short enough for the conditions to be unchanged (Larsen et al., 2019). Therefore, it is also common to define the duration of a sea state to be 20 minutes.

2.2 Sea State Estimation

Sea state estimates can be provided from different online and offline methods. The topic of sea state estimation have been widely explored in the last 15-20 years (Nielsen, 2017). This section encompasses a literature review on sea state estimation. Wave measurements that are of interest for this thesis must be useful for wave load estimation in real-time, and possibly for prediction. Therefore, online methods are mostly considered.

2.2.1 Online Methods

Most model-based methods are based on mathematically relating vessel motions to the sea state. This is known as the wave buoy analogy (Nielsen, 2017). Most commonly, the mathematical model that is in use is the RAO operator, which is an a priori known transfer function. Nielsen (2017) assumes perfect knowledge of this transfer function from several ships with different RAOs. An individual sea state estimate is then calculated for each ship. The final estimate is then obtained by weighting the individual estimates due to different RAOs. The sea state direction is accordingly detected by comparing predefined wave spectrum candidates. This method is offline in terms of the predefined information about the transfer functions. The same method for detecting wave direction was used in Brodtkorb et al. (2018a), together with the spectral calculation method from Brodtkorb et al. (2018b). The provided algorithm resulted in a computationally efficient online method. While several studies tend to show good performance using the wave buoy analogy, Nielsen (2017) states that there are limitations related to the theory as a ship acts like a lowpass filter; thus, vessel motions can not reflect the whole frequency domain. However, this might not be an issue if the estimates only is needed for use by the vessel itself (Nielsen, 2017).

Many published studies on sea state estimation presents online methods. However, most published methods can at best be considered as online methods, since it takes time to perform the optimizations and calculations. Ren et al. (2021) have proposed a near real-time version of the wave buoy analogy, where an L1 optimization algorithm gives a more robust optimization. Desmars (2020) predicts the wave field around a marine structure in real-time with measurements from an optical sensor. The prediction is achieved by fitting known wave models to the observed measurements.

Use of radar measurements is a field of increasing interest within wave parameter estimation (Giron-Sierra, 2010). Li et al. (2020) uses a high-frequency surface wave radar to collect dynamic parameters of the ocean surface. Halstensen et al. (2020) have developed a wave reconstruction and prediction system called RIMARC for forecasting waves in real time, for the next minutes. This is applied for prediction of vessel motions.

2.2.2 Offline Methods

Fast Fourier transform (FFT) is a common way to express a function as a sum of periodic data components (Numpy FFT [software]). This can be utilized to express a short term prediction of the wave behavior. In the wave energy industry, a number of studies investigates the use of FFT in short term prediction of wave behavior (Halliday et al., 2011; Elwood et al., 2010; Conde and Gato, 2008). However, FFT requires typically 30 minutes with collected data to give reasonable results, which is not suited for real-time estimations (Fossen, 2021, chap. 13).

2.3 Sensors and Instruments

In order to make a sea state estimate, measurements have to be provided in some way or another. There are several relevant sensors and instruments for this purpose. This section presents some of them.

2.3.1 Radar

Marine radars are usually x-band radars, used for monitoring surrounding ship traffic and for supporting the navigation systems when the view is restricted. However, the range of use is increasing, and wave parameters can also be stated by different tuning and configuration (Bell, 1999; Giron-Sierra, 2010). There are also S-band radars, but X-band radars are more suitable for detecting wave parameters, due to the higher resolution (Dankert and Rosenthal, 2004; Dankert et al., 2005).

Halstensen et al. (2020) have developed RIMARC, which is a system for estimating the next minutes wave parameters and vessel motion with use of an X-band radar. The research showed promising results, which has resulted in the new project RAIDER.

Use of wave radars tends to involve an issue with back scattered echo from the ocean surface and radio frequency interference (Li et al., 2020).

A radar is a rotating antenna transmitting microwaves throughout the surroundings and detecting the reflected waves. The reflection makes an image of the surroundings. As the radar is a physical rotating component, the update frequency is relatively slow. This will affect how the radar detects wave parameters, which introduces the problem of shadowing. Shadowing is when the radar is unable to detect the water surface due to higher waves covering the field of view (FOV). This can, for instance, happen at the time when the vessel is at the bottom of a wave. Therefore, it is important that the location of the radar is as high as possible. Retrieving the significant wave height from an x-band radar is therefore a challenge, but there are methods for dealing with these issues (Wei et al., 2017).

2.3.2 Pressure Measuring

The direct pressure method presented in Faltinsen (1999, chap. 5) is applied in Quadvlieg et al. (2011), where an improved DP system was developed. Pressure sensors were mounted below the water line, distributed along the hull. Quadvlieg et al. (2011) states that the challenges with these sensors are to select a sensor where the accuracy is high enough to detect the pressure variations of interest. Therefore, these sensors are more suited for full scale experiments than for models.

2.3.3 Inertial Measurement Unit

An inertial measurement unit (IMU) is a composition of two sensors: three axis-accelerometer, and attitude rate sensor (ARS) or gyroscopes. This provides a measurement of 6 DOFs. IMUs are commonly used in an inertial navigation system (INS) (Fossen, 2021, chap. 14). Combining a global navigation satellite system (GNSS) with the INS system provides the vessel position, velocity, attitude, and possibly the accelerations (Bryne, 2017). In Kjerstad and Skjetne (2016), a full state estimate of the acceleration vector in 6 DOFs was obtained and further used to compensate for rapidly changing ice loads, where the acceleration was used as a feedforward term in the control law. The reconstructed acceleration vector was developed by utilizing the distribution of four IMUs located such that at least one of them was in a different plane than the other. Fu et al. (2011) used the same configuration to estimate the directional wave spectra by utilizing the phase difference in the distributed IMUs.

2.3.4 Wave Buoy

Wave buoys are a common way of measuring wave parameters, including wave direction. They are often used for local wave forecasting as they have a fixed, permanent location. The measurements are usually provided by IMUs, estimating the wave parameters. Using these measurements for a DP operation in real-time would require a connection to the operational vessel. However, marine operations are often located where such local forecasts are unavailable (Nielsen, 2008), and installing wave buoys for short time operations would be too expensive. Hence, wave buoys are not well suited for providing measurements of onsite wave parameters. However, there are examples where the wave buoy analogy is applied to a ship's motions (Nielsen, 2008).

2.3.5 Wave Height Sensors

Wave height sensors or wave poles uses two parallel rods, which acts as an electric conduction meter. Quadvlieg et al. (2011) propose that such sensors can be mounted on a ship to measure relative wave height with respect to the water line in calm water. For model experiments in a water tank, multiple wave poles can instead be placed throughout the tank. This is a well-used method in experimental setups for measuring wave height. Although, for a full scale real-life scenario, use of these sensors can be problematic since salt water will cause corrosion and large environmental forces may impact the device.

2.4 DP Control Systems

A DP vessel is defined as a unit or a vessel which automatically maintains its position (fixed location or predetermined track) exclusively by means of thruster force (MSC/CIRC. 645). DP-vessels have implemented a DP-system that consists of three sub systems (power system, thruster system, and DP control system), where the DP control system is the subsystem that is responsible for controlling the position of the vessel (MSC/CIRC. 645).

Most DP control system are based on the same principal design methods, as illustrated in Figure 2.4. Details on each module are outlined in Sørensen (2011).

The control objective for a DP control system is the same either if the DP-vessel are following a predetermined track or a fixed location. That is, the vessel states should converge towards a reference signal. Mathematically, we can describe this by (2.7), where $\tilde{\eta}$ and $\tilde{\nu}$ are defined as the error between the respective state, and its desired state.

$$\tilde{\eta}(t) := \eta(t) - \eta_d \longrightarrow 0 \quad \text{as} \quad t \longrightarrow 0 \tag{2.7a}$$

$$\tilde{\nu}(t) := \nu(t) - \nu_d \longrightarrow 0 \quad \text{as} \quad t \longrightarrow 0 \tag{2.7b}$$

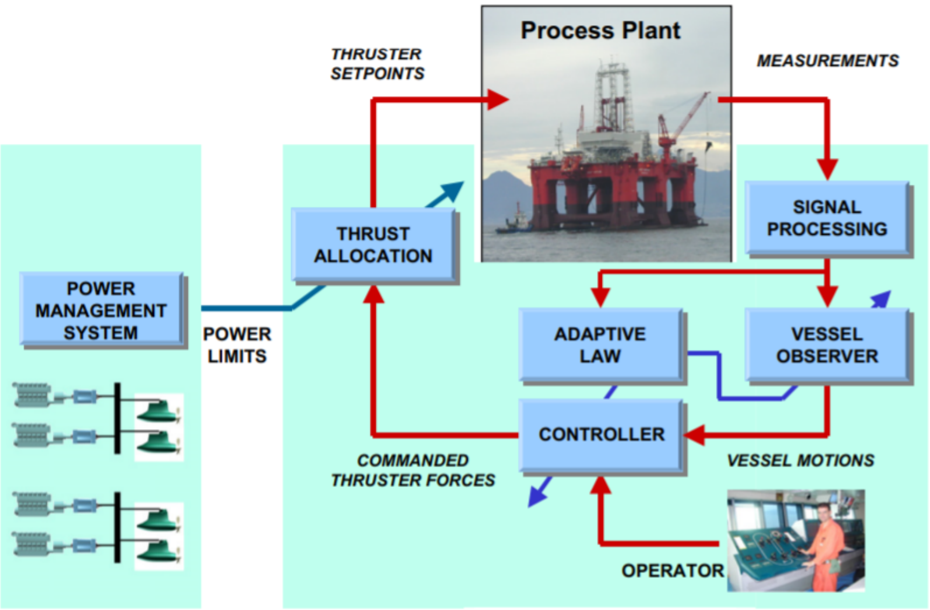

Figure 2.4: DP control system. Courtesy of Sørensen (2011).

A typical topology for a DP control system can be seen in Figure 2.5. It shows how the DP controller (named DPC 21) interfaces the wind sensors, motion reference units (MRU), heading reference (gyro), human operator interface, and position reference systems (DGPS and HiPAP) with the thruster setpoints. For more details, see Breivik et al. (2015).

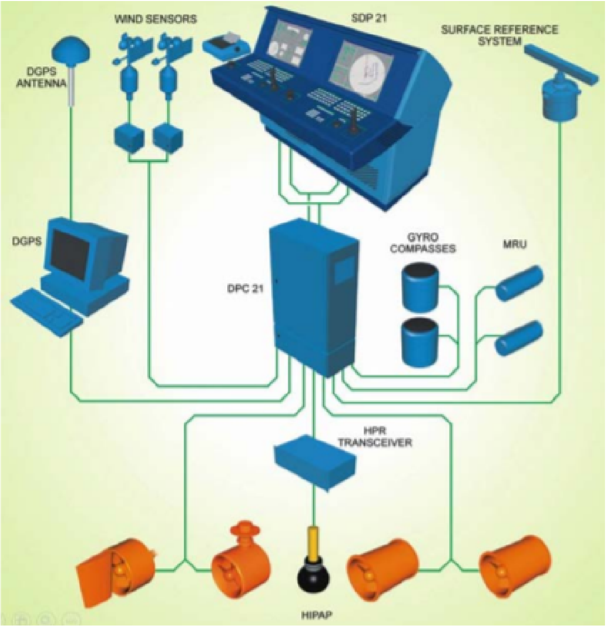

Figure 2.5: Typical topology for a DP control system. Courtesy of Kongsberg Maritime.

2.4.1 Modelling of DP Vessels

A mathematical model of a vessel in DP can often be divided in two categories: a simplified control design model (CDM), and a high-fidelity simulation (verification) model. The former describes only the essential dynamics for the control design. The other describes more accurately the real dynamics of the plant; that is, a more complex model that describes the actual process. This also includes process disturbances, sensor models, actuator models, power plant, etc.

When dealing with the control system for marine surface vessels in DP operations, only 3 degrees of freedom (DOF) are considered; that is, surge, sway, and yaw. Then the kinematics are described by (2.8), where $\nu = col(u, v, r)$ is expressed in the body frame and $\eta = col(x, y, \psi)$ is expressed in the North-East-Down frame (NED).

$$\dot{\eta} = R^T(\psi)\nu \quad \text{, where} \quad R(\psi) = \begin{bmatrix} cos(\psi) & -sin(\psi) & 0 \\ sin(\psi) & cos(\psi) & 0 \\ 0 & 0 & 1 \end{bmatrix} \tag{2.8}$$

The low-frequency (LF) dynamics are generally expressed by (2.9)(Fossen, 2002), where $M \in \mathbb{R}^{3\times3}$, the inertia matrix including added mass, is assumed constant. $C_{RB}(\nu) \in \mathbb{R}^{3\times3}$ and $C_A(\nu_r) \in \mathbb{R}^{3\times3}$ are the Coriolis and centripetal matrix of the rigid body and added mass, respectively. $\nu_r := \nu - \nu_c \in \mathbb{R}^3$ is the relative velocity when current is present. $D(\nu_r) \in \mathbb{R}^3$ is the linear and nonlinear damping matrix, $G(\eta) \in \mathbb{R}^3$ is the generalized restoring force vector. Finally, τ_{wind}, τ_{wave2}, τ_{moor}, $\tau_{thr} \in \mathbb{R}^3$ are loads due to wind, second order wave loads, mooring system and thruster system, respectively.

$$\dot{\eta} = R(\psi)\nu \tag{2.9a}$$

$$M\dot{\nu} + C_{RB}(\nu)\nu + C_A(\nu_r)\nu_r + D(\nu_r)\nu_r + G(\eta) = \tau_{wind} + \tau_{wave2} + \tau_{moor} + \tau_{ice} + \tau_{thr} \tag{2.9b}$$

However, in DP it is sufficient to use the simplified dynamics in (2.10) as CDM, as clarified in Sørensen (2011). Here, the mooring and restoring forces are simplified by $G_{mo}R^T(\psi)\eta$. τ_c is the commanded control input vector, and b is the bias vector.

In this model, a lot of simplifications have been done. These simplifications have to be compensated for, since they lead to unmodelled dynamics. The bias represents this, and can be modelled as a Markov process like in (2.10c).

$$\dot{\eta} = R(\psi)\nu \tag{2.10a}$$

$$M\dot{\nu} = -D\nu + R^T(\psi)b - G_{mo}R^T(\psi)\eta + \tau_c \tag{2.10b}$$

$$\dot{b} = -T_b^{-1}b + E_b w_b \tag{2.10c}$$

The bias tends to be significant as it covers both unmodelled dynamics and slowly-varying environmental loads. Therefore, the bias term is sometimes used as a feedforward term in the control law (Sørensen, 2011). If the vessel is exposed to ice loads, these forces should be modelled explicitly, since ice loads are rapidly varying with large magnitudes. Several ice models are presented in Nguyen et al. (2009).

WF induced motions are often modelled as a damped harmonic oscillator, like (2.11), where $\xi \in \mathbb{R}^6$ is the WF induced dynamics. $A_w \in \mathbb{R}^6$, $E_w \in \mathbb{R}^{6\times3}$, and $C_w \in \mathbb{R}^3$ are constant matrices containing information about the sea states. y is the position measurement containing the sum of LF and WF motions, and some measurement noise v_y. As WF loads are oscillating with zero mean, this will cause wear and tear of actuators, and waste fuel if they are compensated for. In addition, these motions may have a frequency higher than the system's bandwidth. Only higher order wave loads should therefore be compensated; that is, the wave-drift loads as described in section 2.1.2. Sørensen (2011) divides these into three contributions; mean, slowly-varying (difference-frequencies) and rapidly varying (sum-frequencies). This coincides with the theory presented in section 2.1.2. For normal DP operations, the rapidly varying can be neglected (Sørensen, 2011). A method for wave filtering is presented in (Fossen, 2021, chap. 13).

$$\dot{\xi} = A_w \xi + E_w \omega_w \tag{2.11a}$$

$$y = \eta + C_w \xi + v_y \tag{2.11b}$$

2.4.2 Feedback Control

DP controllers are often multi-input multi-output (MIMO) PID-controllers. They depend on a feedback signal that is provided by the estimated LF position and velocity. Such control laws can be mathematically described by (2.12), where $\tilde{\eta}$ and $\tilde{\nu}$ depend on feedback from the measured states. K_p, K_d, $K_i \in \mathbb{R}^3$ are positive injection gains for the proportional, derivative, and integral terms, respectively. Under ideal conditions, it would be sufficient with only proportional- and derivative terms, in order to satisfy the control objective. However, integral action is needed to compensate for slowly-varying (and constant) environmental loads (Sørensen, 2018).

$$\tau_c = -K_p R^T(\psi)\tilde{\eta} - K_d \tilde{\nu} - K_i R^T(\psi) \int_0^t \tilde{\eta} dt \tag{2.12}$$

As these types of controllers are model-based, and simplifications limit the model, there will be some modelling errors. This contributes to unmodelled dynamics in the bias term from (2.10c).

These controllers are often tuned in accordance with (Fossen, 2021, chap. 15), which ensures stability and robustness, and therefore makes PID-controllers the state-of-the-art systems in motion control (Wang and Nie, 2012).

Alternatives to integral action are presented in Værnø et al. (2019), where three controllers for bias compensation (including slowly-varying loads and unmodelled dynamics) were compared to the conventional PID-controller. One method was using the bias estimate provided from the DP-observer directly as a feedforward term, together with a PD-control law. This method is used later in this thesis as a baseline for comparisons. The other methods in Værnø et al. (2019) included a wave filtered estimate of the bias, and finally a separate bias observer for a more accurate estimate of the bias. Results showed the latter to be most satisfying.

A downside of using feedback-mechanisms, is that the system will have to perform unnecessary work as the disturbances already have induced a motion before the control law execute counteractions (Kjerstad et al., 2011). This motivates feedforward control.

2.4.3 Feedforward Control

Since the integral action in a conventional PID-controller only covers slowly-varying loads, it is often necessary to add a feedforward term to the control law for counteracting rapidly changing loads.

The most common feedforward in DP-systems is wind feedforward. This requires measurements of wind speed and direction for estimating wind induced loads acting on the vessel. These estimates are then used to counteract the rapidly changing wind loads instantaneous (Sørensen, 2018).

An ideal controller would have the quality of rejecting disturbances entirely, and some feedforward controllers are close to having this ability. However, many feedforward controllers require predefined knowledge of the environmental disturbances, and such models are rarely simple enough to be modelled mathematically.

With that being said, Kjerstad and Skjetne (2016) have applied acceleration measurements in order to counteract ice loads by acceleration feedforward. The results showed good performance even for unmodelled dynamics. Ice loads are typically very large and dominating, as well as being rapidly varying (Nguyen et al., 2009). Kjerstad and Skjetne (2016) presents the use of four IMUs that provides a reconstructed acceleration vector in 6 DOFs. This replaces the integral action and enables almost immediate counteraction against ice loads and unmodelled dynamics.

Traditionally, a DP control system's control objective is to follow a reference signal for position and velocity states, by measuring the corresponding states. Acceleration measurements are typically not being used (Kjerstad and Skjetne, 2016). The reason for this is the problems that come with the use of these measurements. First of all, the measurements do not provide direct measures of the dynamic acceleration of the vessel. The second problem is to remove the gravitational component from the measurement, since this will affect linear acceleration in roll and pitch. The last is that acceleration measurements contains high levels of noise, bias, and nonlinearities. Kjerstad et al. (2011); Kjerstad and Skjetne (2016) addresses these challenges and proposes methods for dealing with them. Note that this constitutes the background for one of the proposed strategies later in this thesis.

2.4.4 Internal Model Principle

As seen in section 2.1.2, slowly-varying disturbances, in terms of second order wave loads, can be described as sums of oscillating components with different frequencies. These oscillating contributions are typically not known, and subject to randomness. However, if the disturbance can be modelled mathematically by an internal model, other strategies for disturbance rejection can be applied. This is known as the internal model principle (Francis and Wonham, 1976). Espíndola-López et al. (2016) have proposed a self-tuning controller utilizing the internal model principle in terms of Fourier series describing disturbances, with the mentioned characteristics. The disturbance is described as a sum of multiple oscillating terms with different frequencies ω_i and magnitudes. The control input was expressed as in (2.13), where a_0, a_n, and b_n are coefficients defining the magnitude of each oscillating element. These magnitudes were tuned by a neural network, learning the disturbance's behavior, and adapting the magnitudes based on state feedback. The results showed some promising indications of reducing the influence of random disturbance, and suppressing errors caused by unmodelled dynamics and deterministic uncertainties (Espíndola-López et al., 2016).

$$u(t) = \frac{a_0}{2} + \sum_{n=1}^{N} a_n cos(\omega_i t) + b_n sin(\omega_i t) \tag{2.13}$$

The reader should be aware that one of the control strategies proposed in this master thesis is motivated by the method in Espíndola-López et al. (2016).

2.5 MC-Lab and C/S Arctic Drillship

C/S Arctic Drillship (CSAD) is a model vessel made by Bjørnø (2016) and is now a part of the fleet in Marine Cybernetics Teaching Laboratory (MC-Lab) at the Norwegian University of Science and Technology (NTNU). This was originally a $1 : 90$ model scale of an arctic drillship, but the full scale was never built. CSAD is the largest model in the MC-Lab fleet as of today, with the dimensions presented in table Table 2.1.

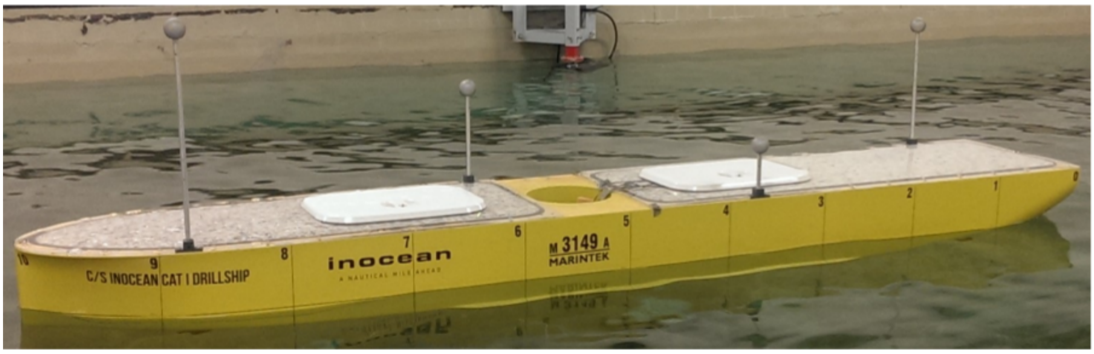

Figure 2.6: CSAD in the MC-Lab. Courtesy of Bjørnø (2016).

The vessel is operated by six azimuth thrusters, and the control system runs on a Raspberry Pi, which is accessed through the local network by secure shell (SSH). Through SSH, the control system can communicate with external systems in the ROS environment. All equipment is powered by six batteries, or optionally land power. Details about the system and mathematical modelling can be read in Bjørnø (2016); Bjørnø et al. (2017).

During the period of the preproject in Brørby (2021), the moon pool was sealed, and four new IMUs were installed, which provide measurements through ROS. In addition, the original CompactRIO-9024 from 2016 have been replaced with a Raspberry Pi in 2021.

Table 2.1: CSAD dimensions. Courtesy of Bjørnø (2016).

Description	Data [m]
Length over all (L)	2.578
Breadth (B)	0.440
Depth (D)	0.211
Design draft (T)	0.133

The MC-Lab is made for testing marine motion control systems, and has multiple instruments, rendering this possible. The laboratory has a water tank with a wave generator for making both regular and irregular sea sates. It consists of a flap that is $6m$ wide, and has the following capacity (MC-Lab, 2021):

- Regular waves: H $<$ 0.25 m, T = 0.3 - 3 s.
- Irregular waves Hs $<$ 0.15 m, T = 0.6 - 1.5 s.
- Available Spectrum: JONSWAP, Pierson-Moskowitz, Bretschneider, ISSC, ITTC.
- Control update rate = 10 Hz.
- Number of wave gauge on paddle = 4

- Stroke length on actuator = 590 mm.
- Speed limit = 1.2 m/s.

The dimensions of the water tank are $L \times B \times D = 40m \times 6.45m \times 1.5m$. This makes the tank suitable for small scale model vessels.

In order to imitate a full scale global navigation satellite system (GNSS), Qualisys is installed. This is a real-time system providing position and attitude measurements in 6 DOFs, which is made available to the control systems through the Robot Operating System (ROS) environment. Qualisys consists of three Oqus cameras and the Qualisys Track Manager System (QTM) (MC-Lab, 2021). For Qualisys to be able to detect a vessel, four reflective spheres are distributed along the deck. Three of these four have to be visible for two Oqus cameras; otherwise no detection can be made.

For more details about the MC-Lab, see MC-Lab (2021); Bjørnø (2016).

Chapter 3

Problem Formulation

This master thesis addresses control systems for wave load compensation in dynamic positioning operations. Marine vessels are subject to various disturbances during such operations, on which wave loads makes a huge contributor. DP control systems must compensate the hydrodynamic wave-drift part of these loads, which are done through integral action in a feedback mechanism. This method of wave-drift compensation is subject to changes caused by low-frequency (and possibly mid-frequency) contributions, which are observed as an offset. Therefore, the research question in this master thesis is about whether there exists better strategies for eliminating such offsets.

The control objective is to control $\eta(t) \rightarrow 0$ and $\nu(t) \rightarrow 0$, while the vessel is exposed to disturbances $d(t)$, in terms of wave loads. These wave loads are assumed to be bounded such that
$max\{\parallel d(t) \parallel, \parallel \dot{d}(t) \parallel\} < \infty$.

Five control methods are designed and discussed. Two of the proposals are feedback mechanisms that are commonly used today. The others are methods which are, to the author's knowledge, not applied to marine DP operations yet. The most promising proposals are implemented and tested. In order to test the methods in realistic conditions, a case study of the model vessel CSAD is considered. The original agenda of the thesis, was to decide on some promising control methods and test them through simulations. After which, the simulation results should have given a qualified indication of what controllers to test further in a physical test case in MC-Lab. Unfortunately, problems with the physical model made it impossible to run physical tests. Thus, only simulations have been made, and further physical test are left for further work.

To fulfill a complete control system, an observer, and a thrust allocation algorithm are required. The thesis is not diving deep into the thrust allocation, apart from where the discussion requires such considerations.

A high-fidelity simulator in 6 degrees of freedom (DOF) is developed. Sensor measurements are simulated and suited to meet the requirements for all control methods presented in this thesis. A realistic environmental load module, containing first order wave loads and second order wave loads, are also implemented. Wind and current loads are not considered.

Finally, a performance analysis of the proposed controller designs are performed. The agenda for the performance analysis, is to find sea states that provoke weaknesses in the conventional DP controllers; and accordingly, investigate the response of the other controllers in the same sea state. All methods are tested on the same groundings, in terms of model parameters and conditions, such that comparisons are made as fairly as possible. The comparisons are based on two key performance indicators (KPIs); that is, positioning performance and thrust effort.

Even though the thesis aims to consider as high-fidelity cases as possible, some simplifications had to be made due to various reasons. These are specified where relevance occur.

Chapter 4

System Design and Implementation

This section describes the design and implementation of all contributions to this master thesis. First, a general overview of the system design is described. Secondly, a brief description of the 6 DOF simulator is given, including sensor simulation and wave load simulation. Then, observer design and thrust allocation is described, followed by the design of five different strategies for wave load compensation in DP-operations. Some of the designs in this chapter are taken from specified references, others are designed by the author. All implementations mentioned in this chapter are done by the author if not otherwise is specified. The source code is attached in the digital appendix.

4.1 Design Overview

The design of the implemented system, as a whole, is made such that the control system can be tested on both a virtual and a physical vessel, in this case the CSAD. The idea was to make a platform that enables switching between simulation and physical tests without rewriting or modifying the source code. Therefore, the simulator had to be able to communicate with the control system in the same way as the physical vessel requires. In theory, the simulation and physical test can be launched simultaneously, but this will probably require the system to run on multiple threads.

The physical vessel uses the Robot Operating System (ROS) as a framework for communication between modules within the system. Hence, the rest of the system design was also implemented within the ROS framework. ROS uses nodes that communicate by publishing and subscribing messages on specified topics. That way, ROS enables full access to all signals for all nodes that subscribes to that specified topic. This is also useful for monitoring signals in real-time, as well as for debugging purposes. Figure 4.1 showing how the system is connecting nodes to each other, where the names on each arrow is the name of the topic, and the direction of the arrow indicates what node that is subscribing to the topic, and where the topic is published from. The circles indicate nodes. Note that Figure 4.1 is only an example. The structure depends on what control strategy that is used.

How the modules are connected is more explainable by considering Figure 4.2, where the environmental load module, marine vessel module, and a control system module are separated. The simulator consists of the two modules; marine vessel module, and environmental load module. The marine vessel module includes a sensor module for representing IMU, GNSS and wave measurements. The light gray field in Figure 4.2 (”6 DOF simulator”) is the part that needs to be exchanged with the physical vessel if physical tests are desired.

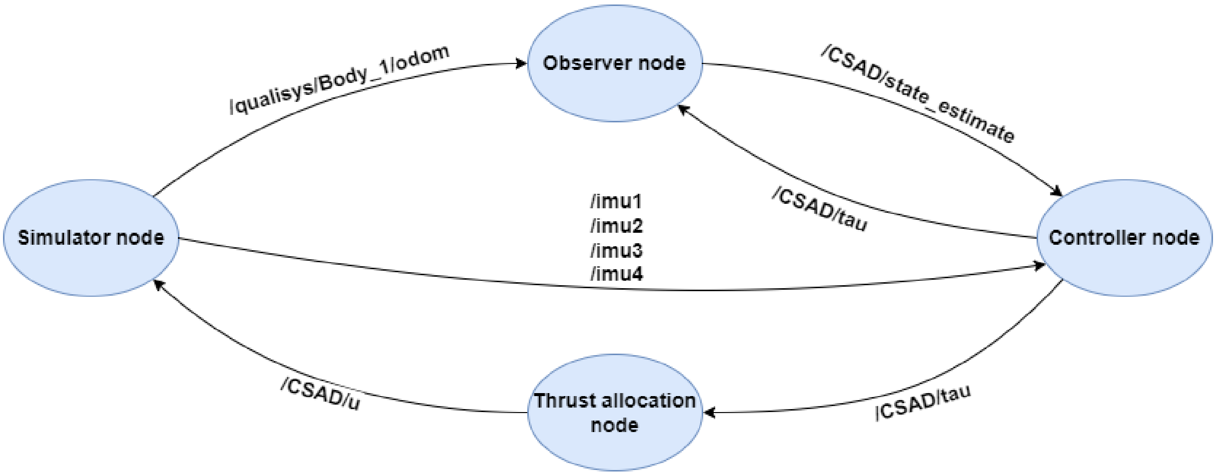

Figure 4.1: Graph describing nodes and the connected topics.

All nodes are running on the same sampling frequency; 50 Hz. This is possible to change, but different frequencies have been tried out. 50 Hz was chosen because of time-consuming calculations within the source code, especially in the environmental load module, and some control methods. Ideally, the sensor module should have been running on higher frequencies than the other nodes. For instance, IMU measurements are typically at 100-200 Hz. As addressed in Brørby (2021); Park et al. (2020), using ROS introduces issues with high communication rates, and is therefore not really suited for real-time control systems (Park et al., 2020). Different frequencies of the nodes individually were tried out, but due to the way the system is designed, significant loss of data occurred. To fix this, a more extensive change in the implementations have to be done. Therefore, this is not prioritized in this thesis.

In Bjørnø (2016), the system parameters for the 6DOF vessel model were calculated using ShipX Vessel Responses Plug-In (VERES) (Sintef, 2022). The data was further converted from ShipX files to MATLAB by using MSS Toolbox (Fossen and Perez, 2022). A complete overview of available parameters are listed in Fossen and Perez (2022), and the relevant parameters for the simulator are listed in Table 4.1. In Bjørnø (2016), a simulator was implemented in MATLAB and Simulink. And could have been used in this thesis. However, since the physical vessel's control system was running on Python, it was decided that a new simulator in Python was needed, for the seamless switch between simulations and physical tests.

Table 4.1: Extract from available system values for 6DOF vessel module.

Parameter	Structure	Content
MRB	6x6 double	Rigid body system inertia matrix
A	6x6x47 double	Added mass 6DOF for 47 frequencies
B	6x6x47 double	Potential + viscous damping 6DOF for 47 frequencies
C	6x6x47 double	Restoring forces 6DOF for 47 frequencies
freqs	1x47 double	Frequencies defined for system parameters
headings	1x36 double	Headings defined for the system parameters
velocities	0	Valid forward speeds for systems parameters
forceRAO	1x1 struct	Transfer function from wave amplitude to first order wave loads, containing amplitude, phase and frequencies
motionRAO	1x1 struct	Transfer function from wave amplitude to first order wave induced motions, containing amplitude, phase and frequencies
driftfrc	1x1 struct	Diagonal of QTF, containing amplitude and frequencies

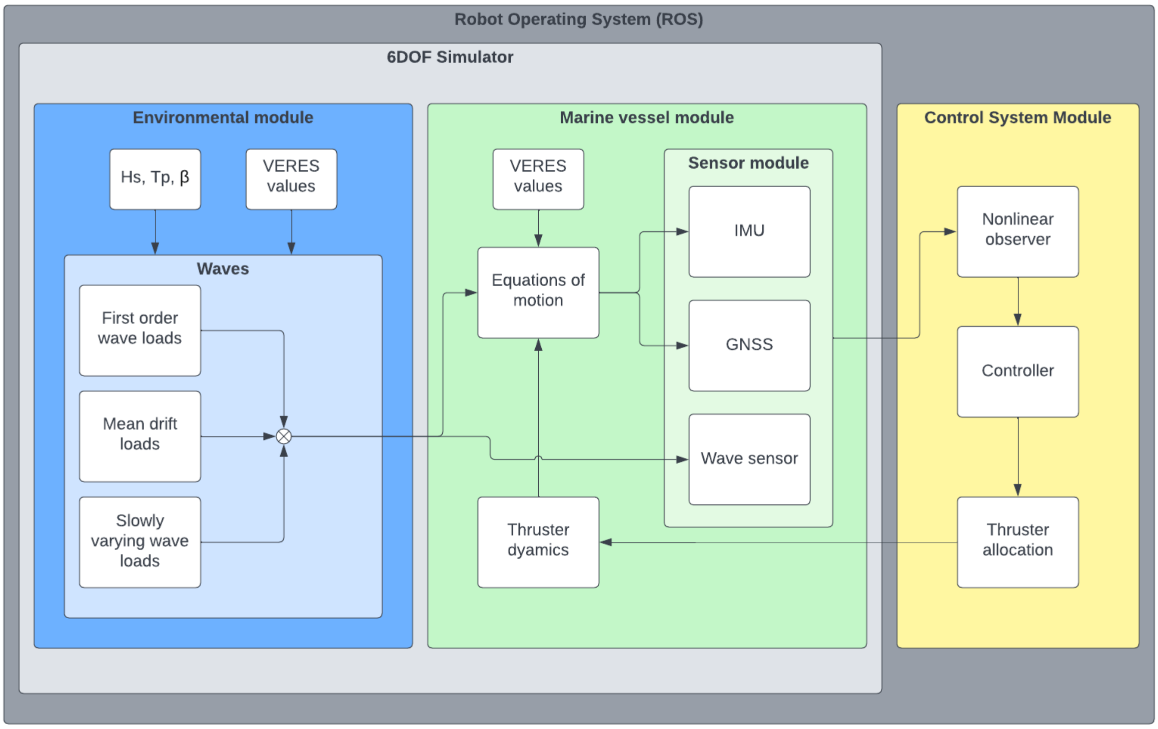

Figure 4.2: Block diagram of the implemented system, showing how the submodules are connected.

4.2 Simulator Design

This section describes how the 6 DOF high-fidelity simulator is implemented. A guide on how to run the simulator is attached in Appendix A.

4.2.1 Marine Vessel Module

A 6 DOF high-fidelity simulator has been implemented. The simulator is based on the VERES database that were calculated in Bjørnø (2016). The values are used to express the vessel's motions in (4.1), where $\eta = col(x, y, z, \phi, \theta, \psi) \in \mathbb{R}^6$ is the pose in the NED frame, and $\nu = col(u, v, w, p, q, r) \in \mathbb{R}^6$ is the velocities in the body-fixed frame. $\tau_{wave} \in \mathbb{R}^6$ which is the wave induced loads expressed in the body-fixed frame. $b \in \mathbb{R}^6$ is the bias in NED frame describing modelling errors and slowly-varying disturbances (except the slowly-varying wave loads), described as a Markov process, where T_b is a time constant, and w_b is some white noise. The mass matrix $M \in \mathbb{R}^{6\times6}$, the damping matrix $D \in \mathbb{R}^{6\times6}$, and a matrix holding the restoring forces coefficients $C \in \mathbb{R}^{6\times6}$, are all given by the VERES database. The transformation matrix $J(\eta) \in \mathbb{R}^{6\times6}$ is defined in (4.2), where c and s is short for $cos(\cdot)$ and $sin(\cdot)$, respectively.

$$\dot{\eta} = J(\eta)\nu \tag{4.1a}$$

$$\dot{b} = -T_b^{-1}b(t) + E_b w_b \tag{4.1b}$$

$$M\dot{\nu} = -D\nu - CJ(\eta)^T\eta + J(\eta)^T b(t) + \tau_{wave} + \tau_{thr} \tag{4.1c}$$

$$J(\eta) = \begin{bmatrix} R(\eta) & 0_{3\times 3} \\ 0_{3\times 3} & T(\eta) \end{bmatrix} \tag{4.2a}$$

$$T(\eta) = \begin{bmatrix} 1 & s\phi t\theta & c\phi t\phi \\ 0 & c\phi & -s\phi \\ 0 & s\phi/c\theta & c\phi/c\theta \end{bmatrix} \tag{4.2b}$$

$$R(\eta) = \begin{bmatrix} c\psi c\theta & -s\psi c\phi + c\psi s\theta s\phi & s\psi s\phi + c\psi c\phi s\theta \\ s\psi c\theta & c\psi c\phi + s\phi s\theta s\psi & -c\psi s\phi + s\theta s\psi c\phi \\ -s\theta & c\theta s\phi & c\theta c\phi \end{bmatrix} \tag{4.2c}$$

The matrices M, D, and C are defined for 47 different wave frequency in the range of $[0.2094, 9.364]$. This allows the vessel module to be dependent on the relevant sea state. Note that the matrices are defined for zero speed only. Hence, the matrices define a zero-speed model.

Since the VERES data only is defined for some specific frequencies and headings, it was necessary to find the values that corresponds to these valid frequencies. This can either be done by finding the closest value or performing an interpolation between two known values. The latter will be more accurate, but increase the number of frequency components that are considered. However, the VERES calculations are not accurate, and since the system already holds a lot of errors in terms of modelling and simplifications, it was concluded that the first option was sufficient.

Thruster Dynamics

The capacity of the real-world actuators are limited, consequently the maneuvering properties are limited. Therefore, in order to obtain a high-fidelity behavior of the simulated vessel, some limitations on the control inputs needs to be applied. The objective of the thruster dynamics is to saturate and limit the rate of actuator set points coming from the thrust-allocation, and then convert the actuator outputs into generalized forces in the body frame. Finally, generalized loads can be applied in the equation of motion (4.1c). Table 4.2 shows an overview of the actuator restrictions.

Table 4.2: Actuator properties for CSAD. Courtesy of Bjørnø et al. (2017)

Parameter	Value
Propeller diameter	0.03 [m]
Max torque	0.0015 [Nm]
Max thrust	1.5 [N]
Max shaft speed	94.9 [RPS]
Steering speed	114 [deg/s]

CSAD is equipped with a total of six actuators. All are azimuth thrusters, and the configuration can be seen in Figure 4.3. For azimuth thrusters, actuator set points include both the angle α_i and thrust u_i. In fact, it is the shaft speed n_i that controls the thrust u_i, and therefore n_i is the parameter that needs to be limited.

The thrust force T_i produced by each actuator is calculated by (4.3) (Fossen, 2021, chap. 9), where ρ is the water density, D is the diameter of the propeller, K_{iT} is a thrust coefficient. u_{iy} and u_{ix} are the decomposed thrust set points in the body frame. α_i is defined as zero when the force vector is pointing in the vessel's surge direction, and positive clockwise.

$$T_i = \rho D^4 K_{iT} \mid n_i \mid n_i \tag{4.3a}$$

$$n_i = sgn(u_i)\sqrt{\mid u_i \mid} \tag{4.3b}$$

$$u_i = \sqrt{u_{ix}^2 + u_{ix}^2} \tag{4.3c}$$

$$\alpha_i = \arctan(\frac{u_{iy}}{u_{ix}}) \tag{4.3d}$$

For a surface vessel with azimuth thrusters, (4.4) can be used to convert the actuator thrust loads into generalized loads in the body frame (Fossen, 2021, chap. 9). Here, $\tau = col(X, Y, N)$ is a vector holding forces and moments in the horizontal plane, and $l = col(l_x, l_y)$ is the position vector of the azimuth's location expressed in body frame.

$$\tau_i = \begin{bmatrix} T_i cos(\alpha) \\ T_i sin(\alpha_i) \\ l_{ix} T_i sin(\alpha_i) - l_{iy} T_i cos(\alpha_i) \end{bmatrix} \tag{4.4}$$

Figure 4.3 shows some red zones for which the direction of the jet from one actuator will affect the flow of water into another actuator. The turbulent flows that occur, in this case, will affect the thrust significantly. However, these turbulent effects are not considered in the simulations, because of the complexity of such hydrodynamic simulations.

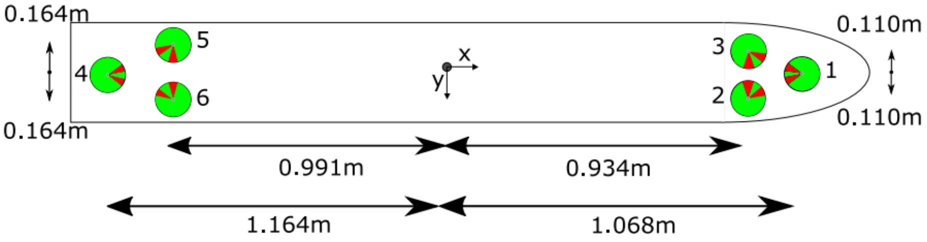

Figure 4.3: Dimensions and constraints of CSAD's actuators. Courtesy of Bjørnø et al. (2017)

4.2.2 Sensor Sub-Module

When designing a high-fidelity simulator, there has to be realistic sensor simulations as well. For the purpose of wave load compensation and the control strategies presented in this thesis, three sensors are required: Global Navigation Satellite System (GNSS), Inertial Measurement Unit (IMU), and a wave sensor providing wave elevation measurements.

GNSS Measurements

In this thesis, it was assumed that positions and velocities are given by the GNSS system. This is because the physical model will obtain these states from the odometry system in MC-Lab, which hereafter will be referred to as the GNSS. The odometry system is described in section 2.5.

Strictly speaking, the GNSS submodule and the calculation of vessel motions, is implemented as the same module in the source code. That is because the odometry system in MC-Lab provides the same states which are provided by the equations in (4.1a) and (4.1c).

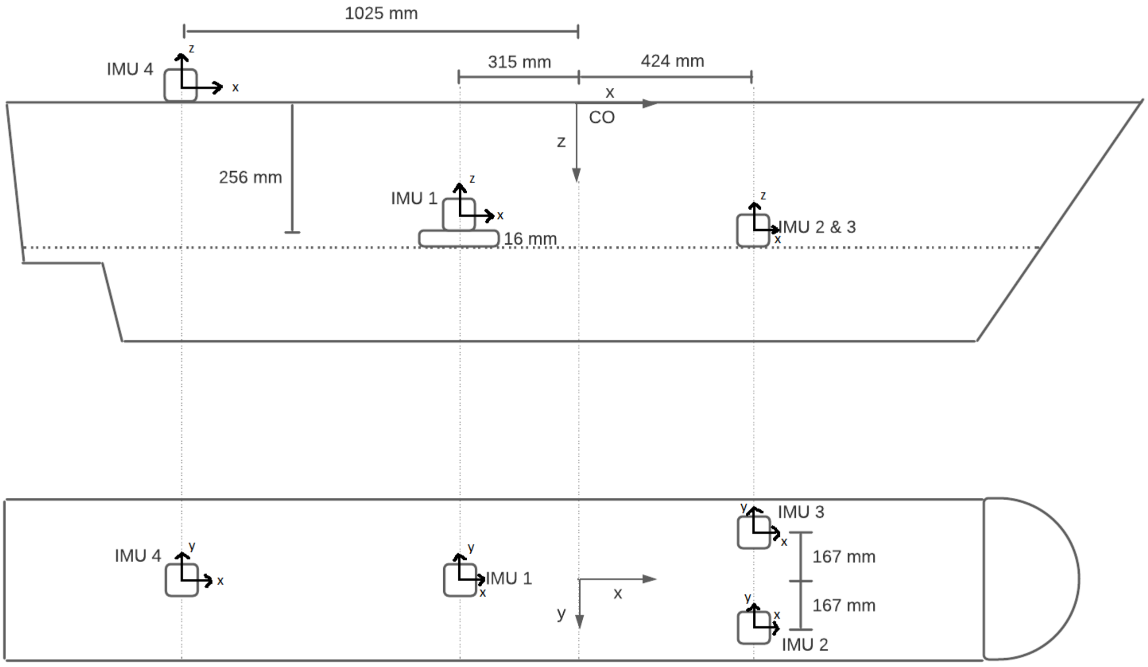

Figure 4.4: Configuration of the IMU locations on CSAD. Courtesy of Brørby (2021)

In the ROS network (Figure 4.1) these messages are published on the topic *"/qualisys/Body_1/odom"*.

IMU Measurements

By containing accelerometers, gyroscopes, and magnetometers, an IMU measurement can provide useful information in applications for motion-control. In this thesis, only accelerometer measurements were considered. The physical model vessel is equipped with four IMUs distributed as shown in Figure 4.4. The reason for this particular configuration is later explained in section 4.5.3.

From the equations of motions in (4.1), we have access to the velocities and position in 6 DOFs in the body frame. Hence, we also have access to the true 6 DOF acceleration vector expressed in the body frame. However, we want to simulate the linear acceleration measurements expressed in the sensor frame. Since the simulator provides 6 DOF calculations, it is possible to calculate the motion of an arbitrary point on the vessel. Assuming that the sensor frame is aligned with the body frame, the acceleration measurements, $a_m = col(a_x, a_y, a_z)$, can be modelled as in Batista et al. (2011). This is shown in (4.5a), where $a_m \in \mathbb{R}^3$ is the sensor output, and $a_l \in \mathbb{R}^3$ the linear acceleration at the location where the sensor is located. $\omega = col(p, q, r)$ is the body's angular velocities relative to NED frame, $\nu = col(u, v, w)$ is the linear velocity of the body, $g \in \mathbb{R}^3$ is the gravitational component in the body frame. $b \in \mathbb{R}^3$ is a sensor bias, and $w \in \mathbb{R}^3$ is sensor noise.

Since the sensors are not located in the body's origin (CO), the linear acceleration a_l must depend on the distance between CO and the sensor frame's origin, $l = col(l_x, l_y, l_z)$. If we express this lever arm as a distance vector in the body frame, the linear acceleration a_l can be described by (4.5b). Here, $a_{co}, \alpha \in \mathbb{R}^3$ is the linear acceleration and angular acceleration in CO, respectively.

It has to be noted that the simulations assumes that the sensor frame is aligned with the body frame. However, this is not the case for the physical model. Therefore, a transformation of the measurements has to be done if the signals should correspond to the physical case. This is left for further work.

The gravitational component g will have an impact on the linear accelerations in roll and pitch. This can be modelled as in (4.5c).

$$a_m = a_l + \omega \times \nu + g + b + w \tag{4.5a}$$
$$a_l = a_{co} + \alpha \times l + \omega \times (\omega \times l) \tag{4.5b}$$
$$\dot{g} = -\omega \times g \tag{4.5c}$$

Drifting measurements are a characteristic inconvenience for acceleration measurements. This is modelled by a random walk process of the bias b. That is, $\dot{b} = w_b$, where w_b is some noise.

In the ROS network (Figure 4.1), the measurements from the four sensors are published on the topic *"/imu1"*, *"/imu2"*, *"/imu3"*, *"/imu4"*. In the physical setup, the IMU measurements also include gyroscope measurements, but is not being used in this thesis.

Wave Measurements

This submodule is closely related to the environmental load module described later in section 4.2.3. Figure 4.5 shows how the wave elevation is both part of the environmental load module (blue sections) and the marine vessel module (green sections). Strictly speaking, the sensor submodule is calling the environmental module for information about the sea state's wave elevation, and publishes the measurement from the sensor submodule.

Sea state parameters T_p, H_s, and β are defined by the user before starting the simulator. How this is done is explained in Appendix A. The simulations are only defined for long-crested waves, both regular and irregular sea states.

To describe how the wave measurements are produced, recall (2.1b) from section 2.1.1, which describes wave elevation for long-crested waves:

$$\zeta(x,t) = \sum_{j=1}^{N} \sqrt{2S(\omega_j)\Delta\omega} sin(\omega_j t - k_j x + \varepsilon_j)$$

where ζ is the wave elevation relative to the surface. When starting the simulator, the environmental load module is initialized with a predefined wave spectrum $S(\omega)$ for some defined range of wave frequencies $[\frac{1}{2}\omega_p, 2\omega_p]$, where ω_p is the sea state's peak frequency. The distribution of wave frequencies ω_j within the mentioned frequency domain, are defined by $\Delta\omega = (2\omega_p - \frac{1}{2}\omega_p)/N$, where N denotes the number of frequency components.

Note that (2.1b) is expressed for all locations x, which is the distance from the defined origin of measurements. That is, the body frame's CO. If, for instance, the wave measurements were provided from a wave radar, the point of measure would be in front of the vessel. That way, by setting x to some measure distance, more realistic measurements can be provided. Note that the measurement then assumes the wave number k is given for an infinitely large water depth. Also note that the MC-Lab has no way of providing wave measurements to the physical vessel. Therefore, control systems, depending on these measurements, can only be tested with simulations as of today.

Wave elevation measurements are published to the topic *"/waveElevation"* in the ROS network.

4.2.3 Environmental Load Module

As implied in the problem formulation in Chapter 3, only wave induced loads are considered in the environmental load module. Hence, the purpose of the module, is to generate wave loads in terms of the three contributions stated in section 2.1.2; that is, first order, mean-drift, and slowly-varying loads. The loads generated are dependent on wave parameters defined by a user input, in terms of peak period T_p, significant wave height H_s, and propagation angle β expressed in NED frame. Since this is where the information of the sea state is generated, the wave measurements also had to be provided by this module, and not by the sensor module. However, the wave measurement is published from the sensor submodule, as described in section 4.2.2.

The reader is encouraged to give attention to Figure 4.5 while reading this section. Blue regions and blocks are members of the environmental load module, while green implies affiliation to the marine vessel module.

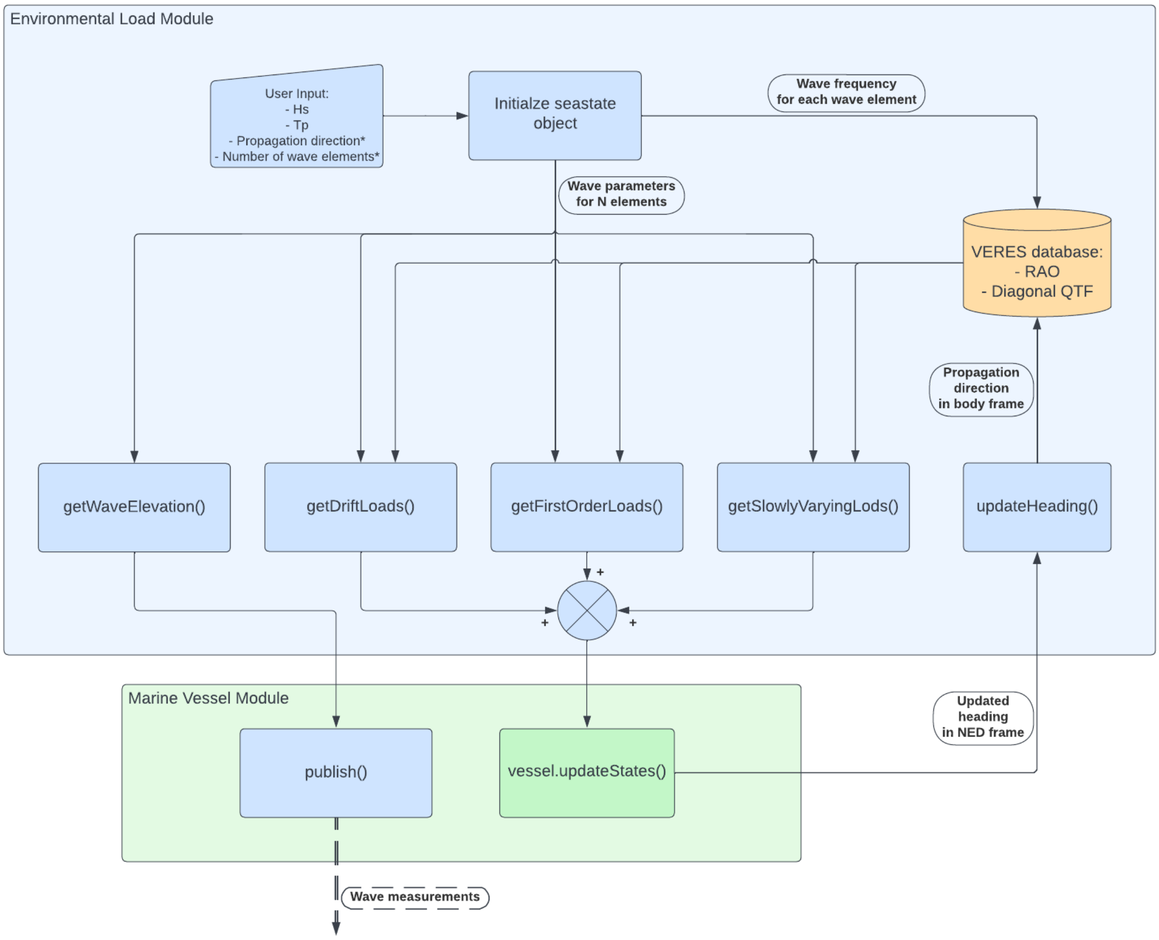

Figure 4.5: Flowchart of environmental load module.

The module simulates wave loads, expressed in body frame, and are calculated by utilizing the transfer functions provided by the VERES database. The parameters used from the database in this module is:

- First order load RAO, for describing first order wave loads. A transfer function from wave amplitude to first order wave loads. Called *"forceRAO"* in the VERES database.

- Diagonal of the QTF, for describing the mean-drift load and the slowly-varying loads. A transfer function from wave amplitudes to mean-drift loads. Called *"driftfrc"* in the VERES database.

The mentioned values are presented in 6 DOFs, and are defined for 47 different wave frequencies in the range of $[0.2094, 9.364]$, and for 36 different headings in the range of $[0, 2\pi)$. This makes it possible to express wave induced loads in a wide range of conditions.

In order to test various cases, this module provides the user to choose between regular and irregular sea states. However, only long-crested waves can be considered; that is, only unidirectional waves are simulated. For irregular sea states, a wave spectrum is generated when initializing the module. From this generation, a set of wave amplitudes, frequencies, and phases are saved for generating wave loads in real time. The JONSWAP spectrum presented in section 2.1.1 is used. Parameters for the spectrum are listed in Table 4.3.

Table 4.3: Extract from available system values for 6DOF vessel module.

Parameter	**Value**
α	0.0081
γ	3.3
σ_a	0.07
σ_b	0.09

Wave induced loads will affect the vessel's heading, even if the wave direction is along the body's surge direction. This is due to unmodelled dynamics and imperfect values from VERES. Since the transfer functions depends on heading, this module have to be updated with the new heading for each iteration, as showed in Figure 4.5.

As already mentioned, the VERES database are only defined for specific headings and frequencies. Therefore, a search for the closest valid condition is performed to find the corresponding values from the database. Since there are a lot of uncertainties in terms of unmodelled dynamics and imperfect hydrodynamic calculations by VERES, it was considered unnecessary to make an interpolation between the values.

The wave amplitudes A_k are associated to the wave spectrum $S(\omega_k)$ by (4.6), where ω_{min} and ω_{max} are defining the range where the major part of the energy is located in the spectrum (Faltinsen, 1999, chap. 5). Faltinsen (1999, chap. 5) states that we should let $N \longrightarrow \infty$, $\omega_{min} \longrightarrow 0$ and $\omega_{max} \longrightarrow \infty$, such that the area under the spectrum becomes an integral. However, choosing a finite large N will affect the calculation time drastically when simulating irregular sea states. Hence, a trade-off between completeness of the sea state and run time are introduced. Therefore, the number of wave elements N should be chosen wisely. In this simulator, it is by default $N = 25$, but the user is free to redefine it.

In addition, the signal will repeat itself after a period of $2\pi N/(\omega_{max} - \omega_{min})$ (Faltinsen, 1999, chap. 5). In order to avoid this, the frequencies ω_j are chosen randomly in each sub interval $\Delta\omega_j$.

$$\frac{A_k^2}{2} = S(\omega_k)\Delta\omega = S(\omega_k)\frac{\omega_{max} - \omega_{min}}{N} \tag{4.6}$$

The first order wave loads are calculated by utilizing the force RAO from VERES. The RAO provided from the VERES values contains both force amplitudes, and the phase angle between the wave and the wave induced force acting on the vessel. The usage of the transfer function is taken from Fossen (2021, chap. 10) and presented in (4.7), for all 6 DOFs ($i = 1, ..., 6$). The formula is a sum over N wave components. Here, H_i is the force RAO depending on the wave frequency ω_k and the wave direction β expressed in body frame. $S(\omega_k)$ is the spectrum as earlier described. The first order loads oscillate with time t, at the frequency of ω_k and a phase delay of $\angle H_i(\omega_k, \beta) + \varepsilon_k$, where $\angle H_i$ denotes the phase angle of the load relative to the incoming wave. ε_k is the phase angle of the wave element between 0 and 2π.

$$\tau^i_{wave1} = \sum_{k=1}^{N} \rho g \mid H_i(\omega_k, \beta) \mid \sqrt{2S(\omega_k)\Delta\omega} \cdot cos(\omega_k t + \angle H_i(\omega_k, \beta) + \varepsilon_k) \tag{4.7}$$

Mean-drift loads are simulated by (4.8), where $T_i(\omega_k, \beta)$ is the diagonal element of the QTF for frequency ω_k.

$$\tau^i_{mean} = \sum_{k=1}^{N} \rho g \mid T_i(\omega_k, \beta) \mid 2S(\omega_k)\Delta\omega \tag{4.8}$$

The slowly-varying wave loads are not as straight forward to simulate as the other contributions. Even if there are several proposals for describing these loads in the literature, most methods are even very time-consuming or does not describe the slowly-varying loads as a whole. OrcaFlex (2021) presents a method (4.9a) that contains a double summation, which results in 2^N calculations, which is a lot when the calculations have to be done in real-time. The reason for the double summation, is that the difference frequencies $\omega_k - \omega_j$ and $\omega_j - \omega_k$ of all wave frequencies are accounted for. It was decided to manipulate this method in order to decrease the run-time, by shorten the inner summation to only cover half of these combinations. By assuming that the full QTF is symmetric; that is, $T(\omega_k - \omega_j) = T(\omega_j - \omega_k)$, we can rewrite the summation to (4.9b). Note the upper limit of the inner sum.

$$\tau^i_{sw} = \sum_{k=1}^{N}\sum_{j=1}^{N} Re\{T_i(\beta_k, \beta_j, \omega_k, \omega_j) A_k A_j \exp\left[\mathrm{i}(\omega_k - \omega_j)t - (\phi_k - \phi_j)\right]\} \tag{4.9a}$$

$$= 2\sum_{k=1}^{N}\sum_{j=1}^{k} Re\{T_i(\beta_k, \beta_j, \omega_k, \omega_j) A_k A_j \exp\left[\mathrm{i}(\omega_k - \omega_j)t - (\phi_k - \phi_j)\right]\} \tag{4.9b}$$

Since only the QTF diagonal is available from VERES, we use an estimate for the off-diagonal terms (4.10)(Faltinsen, 1999, chap. 5), and we get an estimate of the slowly-varying wave loads (4.11).

$$\bar{T}_i(\beta_k, \beta_j, \omega_k, \omega_j) = \frac{1}{2}(T_i(\beta_k, \beta_k, \omega_k, \omega_k) + T_i(\beta_j, \beta_j, \omega_j, \omega_j)) \tag{4.10}$$

$$\Downarrow$$

$$\tau^i_{sw} \simeq 2\sum_{k=1}^{N}\sum_{j=1}^{k} Re\{\bar{T}_i(\beta_k, \beta_j, \omega_k, \omega_j) A_k A_j \exp\left[\mathrm{i}(\omega_k - \omega_j)t - (\phi_k - \phi_j)\right]\} \tag{4.11}$$

Eventually, as shown in Figure 4.5, the three contributions τ^i_{wave1}, τ^i_{mean}, and τ^i_{sw} are added and used in the equation of motions in the marine vessel module.

Note that the VERES database are offering a motion RAO as well (see Table 4.1). This could have been used to simulate the corresponding wave induced vessel motion, instead of the wave loads. The reason for not using motion RAO is that it only represents the first order wave loads. Consequently, second order wave loads still need to be added (Fossen, 2021, chap. 10).

4.3 Thrust Allocation

There are several methods for solving the thrust allocation problem. In this case, a pseudoinverse algorithm was used. The author considers the choice of allocation solver to not be conclusive for the scope of this master thesis. Therefore, more details can be seen in Fossen (2021, chap. 9).

It should be noted that with a view to avoid thrust in the restricted zones (recall Figure 4.3 from section 4.2.1), a constraint version of the pseudoinverse would have been a more reasonable choice. However, for the purpose of simulations, and the fact that thrust loss due to turbulent flow was neglected, the simple version was implemented. On the other hand, for the physical test case, a constraint version should be implemented in further work, as the turbulent effects can no longer be neglected.

4.4 Observer Design

In most DP operations for surface vessels, only surge, sway, and yaw motions from (4.1) are considered. In order to estimate the LF position η, velocity ν, and bias b in 3 DOFs, the nonlinear observer (NLO) from Fossen and Strand (1999) was selected. The observer model is presented in (4.12), where $\dot{\hat{\eta}}$, $\dot{\hat{\nu}}$ and $\dot{\hat{b}}$ are estimates of the named states, respectively. $\hat{\xi} \in \mathbb{R}^6$ is the estimate of the first-order wave induced dynamics, and $A_w \in \mathbb{R}^6$ is a matrix containing peak frequencies and damping ratios for the relevant sea state. $\tilde{y}$ is the measurement error, and $C_w = [0_{3\times3} \quad I_{3\times3}]$ is simply a selection matrix. The matrices $L_1 \in \mathbb{R}^{6\times3}$, L_2, L_3, and L_4 are injection gains. L_1 is used to tune the observer for proper wave-filtering.

$$\dot{\hat{\xi}} = A_w\hat{\xi} + L_1\tilde{y} \tag{4.12a}$$

$$\dot{\hat{\eta}} = R(\psi)\hat{\nu} + L_2\tilde{y} \tag{4.12b}$$

$$\dot{\hat{b}} = L_3\tilde{y} \tag{4.12c}$$

$$M\dot{\hat{\nu}} = -D\hat{\nu} + R(\psi)^T\hat{b} + \tau + L_4R(\psi)^T\tilde{y} \tag{4.12d}$$

$$\hat{y} = \hat{\eta} + C_w\hat{\xi} \tag{4.12e}$$

The reasons for using an observer with wave filtering, is stated in section 2.4.1. Since the objective of this thesis is concentrated on second order wave loads, the filter renders the comparisons between the controllers on the proper foundation; that is, compensation of wave induced motions due to second order effects.

Note that using deterministic observers, like this, will constitute a small delay of the provided estimate, due to integration of the states.

Fossen and Strand (1999) states that the NLO requires $R(\psi)$ to be perfectly known. Which, in our case, is a valid assumption as these measurements are either provided by the odometry system in MC-Lab or signals from the simulation model. Both contains small levels of uncertainty.

4.4.1 Tuning

The method for tuning the observer gains L_1 and L_2 is presented in Fossen and Strand (1999), and is optimized for good wave-filtering. It is possible to consider the gains L_3 and L_4 as an indication of how reliable the design model is compared to the measurements. If the measurements contain high uncertainty, lower values should be used. If the design model has high uncertainty, higher values are recommended. Therefore, a brute force approach is applied for the latter gains, with focus on good η and ν estimates.

4.5 Control Design

This section aims to present the different control methods that are developed and implemented in the thesis. How to launch and test the different controllers, are presented in Appendix A. The following methods are presented:

- **Method 1:**
  Bias estimate provided from the observer as direct compensation in a nominal control law.
- **Method 2:**
  Integral action as direct compensation in a nominal control law.
- **Method 3:**
  Acceleration feedforward term suppressing disturbances, added to a nominal control law.
- **Method 4:**
  An adaptive controller, using a Fourier series as internal model for second order loads.
- **Method 5:**
  A spectrum-based method, using estimates of the wave spectrum for supplying the integral action in a nominal controller.

We consider the 3 DOF CDM in (4.13), where τ is the control input, and $d(t)$ is the disturbance force, in terms of wave loads. The rest is defined as in section 2.4.1.

$$\dot{\eta} = R(\psi)\nu \tag{4.13a}$$

$$M\dot{\nu} = -D\nu + R(\psi)^T b(t) + \tau + d(t) \tag{4.13b}$$

4.5.1 Method 1: DP-Observer Estimate

The first method we consider is a PD control law, supplied by a bias term provided by the observer. The method is taken from Loría and Panteley (1999), where the separation principle is utilized; that is, if a globally exponentially stable feedback controller can be made using the state estimates from a globally exponentially convergent observer, the closed loop system will be globally asymptotically stable (Loría and Panteley, 1999).

We consider the observer presented in (4.12) from section 4.4, providing estimates of position, velocity, and bias. The bias estimate from (4.12c) represents the disturbance and unmodelled dynamics. The estimates are fed into the control law.

We propose a nominal control law (4.14), where $\tilde{\eta} := \hat{\eta} - \eta_d$ and $\tilde{\nu} := \hat{\nu} - \nu_d$ are the error states. K_p, $K_d \in \mathbb{R}^3$ are positive gains. $\tau \in \mathbb{R}^3$ is the control input for surge, sway, and yaw.

$$\tau = -K_p R(\psi)^T \tilde{\eta} - K_d \tilde{\nu} - R(\psi)^T \hat{b} \tag{4.14}$$

It is assumed that the two first terms in (4.14) are known to the reader as a nominal PD-controller. It is the last term that is interesting in this context. The bias estimate is assumed to be represented in the NED frame. Note that (4.12c) is dependent on the measurement error $\tilde{y}$ only, and no other parameters. Hence, this is actually a feedback term, and following the effect of the direct bias compensation will contain a delay equal to the delay that originates from the estimates.

This method is considered as the simplest control method in this thesis, and will be used as baseline when comparing all methods.

4.5.2 Method 2: Direct Integral Action

The second method is the most common for DP operations (Sørensen, 2011). It constitutes the PD controller with an integral term, and fulfills the controller known as the PID-controller. The idea of the integral action is that the error is summarized over time. We define a new state z in (4.15b), such that z is the integral of the position error from $t = 0$ to the current time.

$$\tau = -K_p R(\psi)^T \tilde{\eta} - K_d \tilde{\nu} - K_i R(\psi)^T z \tag{4.15a}$$

$$\dot{z} = \hat{\eta} - \eta_d(t) \tag{4.15b}$$

Like Method 1, this is a model-based control design. Such control systems are popular, as they provide stable and robust control (Fossen, 2021). However, they are not ideal for handling uncertainties in the CDM, and disturbances have to induce positioning offset before the integral action can adapt the system. This motivates the following methods.

4.5.3 Method 3: Acceleration Feedforward

Method 3 was originally presented in Kjerstad and Skjetne (2016). For the full control design, see Kjerstad and Skjetne (2016). Only the most essential details are presented here. The method utilize the (normally unused) acceleration measurements at marine surface vessels. The idea is to make a reconstruction of the 6 DOF acceleration vector for the vessel in body frame, and utilize the fact that acceleration signals holds values proportional to the forces acting on the vessel.

In order to achieve this, Kjerstad and Skjetne (2016) states some problems to overcome:

1. Sensors are typically not located in the body's CO. Therefore, signals needs to be converted from sensor frame to body frame.
2. The converted measurement from the previous item is not containing the angular accelerations. These must be calculated by utilizing the lever arm from CO to the sensor frame.
3. To procure the full acceleration vector $\dot{\nu}$ from the previous points.

We assume that the accelerometers are aligned with the body frame, and sensor scale-factor, cross-couplings, and misalignment errors are negligible (Kjerstad and Skjetne, 2016).

We also assume that signal for position $p = col(x, y, z)$ and orientation $\Theta = col(\phi, \theta, \psi)$ in the NED frame are measured. As well as angular velocities $\omega = col(p, q, r)$ in the body frame, and four acceleration measurements $a_m = col(a_x, a_y, a_z)$ in the sensor frame relative to the NED frame.

Recall the model of acceleration measurements in (4.5) from section 4.2.1:

$$\begin{aligned} a_m &= a_l + \omega \times \nu + g + b + w \\ a_l &= a_{co} + \alpha \times l + \omega \times (\omega \times l) \\ \dot{g} &= -\omega \times g \end{aligned}$$

where all variables are defined as earlier.

Strictly speaking, the procedure for reconstructing the 6 DOF acceleration vector in CO is the opposite of what we did in section 4.2.1 for simulating the acceleration measurements. However, now we make the most of the distribution of the four sensors. From (4.5b), the linear acceleration vector (a_l) at the sensor location point can be parameterized on matrix form as in (4.17), where $I_{3\times3}$ is the identity matrix, $S(l)$ and $H(l)$ is defined by (4.18a) and (4.18b), respectively. $\bar{\omega}$ contains the cross product elements $\bar{\omega} = \begin{bmatrix} \omega_x^2 & \omega_y^2 & \omega_z^2 & \omega_x\omega_y & \omega_x\omega_z & \omega_y\omega_z \end{bmatrix}^T$.

$$a_l = \begin{bmatrix} I_{3\times3} & S(l)^T & H(l) \end{bmatrix} \begin{bmatrix} a_{co} \\ \alpha \\ \bar{\omega} \end{bmatrix} =: W(l)z \tag{4.17}$$

$$S(l) = \begin{bmatrix} 0 & -l_z & l_y \\ l_z & 0 & -l_x \\ -l_y & l_x & 0 \end{bmatrix} = -S(l)^T \tag{4.18a}$$

$$H(l) = \begin{bmatrix} 0 & -l_x & -l_x & l_y & l_z & 0 \\ -l_y & 0 & -l_y & l_x & 0 & l_z \\ -l_z & -l_z & 0 & 0 & l_x & l_y \end{bmatrix} \tag{4.18b}$$

Doing this for all four sensors with their respective locations l, we can compose these matrices, and get (4.19), where $a_c \in \mathbb{R}^{12}$, $l_c = col(l_1, l_2, l_3, l_4)$, and $G(l_c) \in \mathbb{R}^{12\times12}$.

$$\begin{bmatrix} a_{l1} \\ a_{l2} \\ a_{l3} \\ a_{l4} \end{bmatrix} = \begin{bmatrix} W(l_1) \\ W(l_2) \\ W(l_3) \\ W(l_4) \end{bmatrix} z \tag{4.19a}$$

$$\Updownarrow$$

$$a_c = G(l_c)z \tag{4.19b}$$

Now, assume that the configuration of the acceleration sensors are strategically placed in accordance with Zappa et al. (2001), where at least one sensor is not co-planar to the other three (see illustration Figure 4.6). Consequently, $G(l_c)$ is nonsingular; hence, it can be inverted. Then, by substituting (4.19) into (4.5a), we obtain (4.20), where $a_{mc} \in \mathbb{R}^{12}$ is the composed acceleration measurement vector from four measurements.

$$G^{-1}a_{mc} = z + G^{-1} \begin{bmatrix} \omega \times \nu + g + b_1 + w_1 \\ \omega \times \nu + g + b_2 + w_2 \\ \omega \times \nu + g + b_3 + w_3 \\ \omega \times \nu + g + b_4 + w_4 \end{bmatrix} \tag{4.20}$$

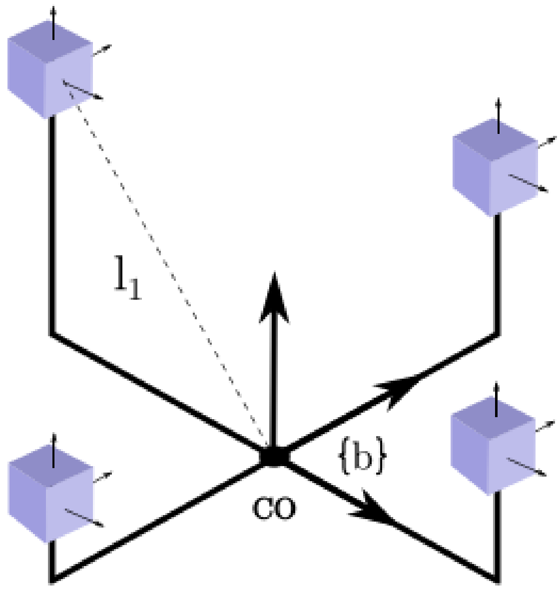

Figure 4.6: A possible setup for accelerometers for obtaining full state acceleration vector. Courtesy of Kjerstad and Skjetne (2016)

Consequently, the two first problems have been solved. To deal with the third problem, a state observer have to be made. This is because the gravitational component g needs to be removed from the signals, and sensor bias have to be accounted for. Kjerstad and Skjetne (2016) propose the observer in (4.21), where p_ν is the position p transformed to the body frame. $\nu = col(u, v, w)$ is here redefined to only contain the linear velocity in body frame. a_{mc} is the acceleration measurement vector from (4.20). b_l and b_ω is the bias from the linear and rotational acceleration that arise with the transformation in (4.20). $B_1,\ B_2 \in \mathbb{R}^{3\times12}$ is selection matrices for the linear dynamic acceleration and angular acceleration, respectively.

$$\dot{p}_\nu = -S(\omega(t))p_\nu + \nu \tag{4.21a}$$
$$\dot{\nu} = -S(\omega(t))\nu - b_l - g + B_1G^{-1}a_{mc} \tag{4.21b}$$
$$\dot{g} = -S(\omega(t))g \tag{4.21c}$$
$$\dot{b}_l = 0 \tag{4.21d}$$
$$\dot{\omega} = b_w + B_2G^{-1}a_{mc} \tag{4.21e}$$
$$\dot{b}_\omega = 0 \tag{4.21f}$$

Consequently, (4.21) constitutes a full state observer; hence, the control law can be designed. Let the control law be divided in a nominal term Γ and a term Δ for compensating the disturbance. To achieve disturbance rejection by acceleration feedforward, the control law (4.22) is proposed (Kjerstad and Skjetne, 2016).

$$\tau = \Gamma - \Delta \tag{4.22}$$

In this master thesis, we choose the nominal control law that is similar to the previous methods, but without the terms for disturbance compensation; namely, the PD-controller in (4.23). Here, $\tilde{\eta}$ and $\tilde{\nu}$ is the error states of the surge, sway, and yaw position and velocity, respectively. All provided by the state observer in (4.21).

$$\Gamma = -K_p R(\psi)^T \tilde{\eta} - K_d \tilde{\nu} \tag{4.23}$$

Since the acceleration measurements contains high levels of noise, a filtered acceleration signal should be used. Kjerstad and Skjetne (2016) suggests (4.24), where μ is a tuning gain for how accurate the disturbance is followed by Δ, and $\rho(\eta, \nu)$ is a function representing the nonlinear dynamics in the CDM (4.13).

$$\dot{\Delta} = \mu(Ma(t) - \Gamma - \rho(\eta, \nu)) \tag{4.24}$$

The method is presented as a block diagram in Figure 4.7.

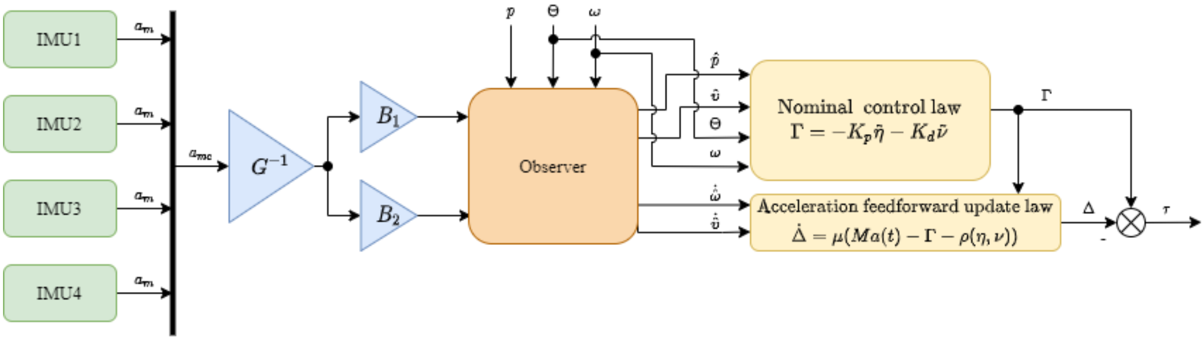

Figure 4.7: Block diagram of the acceleration feedforward method.

4.5.4 Method 4: Adaptive Fourier Series

Method 4 is based on the internal model principle, where a mathematical model for the disturbance is defined. An adaptive control law is designed to adapt parameters in the internal model, and to compensate for the true disturbance.

Consider the CDM in (4.13), and let $d(t) \in \mathbb{R}^3$ describe the disturbance as a sum of the slowly-varying loads and the mean-drift loads, in surge, sway and yaw.

We design an internal model for the disturbance, by assuming that the disturbance $d(t)$ can be described as a Fourier series of harmonic oscillating functions with N different frequencies. This can be written as in (4.25), where ω_n is the wave frequency of the n-th component, and a_{0i}, a_{ni}, b_{ni} are unknown Fourier coefficients, that we want to estimate. If we rewrite (4.25) to matrix form, we get (4.26), where the regressor $\Phi(t)$ is a vector consisting of time-variant functions, and θ is an unknown vector containing the Fourier coefficients. We assume θ to be constant, which is a reasonable assumption for a fully developped sea state.

$$d_i(t) = a_{i0} + \sum_{n=1}^{N} a_{ni} cos(\omega_n t) + b_{ni} sin(\omega_n t) \quad ; \quad i = 1, 2, 3 \tag{4.25}$$

$$d_i(t) = \begin{bmatrix}1 & cos(\omega_1 t) & sin(\omega_1 t) & \dots & cos(\omega_N t) & sin(\omega_N t)\end{bmatrix} \begin{bmatrix} a_{0i} \\ a_{1i} \\ b_{1i} \\ \vdots \\ a_{Ni} \\ b_{Ni} \end{bmatrix} \tag{4.26a}$$

$$=: \Phi(t)^T \theta \tag{4.26b}$$

Note that the first term in (4.26) is a constant. That is, for representing the mean-drift load. Hence, it is assumed that second order wave loads due to both difference-frequency effects and mean-drift are represented in the internal model.

We use LgV-backstepping for the controller design, and we define two new states (4.27), where $\alpha \in \mathbb{R}^3$ is a virtual controller to be defined later.

$$z_1 = R(\psi)^T(\eta - \eta_d(t)) \tag{4.27a}$$

$$z_2 = \nu - \alpha \tag{4.27b}$$

Step 1:

We differentiate (4.27a) with respect to time and get:

$$\begin{aligned} \dot{z}_1 &= \dot{R}^T(\psi)(\eta - \eta_d(t)) + R(\psi)^T(R(\psi)\nu - \dot{\eta}_d(t)) \\ &= -S(r)z_1 + z_2 + \alpha - R(\psi)^T\dot{\eta}_d(t) \end{aligned} \tag{4.28}$$

where we have used that $\dot{R}(\psi) = R(\psi)S(r)$ and $S(r) = -S^T(r) = \begin{bmatrix} 0 & -r & 0 \\ r & 0 & 0 \\ 0 & 0 & 0 \end{bmatrix}$.

We assign a control Lyapunov function (CLF):

$$V_1(z_1) = \frac{1}{2} z_1^T z_1 \tag{4.29}$$

where the time derivative is

$$\begin{aligned} \dot{V}_1 &= z_1^T \dot{z}_1 \\ &= z_1^T(-S(r)z_1 + z_2 + \alpha - R(\psi)^T\dot{\eta}_d(t)) \\ &= z_1^T(z_2 + \alpha - R(\psi)^T\dot{\eta}_d(t)) \end{aligned} \tag{4.30}$$

In order to cancel terms in (4.30), we choose the virtual control law:

$$\alpha = -C_1 z_1 + R(\psi)^T\dot{\eta}_d(t) + \alpha_0 \tag{4.31}$$

where $C_1 \in \mathbb{R}^{3\times3}$ is a positive tuning matrix, and α_0 is a virtual control law for making (4.30) negative, and will be assigned later in the design. Putting the control law (4.31) into (4.30) gives

$$\begin{aligned} \dot{V}_1 &= -z_1^T C_1 z_1 + z_1^T z_2 + z_1^T \alpha_0 \\ &\leq -z_1^T C_1 z_1 + \kappa_1 z_1^T z_1 + \frac{1}{4\kappa} z_2^T z_2 + z_1^T \alpha_0 \end{aligned} \tag{4.32}$$

In (4.32) we have used Young's inequality; that is, $a^T b \leq \kappa a^T a + \frac{1}{4\kappa} b^T b$ for some constant $\kappa > 0$, where $a = z_1$ and $b = z_2$. Then, by choosing the control law for α_0:

$$\alpha_0 = -K z_1 \tag{4.33}$$

where $K = \kappa I_3$. This results in the following:

$$\dot{V}_1 \leq -z_1^T C_1 z_1 + \frac{1}{4\kappa} z_2^T z_2 \tag{4.34}$$

$$\dot{z}_1 = -S(r) z_1 + z_2 - (C_1 + K) z_1 \tag{4.35}$$

Step 2:

Now, considering the z_2-dynamics from (4.27b), where the time derivative is

$$\begin{aligned} M\dot{z}_2 &= M\dot{\nu} - M\dot{\alpha} \\ &= -D\nu + \Phi(t)^T \theta + \tau - M\dot{\alpha} \end{aligned} \tag{4.36}$$

We assign a new CLF for Step 2:

$$V_2(z_1, z_2) = V_1(z_1) + \frac{1}{2} z_2^T M z_2 \tag{4.37}$$

Differentiating (4.37) gives

$$\begin{aligned} \dot{V}_2 &= \dot{V}_1 + z_2^T M z_2 \\ &\leq -z_1^T C_1 z_1 + \frac{1}{4\kappa} z_2^T z_2 + z_2^T (-D\nu + \Phi(t)^T \theta + \tau - M\dot{\alpha}) \\ &= -z_1^T C_1 z_1 + \frac{1}{4\kappa} z_2^T z_2 + z_2^T (-D z_2 - D\alpha + \Phi(t)^T \theta + \tau - M\dot{\alpha}) \end{aligned} \tag{4.38}$$

Let $\hat{\theta}$ be an estimate of θ, and let $\tilde{\theta} = \theta - \hat{\theta}$ be the error state. Recall that θ is a constant vector. Hence, the error dynamics becomes: $\dot{\tilde{\theta}} = -\dot{\hat{\theta}}$.
Based on the terms in (4.38), we choose the control law

$$\tau = -C_2 z_2 + D\alpha + M\dot{\alpha} - \Phi(t)^T \hat{\theta} \tag{4.39}$$

where $C_2 \in \mathbb{R}^{3\times3}$ is a positive tuning matrix. Note that we do not want to counteract the $-Dz_2$ term in (4.38), since it adds more stability to the system.

Putting the control law (4.39) into (4.38) gives

$$\dot{V}_2 \leq -z_1^T C_1 z_1 - z_2^T (C_2 - \frac{1}{4\kappa} + D) z_2 + z_2^T \Phi(t)^T \tilde{\theta} \tag{4.40}$$

$$M\dot{z}_2 = -(D + C_2) z_2 + \Phi(t)^T \tilde{\theta} \tag{4.41}$$

For simplicity, we define $C_3 = C_2 - \frac{1}{4\kappa} + D$.
Finally, we assign a last CLF in order to achieve an update law for the estimate $\hat{\theta}$:

$$V(z_1, z_2, \tilde{\eta}) = V_2 + \frac{1}{2} \tilde{\theta}^T \Gamma^{-1} \tilde{\theta} \tag{4.42}$$

where $\Gamma \in \mathbb{R}^{2N+1}$ is a tuning matrix, implying how fast the Fourier coefficients will be updated.

Differentiating (4.42) gives

$$\begin{aligned}\dot{V} &= \dot{V_2} + \tilde{\theta}\Gamma^{-1}\dot{\tilde{\theta}} \\ &\leq -z_1^T C_1 z_1 - z_2^T C_3 z_2 + \tilde{\theta}^T(\Phi(t)z_2 - \Gamma^{-1}\dot{\hat{\theta}})\end{aligned} \tag{4.43}$$

Then, in order to cancel the last term in (4.43), we choose the update law

$$\dot{\hat{\theta}} = \Gamma\Phi(t)z_2 \tag{4.44}$$

which renders

$$\dot{V} \leq -z_1^T C_1 z_1 - z_2^T C_3 z_2 \leq 0 \tag{4.45}$$

In other words, $\dot{V}$ becomes negative semi-definite. Hence, by Lyapunov's direct method, we can conclude that the equilibrium $(z_1, z_2, \tilde{\theta}) = 0$ is UGS. In addition, according to LaSalle (1968) and Yoshizawa (1966), (z_1, z_2) will converge to zero as time goes to infinity.

Note that this control method will not give guaranties for convergence of $\tilde{\theta} \longrightarrow 0$, only $(z_1, z_2) \longrightarrow 0$. To achieve such guaranties, it is required that the preliminary assumptions holds, and that the CDM is accurate enough. In addition, the true disturbance $d(t)$ would have to be persistently exciting the regressor $\Phi(t)$ (Anderson et al., 1986).

Also note that the frequencies ω_n are equally distributed within the set $[2\pi/20 \quad 2\pi/2]$, where N is a natural number to decide the number of frequency components to consider in the Fourier series. A higher value of N gives a more accurate disturbance estimate, but will also increase the size of the matrices $\Phi(t)$ and $\hat{\theta}$ with $2N + 1$; hence, increase the calculation time. $T_{min} = 2$ seconds and $T_{max} = 20$ seconds is chosen to cover a wide range of slowly-varying frequencies, but this may also be considered as tuning parameters.

A block diagram of the method is presented in Figure 4.8.

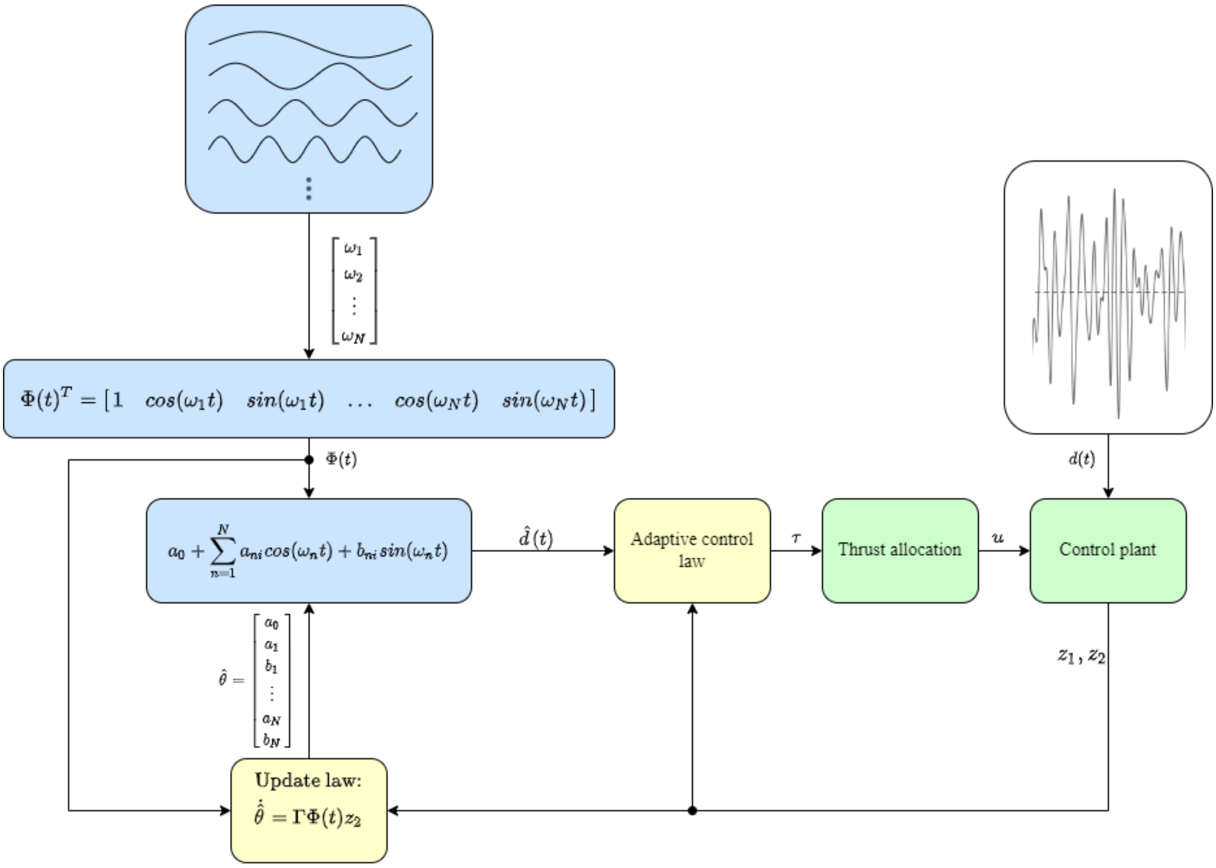

Figure 4.8: Block diagram from Method 4.

4.5.5 Method 5: Spectrum-Based Estimation

This method was first presented in the preproject written by the author (Brørby, 2021). The design is here reproduced and improved for this master thesis. As mentioned in section 2.4, the bias $b(t)$ tends to be significant as it covers both unmodelled dynamics and slowly-varying environmental loads (Sørensen, 2011). In conventional PID-controllers, integral action is used to compensate for the bias in its entirety. The idea of Method 5 is to relieve the integral action by extracting the mean-drift loads, and compensate these in a separate term (see Figure 4.9). In order to do so, a strategy for estimating the mean-drift loads is proposed, which is further used as a supplement to the conventional PID controller.

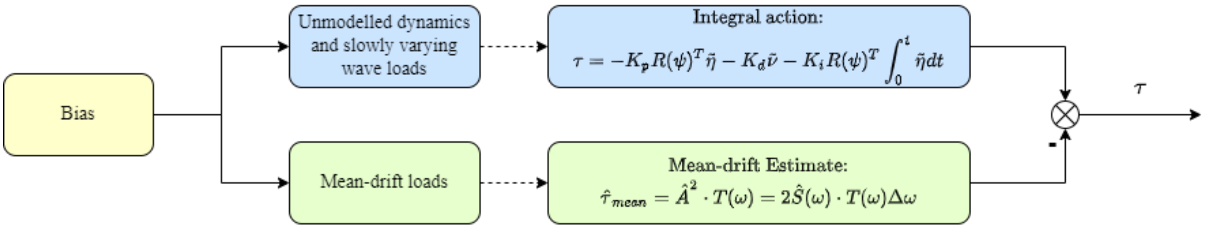

Figure 4.9: Block diagram of Method 5.

Two main challenges must be overcome:

1. The current sea state needs to be estimated and modelled, based on wave measurements.
2. The mean-drift load must be estimated using the gained knowledge of the current sea state.

In Brørby (2021), some strategies were proposed to deal with the first challenge. Here, we choose to estimate a wave spectrum based on historical data, gained online.

Assume that raw wave measurements are provided in terms of wave amplitudes A_m from some sensor with sampling time T_A. Let $\bar{A} = [A_1, A_2, ..., A_N] \in \mathbb{R}^N$ be a vector holding the historical measurements for N samples. A shift register holding the historical data for the wave measurements are defined in (4.46), where the superscript $+$ denotes the new value of position i of a total of N historical samples.

$$A_0 = A_m \tag{4.46a}$$
$$A_i^+ = A_{i-1} \quad ; \quad i = 1, ..., N \tag{4.46b}$$
$$N^+ = N + 1 \tag{4.46c}$$

Let Ω be a vector containing the available frequencies provided by the VERES database. An estimate of the wave spectrum ($\hat{S}_0(\omega)$) and associated wave frequencies $\hat{\Omega}$, corresponding to the collected measurements $\bar{A}$, can be obtained by performing an FFT of $\bar{A}$ (Fossen, 2021, chap. 13). In the implementations, Welch's method is used to obtain a power spectral density of the sea state (Scipy FFT: Welch).

Let T_{ss} be the period between each time a new estimate of the wave spectrum should be calculated, and let $\bar{S} = [\hat{S}_1(\omega), ..., \hat{S}_M(\omega)]$ be a vector holding the estimated spectrums for each period of $T = M \cdot T_{ss}$. A shift register, carrying the M last estimated wave spectrums $\hat{S}_j(\omega)$, can then be defined as in (4.47). Figure 4.10 illustrates how the period of the estimates evolves.

$$S_j^+(\omega) = S_{j-1}(\omega) \quad ; \quad j = \{1, ..., M\} \tag{4.47a}$$
$$M^+ = M + 1 \tag{4.47b}$$

As stated in section 2.1.1, it is common to say that 20 minutes is enough to express the statistical properties for a sea state (Larsen et al., 2019). However, a sea state will also change with time, depending on how long period a sea state is observed. If we consider shorter time periods isolated, we may observe that the mean-drift will vary from one interval to another, and the actual sea state may not be represented. On the other hand, considering a growing time span, will represent the current sea state more accurately, as time grows. This motivates the choice of considering a growing time span for the wave spectrum estimate (Figure 4.10), and also the final estimate, that is (4.48). Here γ is a weighting parameter, implying how much the older estimates $\hat{S}_j(\omega)$ should be weighted.

$$\hat{S}(\omega) = \frac{\sum_{j=1}^{M} \gamma^j \hat{S}_j(\omega)}{\sum_{j=1}^{M} \gamma^j} \quad ; \quad \gamma \in (0, 1] \tag{4.48}$$

Note that choosing $\gamma = 1$ will weight all estimates equally, while lower values will make $\hat{S}(\omega)$ depend more on the newest estimates.

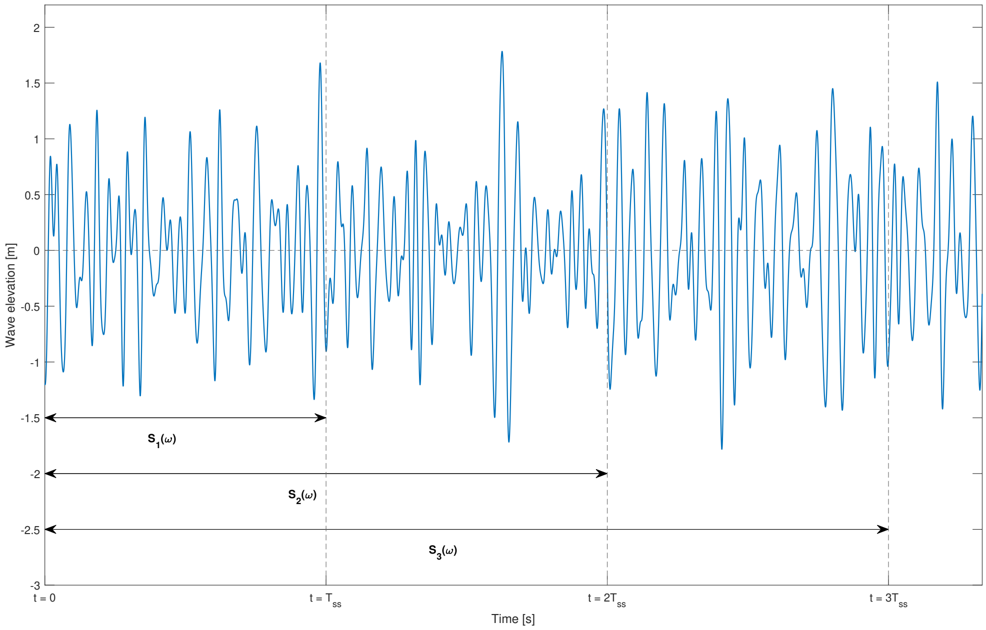

Figure 4.10: Illustration of how to update the estimation of the wave spectrum.

A flowchart of the procedure of sea state estimation is presented in Figure 4.11.

Now that an estimate of the wave spectrum is provided, we can use this to calculate a mean-drift load corresponding to the estimated sea state. Proposing (4.49), where $T(\omega)$ is the diagonal of the QTF, as mentioned earlier. (4.49) is inspired by the mean-drift loads (2.5) from section 2.1.2.

$$\hat{\tau}_{mean} = \hat{A}^2 \cdot T(\omega) = 2\hat{S}(\omega) \cdot T(\omega)\Delta\omega \tag{4.49}$$

Note that, since the estimated spectrum $\hat{S}(\omega)$ will vary over time, $\hat{\tau}_{mean}$ will be a slowly-varying load. However, it is important to emphasize that this is not reflecting the slowly-varying loads due to difference-frequencies.

We fulfill the control law in (4.50).

$$\tau = -K_p R(\psi)^T(\hat{\eta} - \eta_d(t)) - K_d(\hat{\nu} - \nu_d(t)) - K_i R(\psi)^T z - \hat{\tau}_{mean} \tag{4.50a}$$

$$\dot{z} = \hat{\eta} - \eta_d(t) \tag{4.50b}$$

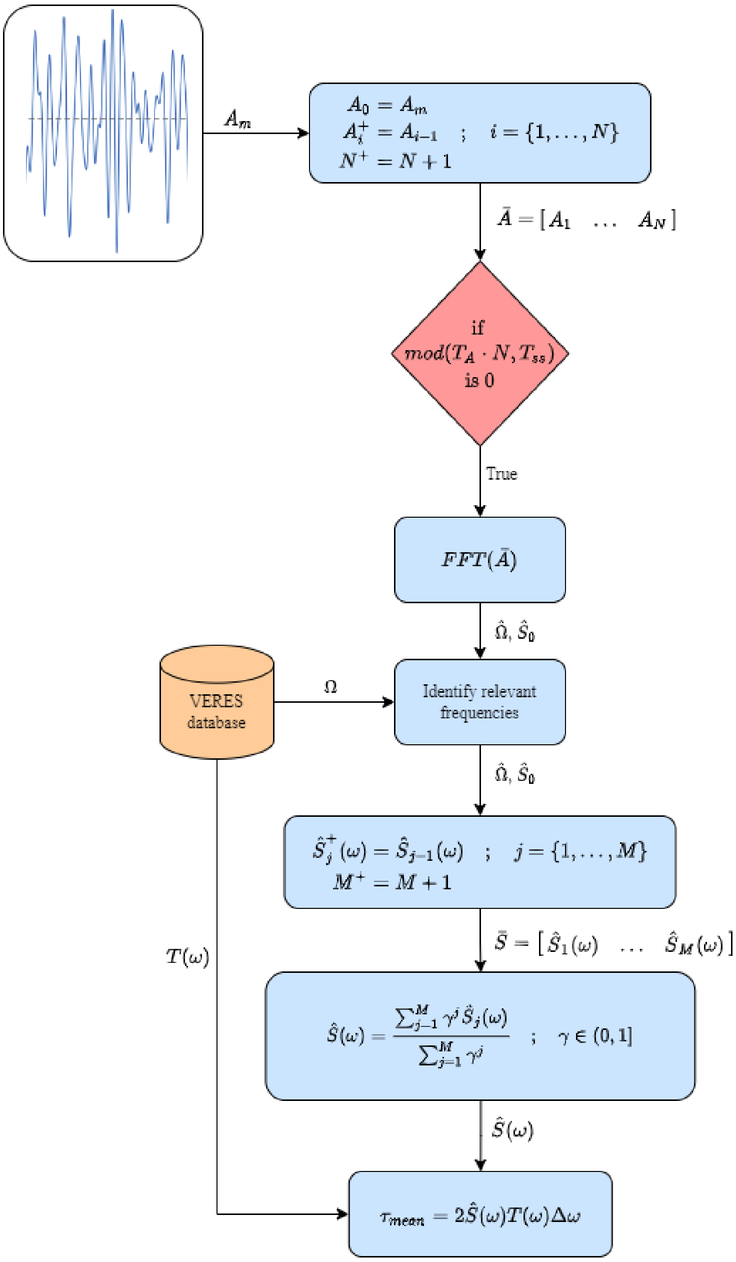

Figure 4.11: Flowchart of the sea state estimation for Method 5.

Chapter 5

Results and Discussion

This chapter presents results from simulations, and a performance analysis of the designed methods that was presented in Chapter 4.

First, some results addressing the high-fidelity simulator's features are visited. Thereafter, results from simulations providing a basis of the performance analysis are considered and discussed.

5.1 High-Fidelity Simulator

Since the scope of this master thesis is to develop DP control systems for wave loads compensation, it is essential that the simulated wave loads are generated in a way that is realistic, and make the performance analysis useful for real world cases.

Figure 5.1 showing the output of the slowly-varying loads only, with the corresponding wave elevation. Since the output contains a lot of spiked samples, a red line showing the contour of the slowly-varying loads is included. Note that the contour is used for illustrating purposes only, to give the reader an intuition of how the slowly-varying component varies with time. It is not part of the output from the generated wave loads.

The reason for the spiky output, comes from an issue with the modelling of second order wave loads, which was presented in section 4.2.3. The issue was already addressed in section 2.1.2; sum-frequency effects will be part of the mathematical expression of the slowly-varying wave loads. Sum-frequency components results in high-frequency loads, which is what we observe in Figure 5.1. However, for a surface vessel, such high-frequency loads will not have any physical impact, since the vessel acts as a lowpass filter itself, and the high frequencies are not in the neighborhood of any natural frequencies in the horizontal plane of the vessel motion.

Another observation from Figure 5.1 is that there are no indications in the wave elevation that should imply the slowly-varying forces that occur. For instance; the swollen loads at about 270 sec, has no corresponding swells in the wave elevation measurements. This supports the statement that the correlation between the wave elevation and the slowly-varying loads, are not a one-to-one correspondence, but a consequence of the vessel's vertical motions in the waves, and hydrodynamic effects.

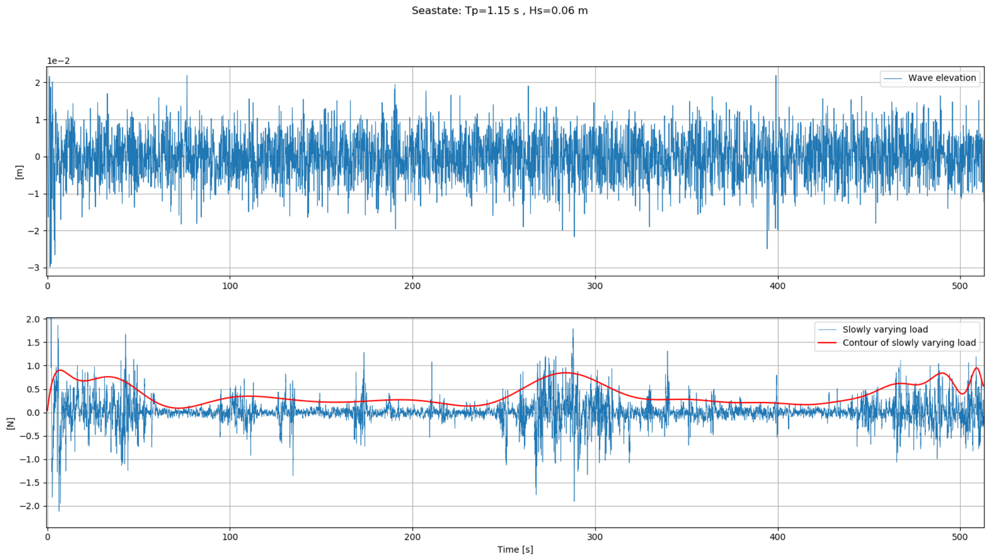

Figure 5.1: Generated slowly-varying loads from the environmental load module, with corresponding wave elevation.

5.2 Observer

The observer is essential for the control system to behave in a desirable way. Figure(s) 5.2 and 5.3 shows results from the tuned observer, in regular and irregular sea states respectively, in surge direction. Note that first order motions are filtered in both sea states, but these motions are harder to observe in an irregular sea state.

An important observation from Figure 5.3 is the delay that comes with the estimated states. The signal will be delayed due to integration within the observer, and due to the time of the estimation itself. Recall that all the ROS nodes are running on a sampling frequency of 50 Hz. If this frequency was higher, the delay could have been shortened, but not eliminated totally. The delay will affect how the control systems compensate disturbances, in terms of how fast they will be able to react; hence, the stability of the controllers are also affected by the observer delay.

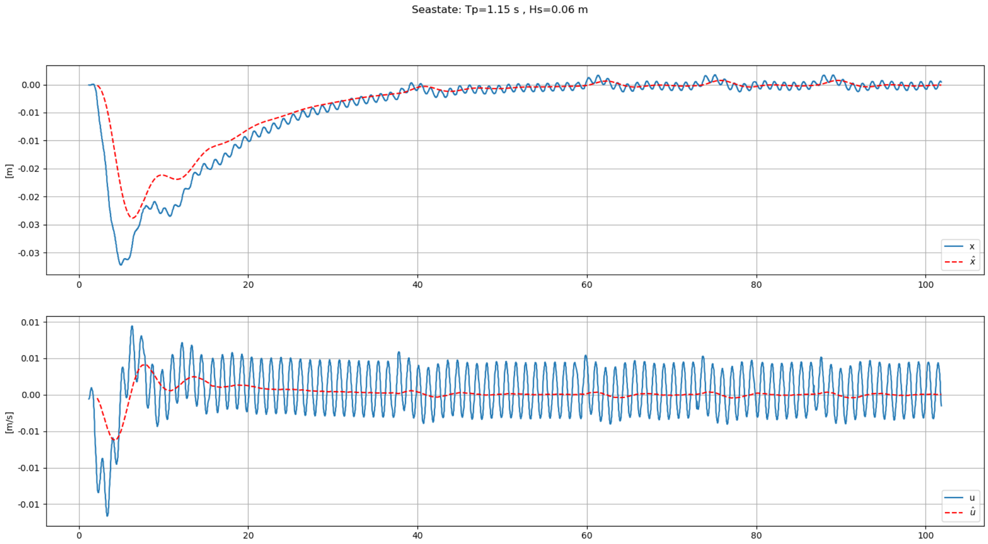

Figure 5.2: η and ν in surge with corresponding estimates from the nonlinear observer, subject to regular waves.

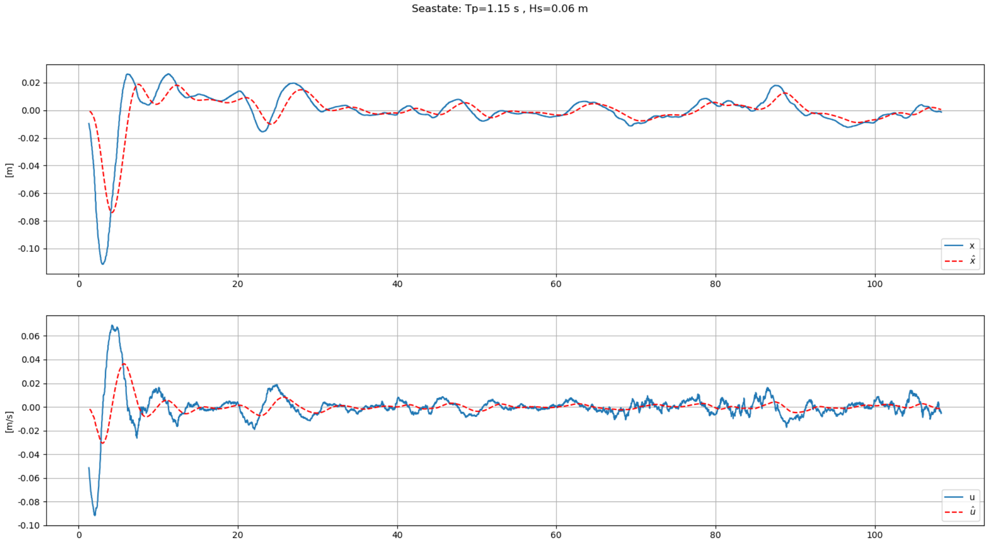

Figure 5.3: η and ν in surge with corresponding estimates from the nonlinear observer, subject to irregular waves.

5.3 Control System Performance

A performance analysis of the designed methods are presented. Table 5.1 showing realistic sea states that are scaled to the size of the model that we are considering (CSAD). The list was used to test the controllers under realistic conditions. The standard of comparison is based on finding sea states that provokes weaknesses in the conventional DP controllers; that is, Method(s) 1 and 2.

The control objective for the performance tests, was to control $\eta(t) \longrightarrow 0$ and $\nu(t) \longrightarrow 0$. Due to time-consuming work, only one DOF of the controllers was tuned properly for η and ν; that is, surge direction. Hence, only controlling the vessel in surge direction is considered in the performance analysis. The consequences of this limitation are discussed later in section 5.3.6.

Table 5.1: Realistic combination of significant wave heights and peak periods: full scale (Price and Bishop, 1974) and model scale (Slåttum, 2021).

		Full Scale		**1:90 Model Scale**	
Sea state	**Description**	**Hs [m]**	**Tp [s]**	**Hs [m]**	**Tp [s]**
0	Calm (glissy)	0.0	-	0.0	-
1	Calm (reppled)	0.0 - 0.1	4.87 - 5.66	0.0 - 0.001	0.51 - 0.6
2	Smooth (wavelets)	0.1 - 0.5	5.66 - 6.76	0.001 - 0.006	0.6 - 0.71
3	Slight	0.5 - 1.25	6.76 - 7.95	0.006 - 0.014	0.71 - 0.84
4	Moderate	1.25 - 2.5	7.95 - 9.24	0.014 - 0.028	0.84 - 0.97
5	Rough	2.5 - 4.0	9.24 - 10.47	0.028 - 0.044	0.97 - 1.10
6	Very rough	4.0 - 6.0	10.47 - 11.86	0.044 - 0.067	1.10 - 1.25
7	High	6.0 - 9.0	11.86 - 13.66	0.067 - 0.1	1.25 - 1.44
8	Very high	9.0 - 14.0	13.66 - 16.11	0.1 - 0.156	1.44 - 1.70
>8	Phenomenal	>14.0	>16.11	>0.156	>1.70

Method 1 was first tested in different sea states defined by Table 5.1. It was concluded that the controller started to show some significant weaknesses related to the "Rough" sea state (level 5 in Table 5.1). Therefore, the performance analysis is based on considerations of the same sea state.

Video recordings from the experiments, from the preproject Brørby (2021), showed that waves with periods longer than one seconds resulted in wavelengths longer than the characteristic length of the vessel. Figure 5.4 illustrates this. The videos from these experiments and corresponding force measurements are included in the digital appendix. Recalling the theory from section 2.1.2, wave-drift loads for such wave periods may be dominated by viscous effects. However, waves of this length are still causing relative motions between the sea surface and the vessel hull.

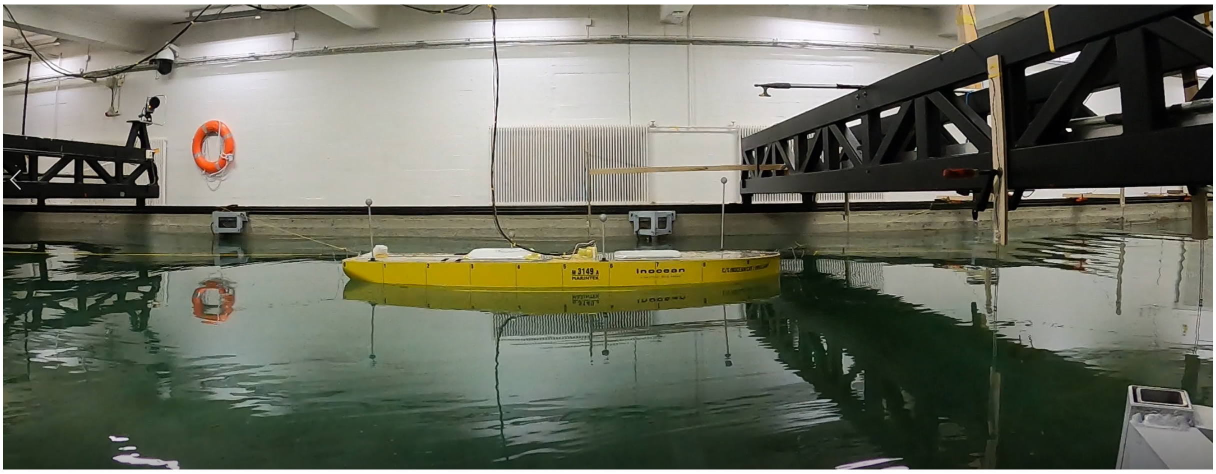

Figure 5.4: Screenshot of video from experiments in Brørby (2021): CSAD in regular waves with wave period of $T = 1.10$ seconds.

5.3.1 Method 1: DP-Observer Bias Estimate

Figure 5.5 shows results for position (upper plot) and velocity (lower plot) in surge direction, from a simulation where Method 1 was tested in a rough sea state. In the initial seconds, a large positioning offset occurs. This is due to the sudden occurrence of the wave loads, which is handled by the PD-regulator. After the sudden negative offset, the controller overshoots above the set point. This is due to that the controller is tuned to be underdamped. Consequently, the sudden change in wave loads will be compensated with high stiffness and not enough damping by the controller. This could have been avoided by a higher derivative gain, providing more damping to the closed loop system.

It can be observed in Figure 5.5 that the surge position is containing a lot of oscillations which the controller do not handle. These are motions induced by the first order wave loads, and are not meant to be counteracted, but filtered by the observer in order to reduce wear and tear of the actuators. With that being said, Figure 5.5 also shows that larger offsets due to slowly-varying loads are present as well. It is these contributions that the bias estimate from the observer are supposed to counteract. However, this assumes that the bias observer is tuned properly, and that it is able to model the bias quite accurate.

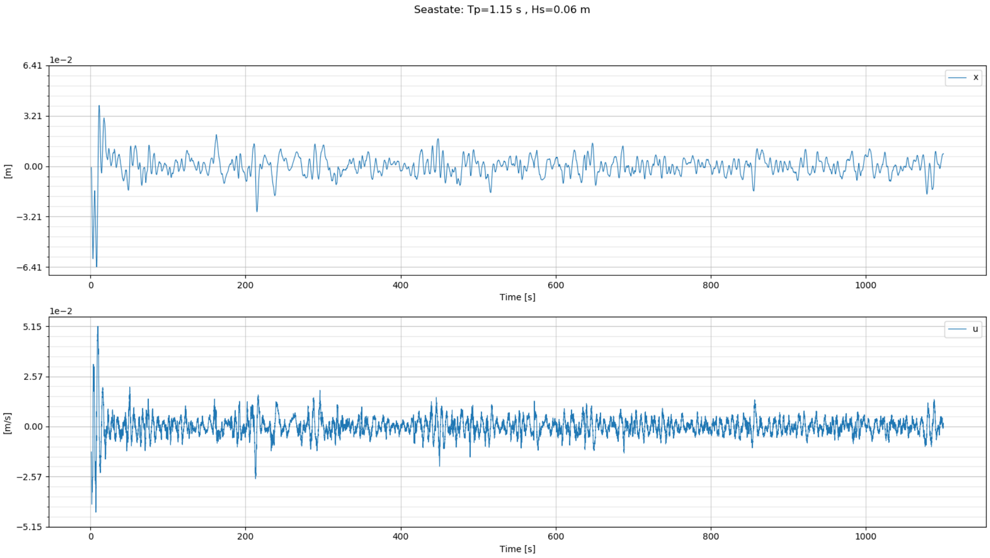

Figure 5.5: Surge response of Method 1. Sea state: $T_p = 1.15$, $H_s = 0.06$, $\beta = 0$.

In Figure 5.6, the desired control input is plotted above the set point for each actuator. The dashed line in the lower plot represents the maximum thrust load that is achievable for one azimuth thruster; that is, the saturation limit of each actuator. Note that the plots shows the output from the controller and thrust allocation, respectively, and is not saturated. In the lower plot, one can see that the desired set points are mostly below the saturation limit, except for a couple of peaks. This implies that the method do not surpass the actuator's thrust capacity, which means that the vessel is able to satisfy the desired control input. At least in terms of magnitude. The actuator's maximum shaft-speed rate will still limit the bandwidth of the closed loop system

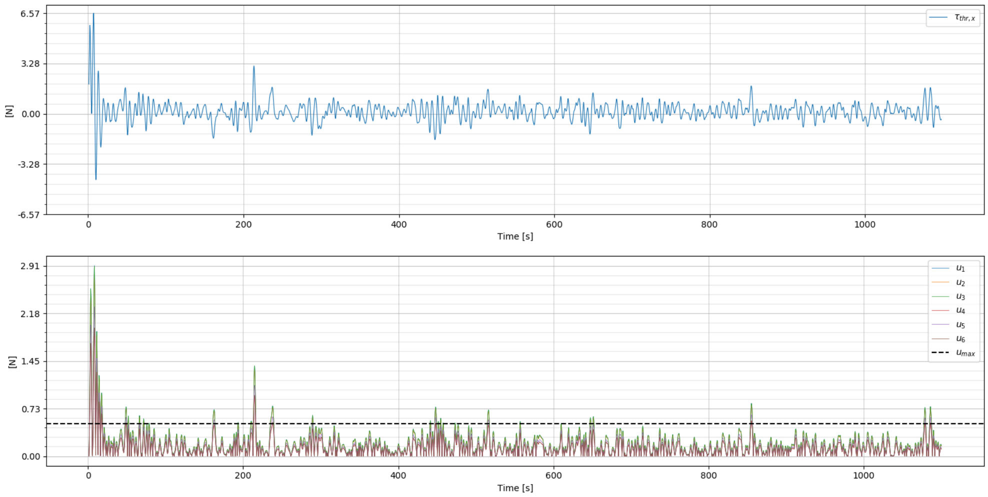

Figure 5.6: Controller output τ in surge, and thrust allocation output u_i for Method 1. Sea state: $T_p = 1.15$, $H_s = 0.06$, $\beta = 0$.

Since the method utilize the bias estimate from Fossen and Strand (1999), which has shown to be robust in terms of disturbances and unmodelled dynamics, Method 1 is a simple and robust strategy for wave load compensation. However, it has some downsides. First and foremost, the controller performance depend on how good the bias model in the observer is. If the model is inaccurate, the DP performance will reflect this uncertainty. As stated earlier; bias in terms of unknown slowly-varying loads are hard to model mathematically, since they contain a lot of randomness, and are often complex systems. In addition, Method 1 depends on how good the CDM is. Since unmodelled dynamics are included in the bias term, it should grow accordingly if the model parameters are uncertain. How uncertain the model parameters are in this case remain unknown, but the fact that parameters comes from the VERES database, which is calculated based on a digital 3D model of the vessel's hull (and not experimental data), we should assume that there are some significant uncertainties.

5.3.2 Method 2: Direct Integral Action

Considering Figure 5.7, we can see that the position plot is not that different from Method 2 in Figure 5.5. Recall that both Method 1 and 2 contains PD controllers with similar tuning parameters, and that it is the disturbance rejection terms which are distinct. Similarly to Method 1, there is an overshoot in the initial seconds. This is as expected since the controller contains the exact same terms and gains as the PD-part of the controller. Hence, too low damping could have been avoided by higher gains of the derivative term, also here.

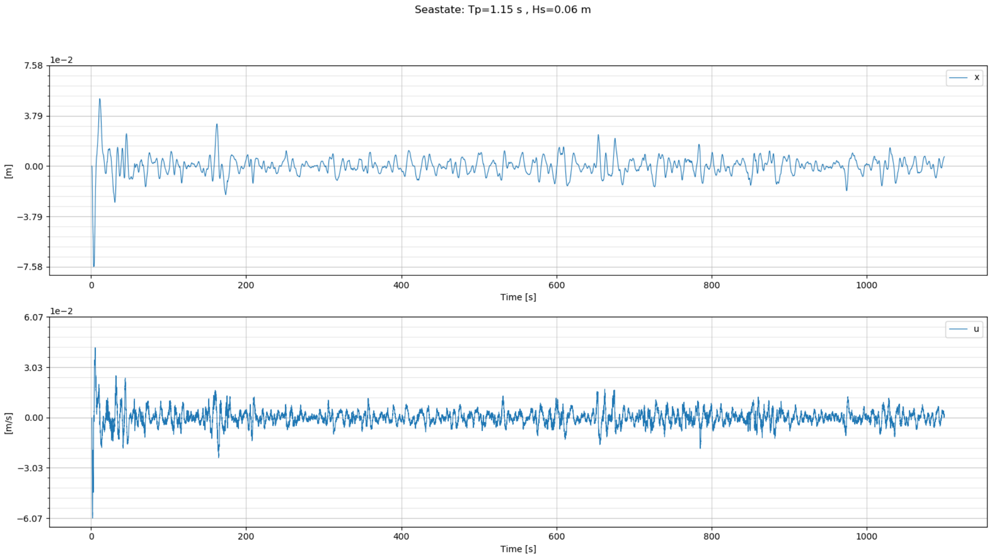

Figure 5.7: Surge response of Method 2. Sea state: $T_p = 1.15$, $H_s = 0.06$, $\beta = 0$.

Similar to Method 1, the controller input is demanding loads from the actuator that is achievable in terms of not surpassing the saturation limit. However, the mean thrust loads of the actuators are slightly lower (0.0284 N) than it was for Method 1 (0.0328 N). This gives an indication of the fuel consumption that the two methods will cause. A more in-depth discussion of this is given later in the chapter.

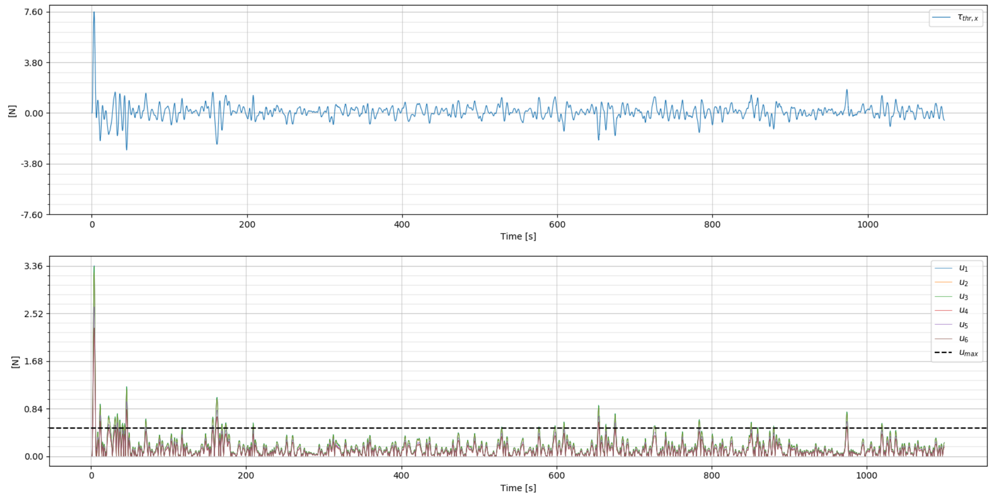

Figure 5.8: Controller output τ in surge, and thrust allocation output u_i for Method 2. Sea state: $T_p = 1.15$, $H_s = 0.06$, $\beta = 0$.

The difference between Method 1 and Method 2 is about how they handle disturbances. Method 2 summarize the positioning error over time, while Method 1 uses the bias estimate from the observer; which is depending on an estimated measurement $\hat{y}$. It is not easy to see how the two methods differs in the irregular sea state. Therefore, consider Figure 5.9, where the two methods are applied on a regular sea state. Recall that for regular waves, the slowly-varying loads will be modelled as a mean-drift load. Hence, first order and mean-drift loads are the only contributions acting on the vessel in Figure 5.9. We can see an obvious difference in the positioning response between approximately 8 seconds to 40 seconds. The integral action responds way faster to the wave induced offset, than the direct bias compensation. With that being said, the integral action is also consisting of some oscillating responses. This introduces a trade-off when using integral action; higher integral action will more effectively compensate for disturbances, but a too high integral action produces oscillatory responses, and adds instability due to a phase lag to the closed loop system. On the other hand; smaller integral gains will give an asymptotic stability of the response, but that is after long time.

The direct bias compensation, on the other hand, is more equal to an overdamped system, as the disturbances are more slowly counteracted, when compared to the integral action.

Note that the small oscillations in Figure 5.9 are the filtered first order wave induced motions, which are filtered in the observer.

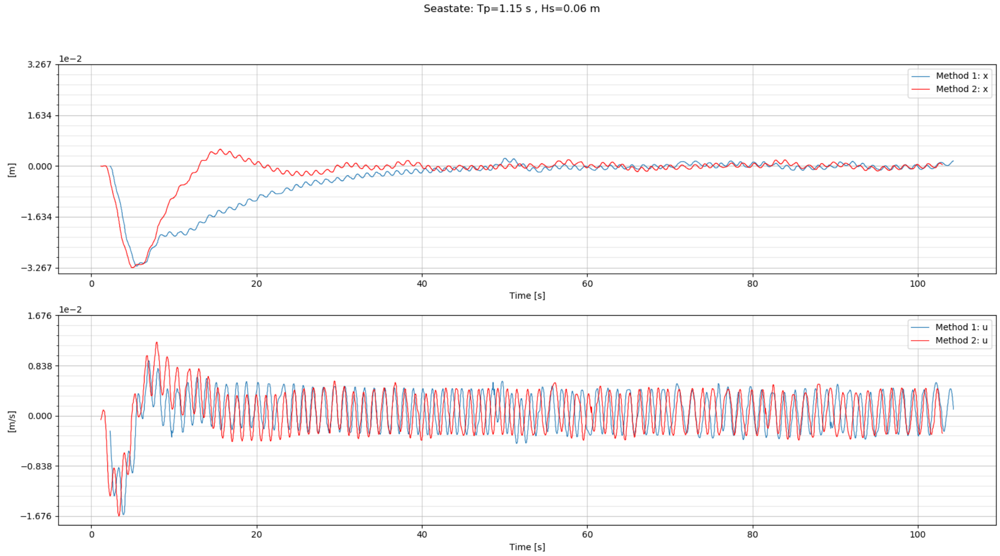

Figure 5.9: Surge responses of Method(s) 1 and 2, compared in a regular sea state.

A downside of using integral action is the problem with integral windup, which may happen when a sudden large offset occur. Then it would take time for the integral to remove this error from the total sum of the integral. This is not the case for Figure(s) 5.7 and 5.8, but it may be a problem for higher sea states, in transients, or wave trains.

Another downside with Method 2 is that, the estimated states provided by the observer, comes with a delay due to integrations within the observer, and the signal processing itself (as seen in Figure 5.3). Due to this, it is not achievable with an immediate counteraction when a sudden change in the environmental loads occurs. This is in general an issue with feedback mechanisms, including Method 1 and 2; an offset will have to be induced before any counteractions are carried out.

5.3.3 Method 3: Acceleration Feedforward

Figure 5.10 presents the surge response when the acceleration feedforward controller is applied. First thing to notice, is the immediate response in the initial seconds. Since the sudden occurrence of the experienced wave loads are proportional to the dynamic acceleration, the feedforward term is able to react quickly to the offset. In addition, the proportional term in the PD controller is providing stiffness in the nominal controller. Consequently, an aggressive control response is provided.

We can see from Figure 5.10 that the velocity and position is oscillating more the first 150 seconds. At this point, the sea state is not considered as steady state yet, and is still in the transient condition. This is reflected by the control input from Figure 5.11, where we can see that the actuators are much more active for the first 150 seconds, and the saturation limit u_{max} is exceeded much more than the previous methods. However, the control input seems to be relatively stable, while the mean of the actuator thrust load (0.0357 N) is higher than for Method(s) 1 and 2.

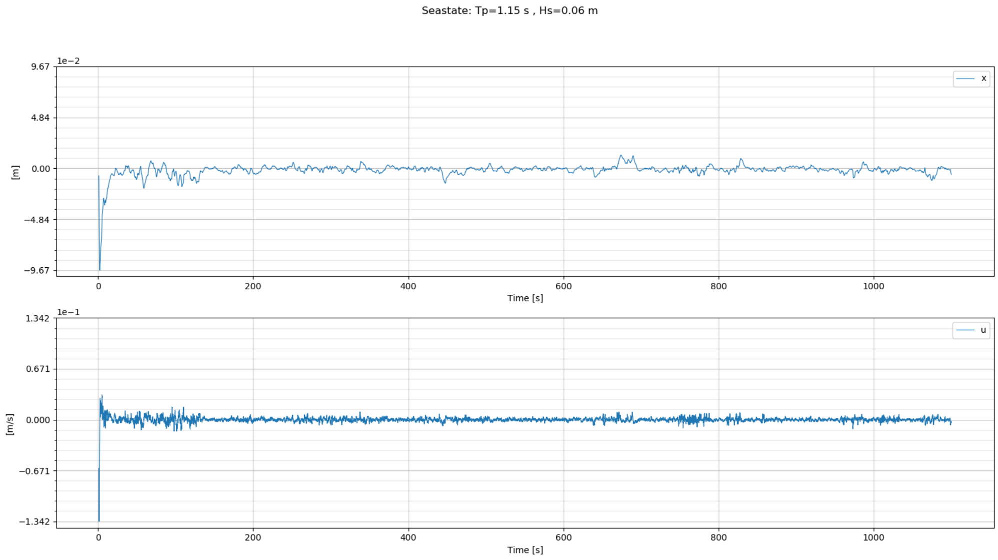

Figure 5.10: Surge response of Method 3. Sea state: $T_p = 1.15$, $H_s = 0.06$, $\beta = 0$.

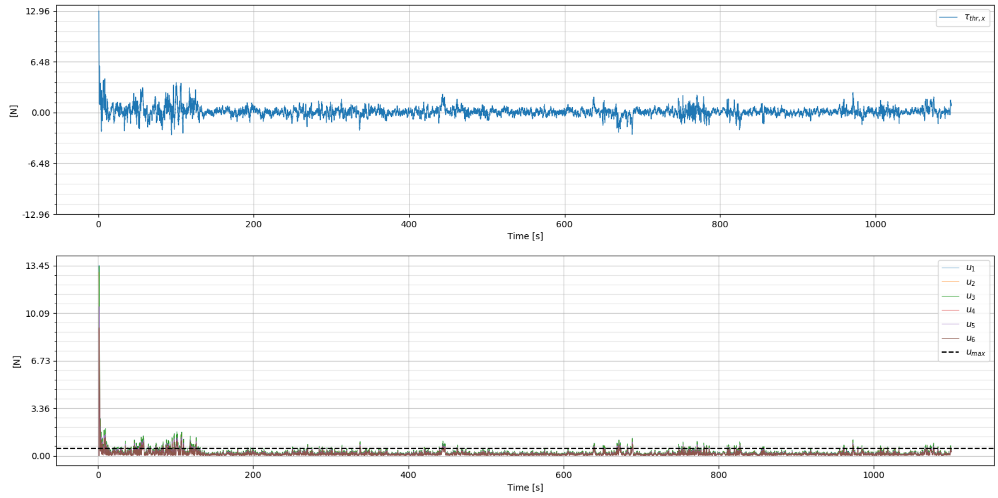

Figure 5.11: Controller output τ in surge, and thrust allocation output u_i for Method 3. Sea state: $T_p = 1.15$, $H_s = 0.06$, $\beta = 0$.

Looking into how the method reacts to regular waves in Figure 5.12, an interesting observation emerges. After approximately 72 seconds, a sudden jump in position is found. Since we are considering regular waves, there is no rapidly varying loads that is inducing this response. If we look into the acceleration measurements in Figure 5.12b, we can see that the measurements contains some sort of break at the same time instance. It seems that this points out a disadvantage with using ROS for a real-time control system. The break comes from a frozen node in the ROS environment holding the last value a bit longer than the sampling period. This affects the integration of the velocity state, which further results in a phase lag for a short period of time. Luckily, the nominal controller manage to rectify this as long as the contribution from the acceleration feedforward is smaller than the nominal terms.

Another observation is the slowly-varying oscillation that is present in Figure 5.12a. Since there are no slowly-varying loads acting on the vessel in the regular sea state simulation, this may be due to some unmodelled dynamics which originates from the transformation of the sensor measurements.

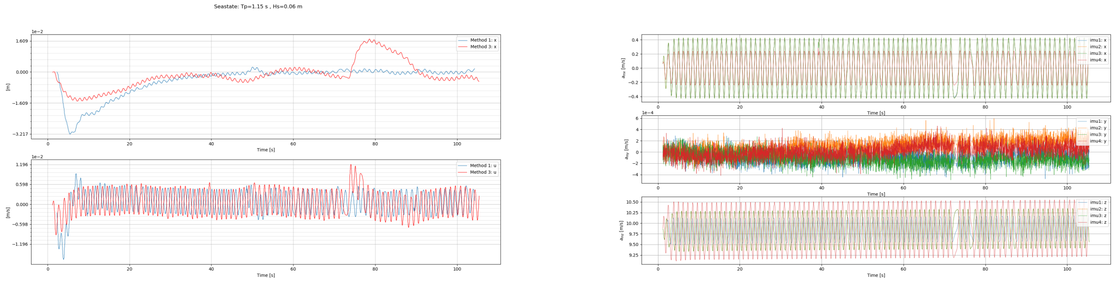

(a) Surge position and velocity.

(b) Acceleration measurements.

Figure 5.12: **(a)** Surge responses of Method(s) 1 and 3 in regular sea state. **(b)** Acceleration measurements provided to controller in Method 3. Here, the noisy measurements are filtered, for illustrating purposes only.

One downside of Method 3 is clearly related to the sensitivity of the frozen ROS node. This is not affecting Method(s) 1 and 2 to the same extent as for Method 3. The reason is that the acceleration measurements are more affected by the frozen node than the nonlinear observer from Fossen and Strand (1999) is. This shows a benefit of using a model-based observer; that is, if measurements are uncertain, the observer can still estimate the states if frozen measurements occurs, by depending the estimates on both measurements and the mathematical design model. For the state observer used in Method 3, the estimates are dependent on measurements only, and no mathematical model. Hence, Method 3 is more sensitive to uncertain measurement than the previous methods.

With that being said, Kjerstad and Skjetne (2016) states that the feedforward control law used in Method 3 is handling unmodelled and uncertain dynamics well; i.e., the model parameters in the CDM can contain uncertainties and simplifications. However, this is not related to the mentioned signal issue.

A possible problem with using the acceleration measurements in a feedforward method for wave load compensation could have been to separate first order wave loads from the second order wave loads. Slowly-varying loads, induces small accelerations, while acceleration due to first order loads are much higher, but the latter is not supposed to be compensated for. However, this is taken care of by the filtered acceleration feedforward term. This is also supported by the observation in Figure 5.12, where the first order wave induced motions are freely oscillating.

An important observation is the constant mean-drift loads induces no acceleration; hence, this is not perceived by the acceleration signals. We can see this in Figure 5.12, where a stationary offset is not compensated for. This shows a disadvantage by Method 3.

5.3.4 Method 4: Adaptive Fourier Series

Results from using Method 4 are presented in Figure(s) 5.13 and 5.14. As we could expect, the response is characterized by a lot of oscillating components. The reason for this is that the internal model, describing the estimated disturbance, is in fact a sum of multiple harmonic oscillating functions. As a consequence, the control input in Figure 5.14 is oscillating with high magnitude in the initial seconds, making Method 4 pushing the saturation limit of the actuators' capacity.

Since Method 4 is an adaptive controller, it takes time for the estimated disturbance to adapt to the true disturbance. For an adapting controller to deal with transients in the initial period of the sea state, is therefore not possible. In addition, the true disturbance is subject to randomness, which can not be predicted by a series of harmonic oscillating functions. With that being said, the sea state is assumed to be steady state after the first transient period is passed. Therefore, there are reasons to believe that an estimate of the slowly-varying loads should be achievable to estimate using the presented internal model.

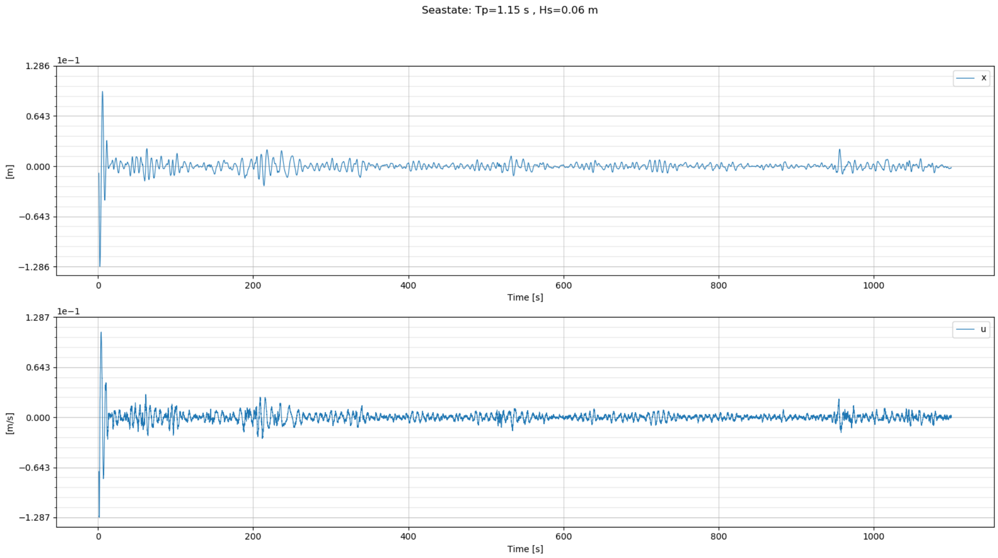

Figure 5.13: Surge response of Method 2. Sea state: $T_p = 1.15$, $H_s = 0.06$, $\beta = 0$.

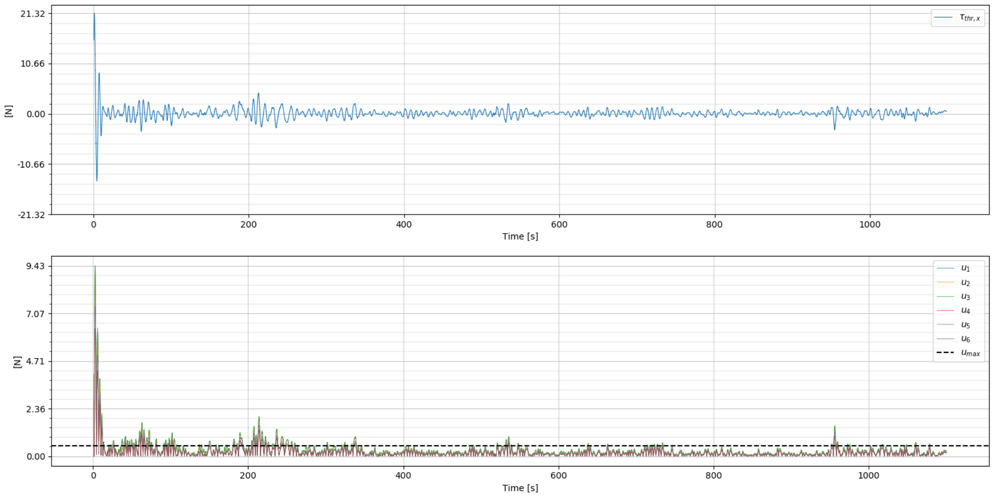

Figure 5.14: Controller output τ in surge, and thrust allocation output u_i for Method 4. Sea state: $T_p = 1.15$, $H_s = 0.06$, $\beta = 0$.

Considering Figure 5.13, shows that there are tendencies of the controller output to converge to some estimate of the slowly-varying loads, as the largest oscillations declines with time. We can investigate this further by looking into the estimated disturbance with its corresponding Fourier coefficients. In Figure 5.15, the estimated disturbance is plotted besides the plot of the corresponding Fourier coefficients in $\hat{\theta}$. Figure 5.15b is presented such that the mean of the five lowest frequencies are represented by the yellow plot ($\hat{\theta}[1 : 5]$), the next five are represented by the green plot ($\hat{\theta}[6 : 11]$), etc., and the coefficient corresponding to the mean-drift load is plotted in blue. We can see that the largest oscillation in Figure 5.15a declines quite fast in the first 400 seconds. This is supported by looking at the Fourier coefficients that belong to the highest frequencies in Figure 5.15b. We can see that the coefficients for the highest 2/3 of the frequency components converges towards zero, while the lowest frequencies are the dominating frequency elements. These observations are very promising, as this coincides to the hydrodynamical theory as the slowly-varying loads are observed as low frequencies, due to difference-frequency effects. Therefore, Method 4 stands out as a promising control design for compensation of second order wave loads.

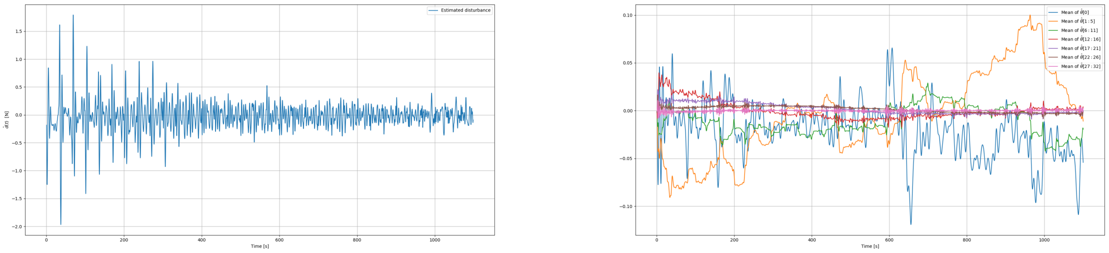

(a) Estimated disturbance

(b) Altering of estimated Fourier coefficients.

Figure 5.15: **(a)** Estimated disturbance provided by the internal disturbance model. **(b)** Corresponding Fourier coefficients, presented as the mean of five coefficients. Yellow is the mean of the five lowest frequencies ($\hat{\theta}[1 : 5]$), green is the next five($\hat{\theta}[6 : 11]$), etc. Blue is the coefficient corresponding to the constant mean-drift load.

Now, considering the response in a regular sea state in Figure 5.16, there seems to be an issue for the update law of $\dot{\hat{\theta}}$ to identify the coefficient for the mean-drift load. Figure 5.16a shows that the position, in steady state, have a stationary offset; even though Figure 5.16b shows that the coefficient for mean-drift are adapting to some value.

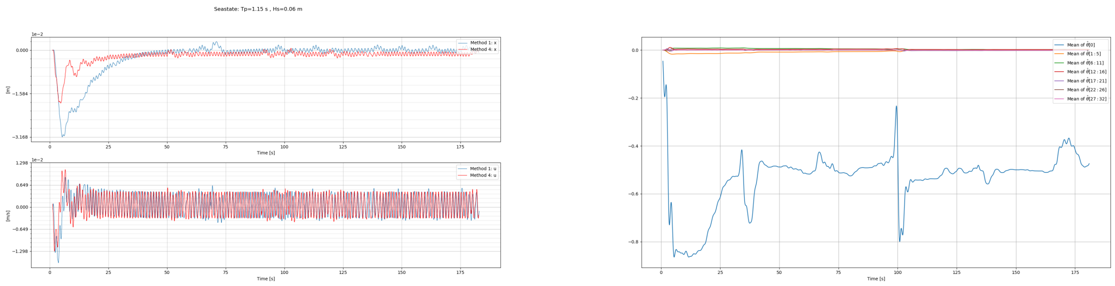

(a) Estimated disturbance

(b) Altering of estimated Fourier coefficients.

Figure 5.16: **(a)** Surge responses of Method(s) 1 and 4 in regular sea state. **(b)** Fourier coefficients, presented as the mean of five coefficients. Yellow is the mean of the five lowest frequencies ($\hat{\theta}[1:5]$), green is the next five($\hat{\theta}[6:11]$), etc. Blue is the coefficient corresponding to the constant mean-drift load.

An alternative approach for Method 4 could have been to use the diagonal QTF as regressor, and adapt coefficients to these transfer functions. Since we know that the QTF is proportional to the second order loads, an internal disturbance model relying on this may have been closer to estimate the true slowly-varying loads, than the Fourier series.

5.3.5 Method 5: Spectrum-Based Estimation

After the algorithm for Method 5 was implemented, initial tests were performed in order to validate if the algorithm was able to run in the real-time simulation. It turns out to be an issue with the calculation time of the sea state estimation. Table 5.2 shows the mean run time for one iteration for all methods. The run time for Method 5 was calculated at the instance of when a new sea state estimation was provided. An estimation taking 0.21 seconds is way too time-consuming when the control system runs at a frequency of 50 Hz. Therefore, no results have been produced for this method.

With that being said, there exists solutions to overcome the run time problem. If the PID-controller and the spectrum-based term runs on separate nodes providing asynchronous control inputs, the PID-controller could have provided the control input continuously; and consequently, not stopped the control process when a new estimate was provided. Then the spectrum-based part could calculate the mean-drift estimate without delaying the whole process. Thus, there are reasons to believe that Method 5 is possible to implement, and requested for further work.

It should be noticed that the sea state estimation procedure will increase in time as the amount of historical data increases with time. Therefore, one should consider deleting the oldest measurements after some specified time.

Table 5.2: Mean run time for each method. Time taken from state measurements are made available to the control signal is generated and ready to be published. (* run time for Method 5 is taken for the instance of when a new sea state estimate is provided.)

Controller	Mean run time [s]
Method 1	0.00044
Method 2	0.00047
Method 3	0.00083
Method 4	0.00063
Method 5*	0.21

The idea of Method 5 is to relieve some of the integral action from the rest of the contributions, since second order wave loads are large contributors to the bias. Consequently, the integral action will have to deal with the slowly-varying loads and unmodelled dynamics. But the question is; after some of the integral action is relieved from the mean-drift loads, is the integral action more suited to compensate the slowly-varying loads? It is hard to tell without any results, but one should believe that integral wind-up may be less problematic if such high values like the mean-drift loads are handled by some other term. Then, the integral can respond better to changes in disturbance, and the time it takes to unwind the built-up error may be reduced.

One should also be aware that creating an FFT frequency spectrum takes time; and consequently, it results in back-dated information (Fossen, 2021, chap. 13). Therefore, the sea state estimates, which are provided by Method 5, may not be good if the sea state changes often, and are rapidly changing its conditions. Fossen (2021, chap. 13) says that FFT can yield a good estimate if the sea state parameters are constant for typically 30 minutes.

One should also consider to use heave responses or acceleration measurements instead of wave elevation measurements. Then the highest frequencies will not have to be considered since they are filtered by the ship acting as a lowpass filter.

5.3.6 Tuning Aspects

Since four of five methods includes a nominal PD-controller with the same tuning parameters, the difference in performance results are not affected too much of the stiffness and damping characteristics of the control systems. The tuning procedure was done in accordance with the tuning rules in (Fossen, 2021, chap. 15). The exception is the adaptive controller in Method 4, which is designed by a LgV-backstepping procedure. Consequently, there are more tuning parameters that have an impact on the performance. In addition, these parameters are harder to tune compared to the conventional nominal controllers, as they are less associated with a physical understanding. Therefore, it is hard to tell whether the control systems are tuned equally good, and compared fairly. To decrease the impact of this source of error, a self-tuning procedure could have been implemented, like the one in Værnø et al. (2019).

The limitation of considering surge direction only, may also constitute to some sources of error. Even if the vessel is exposed to the wave loads from surge direction, the vessel will rotate due to uncertainties in the transfer function from the VERES database, and due to unmodelled dynamics in the equation of motions. When the results in this chapter were produced, this was taken care of by refusing rotational and transverse motions. That way, the impact of poor tuning in sway and yaw were neglected.

Method 4 contains several tuning parameters; N, ω_{min}, and ω_{max} are directly linked to the disturbance we want to suppress. N determines how many frequency components within the set $[\omega_{min}, \omega_{max}]$ that we want the controller to adapt to. Since we want the controller to estimate the environmental disturbance in terms of slowly-varying drift loads and mean-drift loads, we have to determine what frequency domain that can be categorized as "slowly-varying". Therefore, in order to determine these tuning parameters, a closer study on the frequency domain should be prioritized in further work. If N is selected high, the control law would be more capable of adapting the true disturbance. On the other hand, higher N values will have an impact on the computational cost, as the regressor $\Phi(t)$ will increase its dimensions by $2N + 1$.

5.3.7 Comparative Analysis

In order to analyze the performance of the presented methods, a qualified comparison have to be investigated. In this analysis, we are interested in two factors particularly; the positioning accuracy when subject to disturbances, and how much control effort it takes to achieve this.

Now, assume that all controllers are tuned equally good and optimized for good performance of η and ν. In order to evaluate the closed-loop performance on an equal foundation, cost functions are used (5.1), where $J^c_{\tilde{\eta}}$ and J^c_{τ} are the positioning performance and control effort meter factors, respectively. τ and η are defined as in the CDM, t_0 is the initial time, and T is the final time of the test run.

$$J^c_{\tilde{\eta}} = \int_{t_0}^{T} |\eta(t) - \eta_d| dt \tag{5.1a}$$

$$J^c_{\tau} = \int_{t_0}^{T} |\tau(t)| dt \tag{5.1b}$$

Since the generated wave loads includes randomness, some simulations may have more harsh waves than others. Therefore, the results presented here, are taken from a mean of three equally long runs; from $t_0 = 0$ to $T = 1000$.

Now consider Figure 5.17, where the cumulative cost function for positioning errors are normalized such that the worst performing method for the whole test has a total score of 1. Pointing out the most remarkable observation first; is that, the two "new" Method(s) 3 and 4 have a better positioning performance in total than the conventional integral action and direct bias estimate controllers in Method(s) 1 and 2. In fact, the cumulative error of Method 3 is only 60 percent of the same value for Method 2, while Method 4 constitutes just 80 percent of the cumulative positioning error. Method 1 is approximately 90 percent of the value of Method 2. This is surprisingly good results for Method(s) 3 and 4, taken into consideration that PID controllers are the state-of-the-art methods for DP operations.

If we look deeper into the cumulative error of Method 3, we see that the first 100 seconds forms the highest amount of positioning error. This is reasonable as the sea state's transient forces the vessel out of position faster than the controller can react, due to limitations in the thruster dynamics, and the control system's bandwidth. When the sea state have reached its steady state, we can see that the gradient of the graph is relatively small and not far from constant, compared to Method(s) 1 and 2. This is in accordance with the results from the regular case in section 5.3.3, where we could see a stationary offset due to mean-drift loads. In addition, there will always be some small offsets that the controller will not manage to compensate for in irregular sea states.

Considering Method 4, we see that the transient is outstanding for the first seconds, also here. The most interesting about the cumulative development of Method 4, is that the total error is even higher than Method(s) 1 and 2 until about 420 seconds have passed. This illustrates clearly how the internal disturbance model adapts to the sea state, as the cumulative error becomes smaller than for Method(s) 1 and 2 after 600 seconds. This indicates that the adaptive controller perform significantly better after the controller have gained some time to adapt to the sea state.

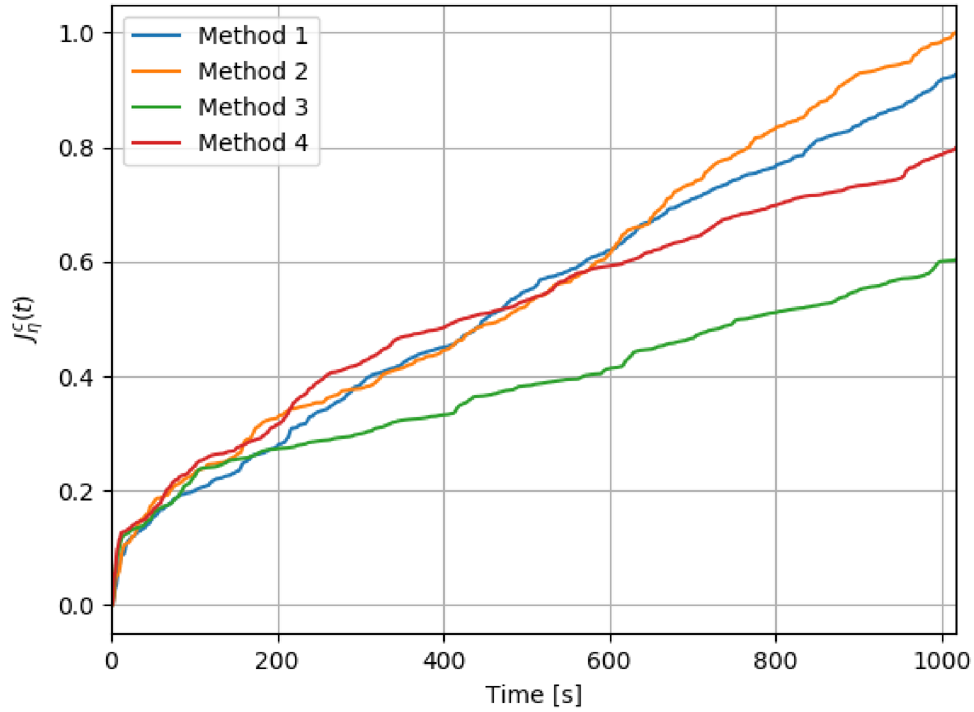

Figure 5.17: KPIs for positioning error $J^c_\eta(t)$, for four wave compensation methods, normalized such that worst performance, have a maximum value of 1 for the whole test.

In Figure 5.18, the cumulative control effort is plotted. The values are normalized the same way as in Figure 5.17. Method 4 stands out as the clearly worst performing method in terms of control effort. This is no surprise, as the initial period involves a lot of oscillating control inputs due to the estimated Fourier series. Therefore, Method 4 will cause much more wear and tear of the actuators, compared to the other Methods.

In contrast to the adaptive controller, Method 3 contends the conventional Method(s) 1 and 2, where the latter is as much as 40 percent better than Method 4. For the acceleration feedforward making Method 3 a quite aggressive controller, it is remarkable that the control effort is relatively low.

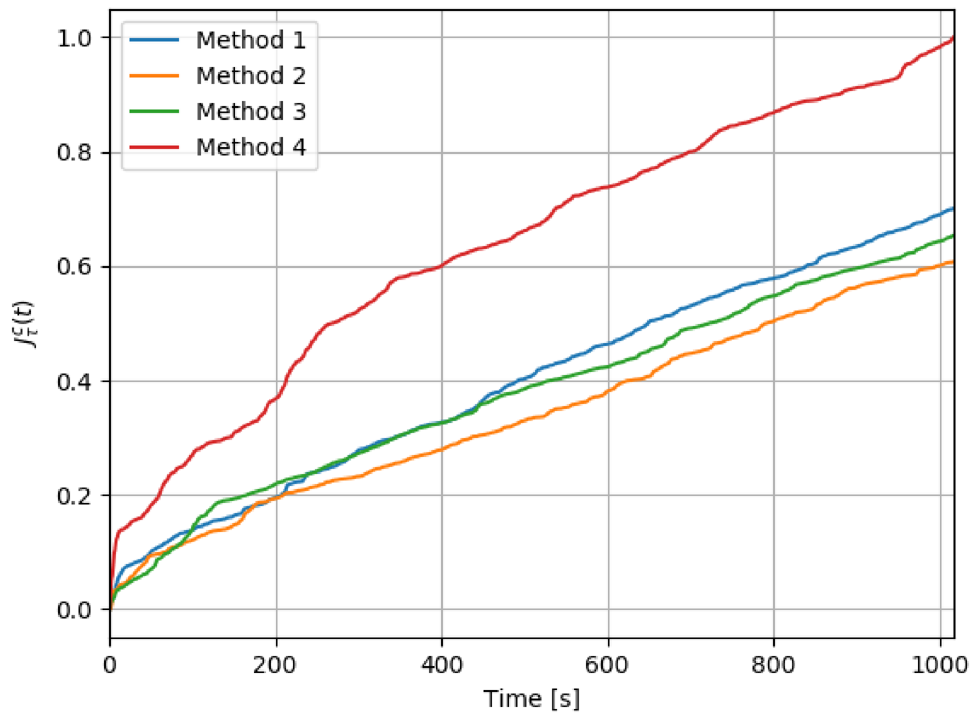

Figure 5.18: KPIs for control effort $J^c_\tau(t)$, for four wave compensation methods, normalized such that worst performance, have a maximum value of 1 for the whole test.

In order to investigate the performance at a shorter term, we consider the same tests, but now in two sub-intervals; 0-500 seconds, and 500-1000 seconds. This means that the cumulative KPIs for the second period are calculated from $t_0 = 500$ to $T = 1000$, so the first 500 seconds is not accounted for. In Table 5.3 the KPIs are listed for each sub-interval, where the results are normalized such that the worst performing in each time interval has a maximum score of 100 points.

For the first 500 seconds, there is a clear distinction between the only feedforward controller (Method 3) and the three feedback controllers (Method(s) 1, 2, 3). The positioning KPI are, already at this point, 32.7 percent better than Method 1. In the first 500 seconds for Method 4 on the other hand, the performance is at the level with Method(s) 1 and 2, while the control effort for the latter is 50.1 percent better than Method 4, which is noteworthy.

It is the last 500 seconds, things becomes really interesting, as Method 4 has started to converge its disturbance estimate to some value. We see that the positioning error have become 42.5 percent better than for Method 2 in the second period. This is a major improvement from the first 500 seconds. With that being said, we can not ignore the fact that the control effort is between 10.9 and 20.3 percent worse for Method 4 than the other methods. For Method 3 in the second period, the positioning performance is 56.4 percent better than Method 2, and approximately on the same level in control effort.

Table 5.3: KPI results for two sub-intervals at 500 seconds.

Time	**0 - 500 s**		**500 - 1000 s**	
Controller	$J^c_{\tilde{\eta}}$	J^c_{τ}	$J^c_{\tilde{\eta}}$	J^c_{τ}
Method 1	100.0	60.8	81.8	89.1
Method 2	95.5	49.9	100.0	82.2
Method 3	67.3	60.3	43.6	79.7
Method 4	97.1	100.0	57.5	100.0
Method 5	-	-	-	-

Chapter 6

Conclusion

This master thesis was backed up by a literature study, conducted to examine earlier and similar studies, and relevant background theory. This has been fundamental for the author's understanding of the problem in question, and for the knowledge needed to solve the problem, both in a control theoretical and hydrodynamical perspective.

The high-fidelity simulator imitating the marine surface vessel CSAD in 6 DOFs was successfully implemented, satisfying the need for credible sensor measurements, and wave induced loads in terms of both first and seconds order loads. Since the physical tests at the MC-Lab were impracticable, the simulator was vital for the analysis and verification of the designed control methods to be performed.

The environmental load module, providing wave loads, made it possible to test control systems in realistic regular and irregular long-crested sea states. However, since especially this module contained were time-consuming calculations, the simulator had to run on a lower update rate than desirable, making the control system subject to signal-delays.

Five strategies for wave-drift load compensation were developed and discussed, where four of them were successfully implemented. The five designs included:

- DP-observer bias estimate and feedforward compensation.
- Direct integral action in a DP PID-control law.
- Acceleration feedforward compensation of residual disturbance loads.
- An adaptive control law, estimating harmonic "residual loads" given by the internal model principle, using a Fourier series.
- Spectrum-based method, estimating mean drift loads.

The latter turned out to be too time-consuming for the proposed design, but possible solutions to overcome the issues were discussed.

A performance analysis was worked out based on results from simulations with the high-fidelity simulator, considering control in surge direction only. The analysis showed that the acceleration feedforward designated as the overall best method compared to the other, in terms of positioning performance. That was, both in shorter and longer periods of time. The positioning performance was 40 percent better than the worst performance when considering a DP operation with duration of 1000 seconds. It was also on the same level as the conventional controllers in terms of control effort performance. However, the method turned out to be sensitive to uncertain measurements, and struggled to compensate for the mean drift loads. The adaptive control law showed tendencies to be better in positioning performance than the conventional controllers, at least after long time. For a shorter time-span, the performance was outnumbered by the other Methods. However, the method required large amounts of control effort compared to the other.

Taken into consideration that only surge direction was analyzed, there are reasons to believe that there exists better strategies for eliminating second order wave induced motions. Utilizing acceleration measurements, or estimating the disturbance by Fourier series seemed to be promising solutions.

6.1 Further Work

Suggestions for further work are:

- Properly tuning of the controllers in sway and yaw, such that performance analysis can be made for all DOFs.
- Implement a spreading function in the environmental module, such that short crested waves can be tested on the control laws.
- Make a separate ROS node for providing the sea state estimate of Method 5, such that the method is less dependent on the time-consuming calculations in the estimations.
- Physical tests on the CSAD in MC-Lab, in order to see how the methods perform in a real world scenario.
- Investigate whether the diagonal QTF can be used as a regressor in an adaptive control law.

Bibliography

Anderson, B.D., Bitmead, R.R., Johnson Jr, C.R., Kokotovic, P.V., Kosut, R.L., Mareels, I.M., Praly, L., Riedle, B.D., 1986. Stability of adaptive systems: Passivity and averaging analysis. MIT press.

Batista, P., Silvestre, C., Oliveira, P., 2011. On the observability of linear motion quantities in navigation systems. Systems & Control Letters 60, 101–110.

Bell, P.S., 1999. Shallow water bathymetry derived from an analysis of x-band marine radar images of waves. Coastal Engineering 37, 513–527. **DOI:** https://doi.org/10.1016/S0378-3839(99)00041-1 **URL:** https://www.sciencedirect.com/science/article/pii/S0378383999000411.

Bjørnø, J., 2016. Thruster-assisted position mooring of c/s inocean cat i drillship. Master's thesis. NTNU.

Bjørnø, J., Heyn, H.M., Skjetne, R., Dahl, A.R., Frederich, P., 2017. Modeling, parameter identification and thruster-assisted position mooring of c/s inocean cat i drillship, in: International Conference on Offshore Mechanics and Arctic Engineering, American Society of Mechanical Engineers. **DOI:** 10.1115/omae2017-61896.

Breivik, M., Kvaal, S., østby, P., 2015. From eureka to k-pos: Dynamic positioning as a highly successful and important marine control technology. IFAC-PapersOnLine 48, 313–323. **DOI:** 10.1016/j.ifacol.2016.01.001.

Brodtkorb, A.H., Nielsen, U.D., Sørensen, A.J., 2018a. Online wave estimation using vessel motion measurements. IFAC-PapersOnLine 51, 244–249. **DOI:** https://doi.org/10.1016/j.ifacol.2018.09.510 **URL:** https://www.sciencedirect.com/science/article/pii/S2405896318321992.

Brodtkorb, A.H., Nielsen, U.D., Sørensen, A.J., 2018b. Sea state estimation using vessel response in dynamic positioning. Applied Ocean Research 70, 76–86. **DOI:** https://doi.org/10.1016/j.apor.2017.09.005 **URL:** https://www.sciencedirect.com/science/article/pii/S0141118717302481.

Brørby, B.T., 2021. Real-time estimation and compensation of wave loads: Establishing case study on c/s arctic drillship. Pre-project written at the Department of Marine Technology at Norwegian University of Science and Technology.

Bryne, T.H., 2017. Nonlinear observer design for aided inertial navigation of ships .

Conde, J.P., Gato, L., 2008. Numerical study of the air-flow in an oscillating water column wave energy converter. Renewable energy 33, 2637–2644.

Dankert, H., Horstmann, J., Rosenthal, W., 2005. Wind-and wave-field measurements using marine x-band radar-image sequences. IEEE Journal of oceanic engineering 30, 534–542.

Dankert, H., Rosenthal, W., 2004. Ocean surface determination from x-band radar-image sequences. Journal of Geophysical Research: Oceans 109.

Desmars, N., 2020. Real-time reconstruction and prediction of ocean wave fields from remote optical measurements. Ph.D. thesis. École centrale de Nantes.

DNV, 2010. Recommended practice dnv-rp-c205: environmental conditions and environmental loads. DNV, Norway .

DNVGL-RP-E306, 2015. DNVGL-RP-E306 Marine Technology Society DP vessel design philosophy. **URL:** https://dynamic-positioning.com/files_mailing/MTS%20DP%20VESSEL%20DESIGN%20 PHILOSOPHY%20GUIDELINES%20(Rev2%20-%20Apr21).pdf **Accessed:** 25-Nov-2021.

Elwood, D., Yim, S.C., Prudell, J., Stillinger, C., Von Jouanne, A., Brekken, T., Brown, A., Paasch, R., 2010. Design, construction, and ocean testing of a taut-moored dual-body wave energy converter with a linear generator power take-off. Renewable Energy 35, 348–354.

Espíndola-López, E., Carrillo-Serrano, R., Gómez-Espinosa, A., 2016. A new self-tuning controller using fourier series neural network.

Faltinsen, O.M., 1999. Sea loads on ships and offshore structures. Cambridge University Press.

Fossen, T.I., 2002. Marine control systems–guidance. navigation, and control of ships, rigs and underwater vehicles. Marine Cybernetics, Trondheim, Norway, Org. Number NO 985 195 005 MVA, www. marinecybernetics. com, ISBN: 82 92356 00 2 .

Fossen, T.I., 2021. Handbook of Marine Craft Hydrodynamics and motion control. 2 ed., Wiley.

Fossen, T.I., Perez, T., 2022. Marine systems simulator (mss) toolbox.
URL: https://github.com/cybergalactic/MSS **Accessed:** 03-Mar-2022.

Fossen, T.I., Strand, J.P., 1999. Passive nonlinear observer design for ships using lyapunov methods: full-scale experiments with a supply vessel. Automatica 35, 3–16.

Francis, B.A., Wonham, W.M., 1976. The internal model principle of control theory. Automatica 12, 457–465.

Fu, T.C., Fullerton, A.M., Hackett, E.E., Merrill, C., 2011. Shipboard measurement of ocean waves, in: International Conference on Offshore Mechanics and Arctic Engineering, pp. 699–706.

Giron-Sierra, J., 2010. State-of-the-art of wave measurement for ship motion prediction, pp. 295–300. **DOI:** 10.3182/20100915-3-DE-3008.00057.

Halliday, J.R., Dorrell, D.G., Wood, A.R., 2011. An application of the fast fourier transform to the short-term prediction of sea wave behaviour. Renewable Energy 36, 1685–1692.

Halstensen, S.O., Vasilyev, L., Zinchenko, V., Liu, Y., 2020. 'next minutes' ocean waves and vessel motion predictions for more efficient offshore lifting operations, in: SNAME Maritime Convention, OnePetro.

Hasselmann, K.F., Barnett, T.P., Bouws, E., Carlson, H., Cartwright, D.E., Eake, K., Euring, J., Gicnapp, A., Hasselmann, D., Kruseman, P., et al., 1973. Measurements of wind-wave growth and swell decay during the joint north sea wave project (jonswap). Ergaenzungsheft zur Deutschen Hydrographischen Zeitschrift, Reihe A .

Kjerstad, Ø.K., Skjetne, R., 2016. Disturbance rejection by acceleration feedforward for marine surface vessels. IEEE Access , 2656–2669 **DOI:** 10.1109/access.2016.2553719.

Kjerstad, Ø.K., Skjetne, R., Jenssen, N.A., 2011. Disturbance rejection by acceleration feedforward: Application to dynamic positioning. IFAC Proceedings Volumes 44, 2523–2528.

Larsen, C.M., Kristiansen, T., Myrhaug, D., Bachynski, E.E., 2019. TMR4182 Marine Dynamics - Compendium. Department of Marine Technology, NTNU.

LaSalle, J.P., 1968. Stability theory for ordinary differential equations. Journal of Differential equations 4, 57–65.

Li, Y., Yue, X., Wu, X., Zhang, L., Zhou, Q., Yi, X., Liu, N., 2020. A higher-order singular value decomposition-based radio frequency interference mitigation method on high-frequency surface wave radar. IEEE Transactions on Geoscience and Remote Sensing 58, 2770–2781. **DOI:** 10.1109/TGRS.2019.2955472.

Loría, A., Panteley, E., 1999. A separation principle for a class of euler-lagrange systems, in: New Directions in nonlinear observer design. Springer, pp. 229–247.

MC-Lab, 2021. Marine cybernetics teaching laboratory. **URL:** https://www.ntnu.edu/imt/lab/cybernetics **Accessed:** 29-Nov-2021.

MSC/CIRC. 645, 1994. MSC/CIRC. 645 Guidelines for vessels with dynamic positioning systems. International Maritime Organization.

Nguyen, D.T., Sørbø, A.H., Sørensen, A.J., 2009. Modelling and control for dynamic positioned vessels in level ice. IFAC Proceedings Volumes 42, 229–236. **DOI:** 10.3182/20090916-3-br-3001.0006.

Nielsen, U.D., 2008. The wave buoy analogy—estimating high-frequency wave excitations. Applied Ocean Research 30, 100–106.

Nielsen, U.D., 2017. A concise account of techniques available for shipboard sea state estimation. Ocean Engineering 129, 352–362. **DOI:** https://doi.org/10.1016/j.oceaneng.2016.11.035
URL: https://www.sciencedirect.com/science/article/pii/S0029801816305388.

Numpy FFT [software], . Fast Fourier Transform (numpy.fft).
URL: *https://numpy.org/doc/stable/reference/routines.fft.html* **Accessed:** 2022-04-03.

OrcaFlex, . Waves: Kinematic stretching. **URL:** https://www.orcina.com/webhelp/OrcaFlex/Content/html/Waves,Kinematicstretching.htm **Accessed:** 05-Apr-2022.

OrcaFlex, 2021. Vessel theory: Wave drift and sum frequency loads.
URL: https://www.orcina.com/webhelp/OrcaFlex/Content/html/Vesseltheory,Wavedriftandsumfrequencyloads.htm **Accessed:** 29-Apr-2021.

Park, J., Delgado, R., Choi, B., 2020. Real-time characteristics of ros 2.0 in multiagent robot systems: An empirical study. IEEE Access PP, 1–1. **DOI:** 10.1109/ACCESS.2020.3018122.

Price, W.G., Bishop, R.E.D., 1974. Probabilistic theory of ship dynamics. Chapman and Hall.

Quadvlieg, F., Hallmann, R., Hughes, G., Harris, R., 2011. Improved dynamic positioning using wave feed forward, in: International Conference on Offshore Mechanics and Arctic Engineering, pp. 765–773.

Ren, Z., Han, X., Verma, A.S., Dirdal, J.A., Skjetne, R., 2021. Sea state estimation based on vessel motion responses: Improved smoothness and robustness using bézier surface and l1 optimization. Marine Structures 76, 102904. **DOI:** https://doi.org/10.1016/j.marstruc.2020.102904
URL: https://www.sciencedirect.com/science/article/pii/S0951833920301969.

Scipy FFT: Welch, . Fast Fourier Transform by Welch's method: Estimateing power spectral density. **URL:** https://docs.scipy.org/doc/scipy/reference/generated/scipy.signal.welch.html
Accessed: 13-May-2022.

Shiach, J., 2008. Numerical modelling of wave run-up and overtopping using depth integrated equations. Ph.D. thesis. Manchester Metropolitan University.

Sintef, 2022. ShipX [software]. **URL:** https://www.sintef.no/en/software/shipx/ **Accessed:** 09-Mar-2022.

Slåttum, S.S., 2021. Data-driven sea state estimation for a DP vessel based on distributed IMUs. Master's thesis. NTNU.

Sørensen, A.J., 2011. A survey of dynamic positioning control systems. Annual Reviews in Control 35, 123–136. **DOI:** 10.1016/j.arcontrol.2011.03.008.

Sørensen, A.J., 2018. Marine cybernetics: Towards autonomous marine operations and systems, lecture notes.

Torsetnes, G., Jouffroy, J., Fossen, T., 2005. Nonlinear dynamic positioning of ships with gain-scheduled wave filtering, pp. 5340 – 5347 Vol.5. **DOI:** 10.1109/CDC.2004.1429657.

Værnø, S.A., Brodtkorb, A.H., Skjetne, R., 2019. Compensation of bias loads in dynamic positioning of marine surface vessels. Ocean Engineering 178, 484–492.

Wang, Q.G., Nie, Z.Y., 2012. PID Control for MIMO Processes. Springer London, London. pp. 177–204.

Wei, Y., Lu, Z., Pian, G., Liu, H., 2017. Wave height estimation from shadowing based on the acquired x-band marine radar images in coastal area. Remote sensing 9, 859.

Xie, S.H., Zhao, Y.S., He, Y.P., Shao, Y.L., Han, Z.L., Gu, X.L., et al., 2020. Prediction of springing-induced extreme responses of a tlp-type floating wind turbine, in: The 30th International Ocean and Polar Engineering Conference, OnePetro.

Yoshizawa, T., 1966. Stability theory by lyapunov's second method (mathematical society of japan, tokyo). Search in .

Zappa, B., Legnani, G., Van den Bogert, A.J., Adamini, R., 2001. On the number and placement of accelerometers for angular velocity and acceleration determination. J. Dyn. Sys., Meas., Control 123, 552–554.

Appendix A - Guides

Guide - Installing CSAD Workspace

1. First, make sure that ROS Melodic is correctly installed. If not, it can be installed by following the guide:
   http://wiki.ros.org/melodic/Installation/Ubuntu
   Note that ROS Melodic requires Ubuntu 18.04 as WSL for windows, and the following guides depends on this.

2. Install the source code in the ROS environment.

3. Type in the following command lines:

```
$ cd csad_dp
$ catkin_make
$ source devel/setup.bash
```

Now the workspace should be correctly installed.

Guide - Running Simulations

For running simulations, the following has to be done:

1. In order to run a simulation you will first need to source the terminal for being able to run on the ROS framework:

```
$ cd csad_dp
$ source /opt/ros/melodic/setup.bash
```

   Note that if *source /opt/ros/melodic/setup.bash* is not written inside your *.bashrc* script, you will either have to modify the file, or source the environment each time a new terminal is created.

2. If the latest code is not built, you will have to do step 3. in **Guide - Installing CSAD Workspace**, before being able to run simulations.

3. A master node needs to be set up, in order to communicate on the ros framework. Open a new terminal and type in:

```
$ roscore
```

4. There are several simulations available in this workspace. Each of them has it's own launch file. Each launch file has it's own controller for wave load compensation. In other words; all controllers presented in section 4.5 are available for simulations. Table 6.1 presents the controllers with their respective launch files.
   In order to run the simulation, type the following in a terminal:

   ```
   $ roslaunch launch/<launcfile>
   ```

   where <launchfile> should be the name of the preferred controller's .launch file.

   Table 6.1: Controller names with their respective launch files.

Controller	.launch file
DP-observer bias estimate	biasController-simulation.launch
Direct integral action	integralAction-simulation.launch
Acceleration feedforward	accFeedforward-simulation.launch
Adaptive fourier series	adaptiveFourierSeries-simulation.launch
Spectrum-based estimation	spectrumController-simulation.launch

5. To store the data from the simulations, it is recommended to use rosbags. There are a lot of data available for recording. The node structure enables all signals within the control system to be recorded. This is done by typing the following in a new terminal:

   ```
   $ cd bags
   $ rosbag record -O <fileName> -a
   ```

   where <fileName> is the name of your rosbag. The flag *-a* means that you record all topics available.
   For more information on how to use rosbags, see:
   http://wiki.ros.org/rosbag.

6. To change sea states, you will have to change the parameters in the source code *simulator_node.py*. In order to choose realistic sea states, see Table 5.1 in Chapter 5. There are also possible to use the gain server feature, but this is not completely implemented as of today.

Guide - Running Physical CSAD Setup

The control system presented in this thesis is made for compatibility with the physical setup for CSAD. CSAD is equipped with a Raspberry Pi, running the controller algorithms. It is recommended that all implementation is done on a local laptop, and then transfer a copy of the source code onto the Raspberry Pi. This can be done by following these steps:

1. In order to save some time and transfer the source code faster, it is preferable to delete the build folder and the devel folder first.

   ```
   $ rm -r build
   $ rm -r devel
   ```

2. Now, the source code needs to be copied through SSH from your local laptop to the Raspberry pi (note that you need to be connected to the MC-lab wifi to manage this). This is done by typing:

   ```
   $ scp -r csad_dp_ws/ pi@192.168.0.123:˜
   ```

3. Log into the Raspberry Pi:

   ```
   $ ssh pi@192.168.0.123
   ```

4. Build the code:

   ```
   $ cd csad_dp
   $ catkin_make
   $ source devel/setup.bash
   ```

5. Check if you are able to access qualisys topics inside the Raspberry Pi:

   ```
   $ rostopic list
   ```

   If qualisys is running properly, it should publish messages on a topic named */qualisys/Body_1/odom*. If you do not see this topic, you will have to export the ros master node from outside the Pi:

   ```
   $ exit
   $ export ROS_MASTER_URI=http://192.168.0.123:11311
   ```

   Now, enter the Rapsberry Pi again by recalling step 3.

6. The control system should now be ready, and launching can be done as described in step 4 in **Guide - Running Simulations**. Note that there are other launch files for the physical setup. Also note that the control system is tuned for simulations as of today.

NTNU

Norwegian University of
Science and Technology